Master's thesis
Theoretical physics

Onset of cosmological turbulence

Jani Dahl

August 12, 2018

Supervisors: Kari Rummukainen, David Weir

Examiners: Kari Rummukainen
David Weir

UNIVERSITY OF HELSINKI
Department of Physics

P.O. Box 64 (Gustaf Hällströmin katu 2a)
FI-00014 Helsingin yliopisto

HELSINGIN YLIOPISTO — HELSINGFORS UNIVERSITET — UNIVERSITY OF HELSINKI

Tiedekunta — Fakultet — Faculty	Laitos — Institution — Department
Faculty of Science	Department of Physics

Tekijä — Författare — Author
Jani Dahl

Työn nimi — Arbetets titel — Title
Onset of cosmological turbulence

Oppiaine — Läroämne — Subject
Theoretical physics

Työn laji — Arbetets art — Level	Aika — Datum — Month and year	Sivumäärä — Sidoantal — Number of pages
Master's thesis	August 12, 2018	100 pages

Tiivistelmä — Referat — Abstract

At the end of the inflationary epoch, about 10^{-12} seconds after the Big Bang singularity, the universe was filled with plasma consisting of quarks and gluons. At some stage the cooling of the universe could have led to the occurrence of first-order cosmological phase transitions that proceed by nucleation and expansion of bubbles all over the primordial plasma. Cosmological turbulence is generated as a consequence of bubble collisions and acts as a source of primordial gravitational waves.

The purpose of this thesis is to provide an overview of cosmological turbulence as well as the corresponding gravitational wave production, and compile some of the results obtained to this day. We also touch on the onset of cosmological turbulence by analysing shock formation. In the one-dimensional case considering only right-moving waves, the result is Burgers' equation. The development of a power spectrum with random initial conditions under Burgers' equation is calculated numerically using the Euler method with sufficiently low step sizes. Both in the viscid and inviscid cases, the result is the presence of a $-8/3$ power law in the inertial range at the time of shock formation.

Avainsanat — Nyckelord — Keywords
cosmology, turbulence, onset

Säilytyspaikka — Förvaringsställe — Where deposited
Kumpula campus library

Muita tietoja — övriga uppgifter — Additional information

Contents

1. Introduction

The prevailing cosmological model implies that the universe was born approximately 13.8 billion years ago in an event called the Big Bang [1]. So far the earliest observed direct source of information from the early universe has been the cosmic microwave background, consisting of the oldest electromagnetic radiation. It is an image of the universe from the time it was about 377 000 years old, the moment when photons could travel freely for the first time[1] and the universe became transparent. This relic radiation has been measured many times, most recently by the Planck probe in 2015 [1], and these measurements have provided invaluable information regarding cosmological parameters, the Big Bang and the composition of the universe. But what about earlier times? Neutrinos decoupled when the universe was around one second old but detecting the neutrino background is not feasible, because neutrinos interact extremely weakly with matter. This leaves us with the gravitational wave background.

Gravitational waves are fluctuations in spacetime that propagate at the speed of light. They were first predicted by Albert Einstein's general theory of relativity in 1916 but were observed directly for the first time only recently in 2015 by LIGO [2]. The reason why the detection took nearly 100 years is that the amplitude of the waves is extremely small, and therefore their detection requires extremely sensitive instruments. In theory, gravitational waves could have decoupled when the universe

[1]This occurs when the particle type in question falls out of thermal equilibrium with respect to other particles. The event is known as decoupling.

was one unit of Planck time old [3] and when this is combined with the fact that they travel undisturbed trough spacetime, they make an excellent (and probably the only) probe of the very early universe. The primordial gravitational wave background is expected to consist of many contributions [4], one of them being the waves generated as a result of cosmological phase transitions.

1.1 First-order cosmological phase transitions

At the end of the inflationary epoch, about 10^{-12} seconds after the Big Bang singularity, the universe was filled with plasma consisting of quarks and gluons [5]. During this period of time the energy content of the universe was dominated entirely by radiation and the Standard Model particles were moving at relativistic velocities. As a result of the expansion of the universe, the temperature fell and the universe cooled down. It is believed that at some stage this could have led to the occurrence of first-order cosmological phase transitions [6].

Cosmological phase transitions are like any other phase transitions but they take place on cosmological scales: Entire regions in the universe can transition from one phase to another extremely rapidly. The general mechanism behind this process can be described, for instance, by quantum field theories (QFTs) [7]. In a QFT each particle species is associated with its corresponding field. For the sake of simplicity, let's focus on a scalar field ϕ. The temperature T in the very early universe was extremely high, hence the effective potential of the scalar field $V(\phi, T)$ is symmetrical and has only one minimum [8]. Let's choose the axes so that the minimum is at $\phi = 0$. In a first-order phase transition a new local minimum develops at some value $\phi > 0$ as the temperature decreases. The minimum at $\phi = 0$ is the global minimum – called the true vacuum state – and the other minimum is called the false vacuum state. The value of the field ϕ in the lowest energy state, which is the true vacuum, is called the vacuum expectation value (VEV).

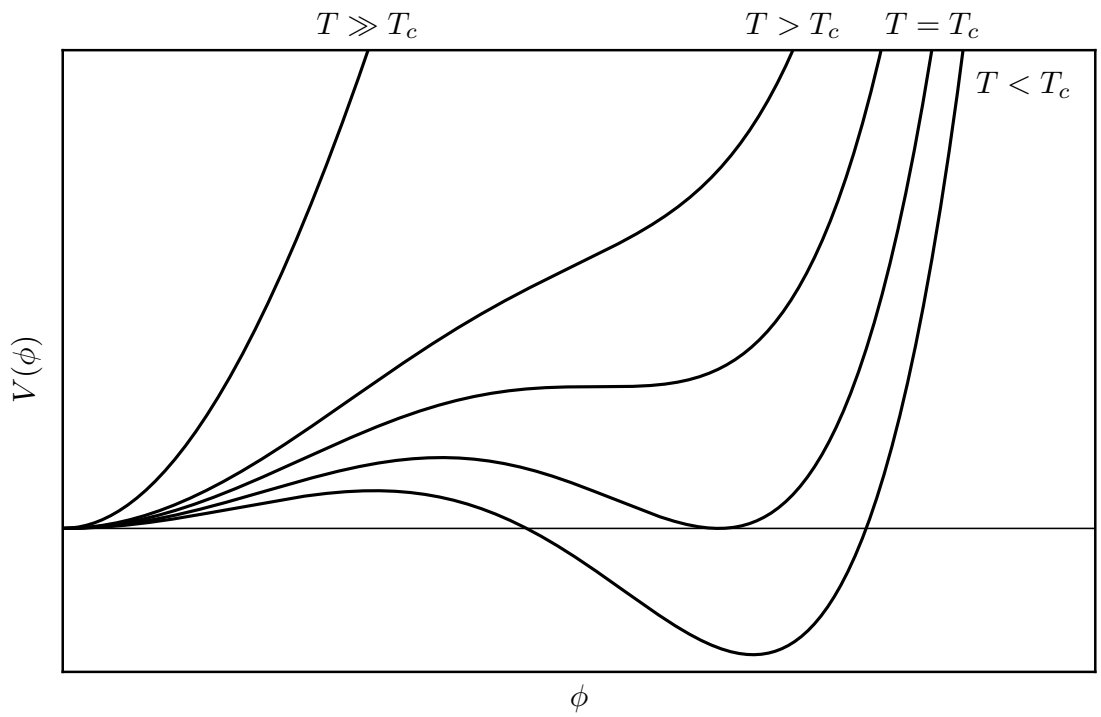

Figure 1.1: The effective potential $V(\phi, T)$ for a first-order phase transition.

As the temperature falls, the shape of the effective potential changes and at some point $V(\phi, T)$ has the same value in both minima. This occurs at the so-called critical temperature T_c. As the temperature falls further, the minimum that was previously the false vacuum state becomes the true vacuum state and, as a result, the value of the VEV changes. The system has moved from the symmetric phase to the broken phase. The scalar field ϕ would like to transition to the new true vacuum state but is unable to do that because of the potential barrier separating the two minima. It is said that ϕ is in a metastable state. The field can get over the barrier in one of two ways, either by quantum mechanical tunneling or by thermal fluctuations [9]. Both of these events are of a random nature, and therefore take place in different parts of the universe at different times. When the field crosses the barrier, the first-order phase transition starts to proceed by nucleation and expansion of a bubble. The mechanism described above is only a toy model but it describes

the general features of first-order phase transitions. They are predicted by many scenarios beyond the Standard Model of particle physics [6].

A bubble is a field configuration, where the bubble wall acts as a phase boundary. Inside the bubble the field has moved to the new true vacuum state and that part of the universe now consists of the new low-temperature broken phase. If the nucleated bubble is large enough, it starts to expand due to a pressure difference between the phases [10]. The expanding bubble converts the old phase into the new low-temperature phase as the phase transition proceeds. The friction between the plasma and the bubble wall slows down the expansion until it reaches constant velocity. It may also be possible under certain circumstances that the bubble wall accelerates without bound, approaching the speed of light. These are known as runaway bubbles [11, 12]. From hydrodynamics one can derive two steady state solutions for the propagation of the phase boundary. In the case of a detonation front, the speed of the phase boundary exceeds the sound speed in the plasma and a rarefaction wave is formed behind it. In the opposite case we have a deflagration front and a shock is formed in front of the bubble wall [13].

After the temperature has fallen low enough that the phase transition begins, bubbles are nucleated and begin to expand all over the universe. An isolated spherical bubble doesn't source any gravitational waves by itself [14]. Instead, gravitational waves are generated when bubbles collide. Collisions can lead to three different sources for gravitational waves [6], the first being gravitational waves generated from the collisions themselves and the resulting shocks in the plasma. Some GWs are also generated from the sound waves that are present in the plasma after the collision. Lastly, there are GWs sourced by turbulence that forms in the plasma after the collision. The gravitational wave background consists of the linear combination of these three contributions, the one featured in this thesis being the one from turbulence. Alongside the turbulent motions, some GWs may also be gen-

erated by the magnetic fields arising from the turbulent dynamo mechanism. We will ignore this so called magnetohydrodynamic turbulence, since its contribution is small compared to regular fluid turbulence [15].

The collision speed is an important aspect when considering the resulting gravitational wave spectrum. Generally, higher velocities lead to stronger gravitational waves [16]. In most models the phase boundaries are assumed to be detonation fronts because it is believed that due to the strength of the electroweak phase transition, the bubble walls can be highly relativistic [17]. If this is indeed the case, the gravitational wave spectrum from first order cosmological phase transitions could be detectable by the LISA (Laser Interferometer Space Antenna) space observatory, which is supposed to be launched into space sometime in the 2030s [6, 18].

1.2 Conventions

Natural units are used throughout this thesis, so that $c = \hbar = k_B = 1$. We also take the signature of the metric to be $(-,+,+,+)$. Then the matrix representation of the Minkowski tensor describing flat spacetime takes the form

$$\eta = \begin{pmatrix} -1 & 0 & 0 & 0 \\ 0 & 1 & 0 & 0 \\ 0 & 0 & 1 & 0 \\ 0 & 0 & 0 & 1 \end{pmatrix}. \tag{1.1}$$

As for indices, the Einstein notation is used meaning that repeated indices are implicitly summed over. Vectors are denoted by boldface letters ($\mathbf{v}$) and their components by subscript indices (v_i). Latin indices contain the spatial components and run from 1 to 3, whereas greek indices run from 0 to 3 and also contain the zeroth temporal component.

The Fourier transform convention used is

$$f(\mathbf{k}) = \int f(\mathbf{x}) e^{-i\mathbf{k}\cdot\mathbf{x}}\, d^3x, \qquad f(\mathbf{x}) = \frac{1}{(2\pi)^3} \int f(\mathbf{k}) e^{i\mathbf{k}\cdot\mathbf{x}}\, d^3k, \tag{1.2}$$

where $\mathbf{k}$ is the wave vector and $k = |\mathbf{k}|$ is the wavenumber. The Laplace transform is defined by

$$F(s) = \int_0^\infty f(t) e^{-st}\, dt. \tag{1.3}$$

Other commonly used functions are the Kronecker delta

$$\delta_{ij} = \begin{cases} 0 & \text{if } i \neq j \\ 1 & \text{if } i = j \end{cases}, \tag{1.4}$$

Heaviside step function

$$\theta(x) = \begin{cases} 0 & \text{if } x < 0 \\ 1 & \text{if } x \geq 0 \end{cases} \tag{1.5}$$

and the Dirac delta function

$$\delta(\mathbf{x}) = \frac{1}{(2\pi)^3} \int e^{i\mathbf{k}\cdot\mathbf{x}} d^3k, \tag{1.6}$$

which has the useful property

$$\int f(\mathbf{x})\, \delta(\mathbf{x} - \mathbf{x}')\, d^3x = f(\mathbf{x}') \tag{1.7}$$

A list of (some of the) symbols appearing in the following chapters contains:

$\bar{a}, \langle a \rangle$	Average value
$\hat{\mathbf{a}}$	unit vector
$\dot{f} = \partial_t = \frac{\partial f}{\partial t}$	Time derivative
$\nabla^2 = \nabla \cdot \nabla = \partial_i \partial_i$	Laplace operator
$\mathbf{u}, \mathbf{v}$	Velocity
ρ	Density (Chapter 2), Energy density (Chapters 3, 4 & 5)
p	Pressure
ν	Viscosity
ϵ	Viscous dissipation
Q_{ij}	Second order correlation tensor
S_{ikj}	Third order correlation tensor
$E(k)$	Energy spectrum of turbulence
$P(k)$	Power spectrum of turbulence
$P_{ij}(\hat{\mathbf{k}}) = \delta_{ij} - \hat{k}_i \hat{k}_j$	Transverse projector operator
$F(k)$	Energy transfer spectrum function
L	Length scale
τ_L	Eddy turnover time on scale L
k_d, k_e	Dissipation-, integral scale
$h_{\mu\nu}$	Metric tensor perturbation
a	Scale factor
$H = \dot{a}/a$	Hubble parameter
h	Reduced Hubble parameter
$T^{\mu\nu}$	Energy-momentum tensor
G	Universal gravitational constant
$\Pi_{ij}(\mathbf{k}, t)$	Transverse and traceless piece of the energy-momentum tensor in Fourier space
$e^{+}_{ij}(\hat{\mathbf{k}}), e^{\times}_{ij}(\hat{\mathbf{k}})$	Polarization tensors
$w = p + \rho$	Enthalpy density
η	Conformal time
$G(x, y)$	Green's function

$\Omega_{\rm GW}$	Spectrum of energy density per logarithmic frequency interval
f	Frequency
ρ_c	Critical density
h_c	Characteristic amplitude
S_h	Spectral density
$\Pi(k,t,t')$	Unequal-time correlator of the tensor-type anisotropic stress (Chapter 3)
T	Temperature
g_{*S}	Number of degrees of freedom associated with entropy
g_*	Number of relativistic degrees of freedom
$m_{\rm Pl}$	Planck mass
$\gamma = \dfrac{1}{\sqrt{1-v^2}}$	Lorentz factor
Γ	Bubble nucleation rate
β	Duration of the phase transition (Chapter 3)
α	Strength of the phase transition (Chapter 3)
v_w	Bubble wall speed
c_s	Speed of sound
$\delta p, \delta\rho$	Pressure, density perturbation
$\delta = \dfrac{\delta\rho}{\rho_0}$	Fractional density perturbation
ϕ	Velocity potential
$\chi = \dfrac{a_0}{a}\mathbf{r}$	Comoving coordinates
$u = x - c_s t$	Coordinates, where left-moving waves travelling at the speed c_s remain stationary
$v = x + c_s t$	Coordinates, where right-moving waves travelling at the speed c_s remain stationary
$\Pi = \dfrac{T^{01}}{\widetilde{T}^{00}}$	Normalized momentum density (Chapters 4 & 5)
$\kappa = \dfrac{2c_s(1+c_s^2)}{1-c_s^2}$	Factor appearing in Burgers' equation

1.3 Outline

Chapter 2 contains basic information about classical fluid turbulence and shows how the equations for turbulent velocity fluctuations arise from averaging the Navier-Stokes equation. The focus is primarily on the simplest possible case of statistically isotropic, homogeneous and stationary turbulence and concepts such as energy cascade, energy spectrum and Kolmogorov turbulence are introduced.

In Chapter 3 the gravitational wave equation is solved for a general stochastic source acting under a FLRW background. The main properties of cosmological turbulence resulting from a first order phase transition are presented and the calculation of the GW spectrum is explained for a specific model of turbulence. It is also briefly mentioned how the quantities characterizing turbulence can be related to those characterizing the phase transition. At the end of the chapter the history of the study of GWs from cosmological turbulence is introduced by looking at what has been done so far and highlighting some of the main differences between the models.

Chapter 4 explains how small amplitude waves in the early universe steepen and form shocks, whose interaction in turn causes vorticity and generates turbulence in the plasma. The relativistic fluid equations for a perfect fluid are expanded to second order in perturbation theory, and when considering only right-moving waves, Burgers' equation is obtained. It is solved using the method of characteristics and analysis gives the time scale for shock formation.

Finally in Chapter 5 Burgers' equation is simulated numerically. The solutions are given random initial conditions by defining an initial power spectrum and giving its amplitude spectrum random phases. The waves are simulated until the moment of shock formation and the corresponding power spectra are calculated and plotted on a log-log scale to see the emergence of possible power laws. A dissipative term

is also introduced to Burgers' equation and the same procedure is repeated in this case as well.

2. Turbulence

2.1 Introduction to turbulent flow

Turbulence occurs all over nature. The winds gusting outside, the currents in oceans, solar flares on the surface of the Sun and convection in the core of the Earth, which maintains its magnetic field, are all examples of turbulent flows. Turbulence also plays a large role in engineering. When designing planes, race cars or skyscrapers, it's necessary to understand and to be able to model the effects of turbulence. In fact, the majority of fluid flows are turbulent and so it can even be described as the natural state of most fluids. Regardless of its ubiquitous nature, turbulence remains the last major unsolved problem of classical physics and one of the six remaining unsolved Millenium Prize problems in mathematics [19].

A flow that is smooth and regular is called a laminar flow. The transition from laminar to turbulent flow takes place when the characteristic speed crosses a certain threshold, assuming the fluid has a sufficiently low viscosity. The quantity that is used to predict the type of flow is called the Reynolds number, whose low values correspond to laminar flows and high values to turbulent flows. As the flow becomes turbulent, eddies, which are swirls in the fluid, begin to emerge. Fully developed turbulence can be described to consist of the superposition of eddies of different sizes. This leads the to concept of scale, which is a profound feature of turbulence. The largest eddies are comparable with the geometric length scale of

the mean flow. Eddies break up into smaller eddies after some time, which in turn break up into ever smaller eddies. This goes on so that eventually a wide range of eddies of different scales exist in fully-developed high Reynolds number turbulence.

The lifespan of an eddy is of the order of its turn-over time, which can be estimated as l/u, where l is the scale and u is the velocity of the fluid. Every eddy has a certain kinetic energy that depends on its vorticity, which is passed onto the smaller eddies upon the moment of breaking down. This results in a transfer of kinetic energy all the way from the largest scales of the flow to the smallest ones, which is referred to by the name energy cascade. The strong diffusive nature of turbulence results from this property. Another important physical phenomenon associated with turbulence is the dissipation of kinetic energy. At the smallest scales the velocity gradients in the eddies grow so large that kinetic energy is converted into heat by viscosity effects that counteract the eddying motion. Therefore the lower limit of the eddies is determined by the viscosity of the fluid and the velocity of the mean flow.

One of the defining characteristics of turbulence is its irregularity. It can be described as a chaotic process, meaning that a small change in the initial conditions will lead to a large change at a later time. Because of this behaviour, it's impossible to describe the motion as a function of time and space coordinates. Hence the only way to get some useful results is to study the statistical properties of turbulence. We write the momentary value of the velocity in the form

$$U(\mathbf{x}, t) = \bar{U}(\mathbf{x}) + u(\mathbf{x}, t), \tag{2.1}$$

where the overbar denotes average value. The first term on the right-hand side of the equation is the smooth laminar component and the latter is the fluctuating turbulent component. We also define the average value as a time average of the

form

$$\bar{U} = \frac{1}{T}\int_0^T U(t+\tau)\,d\tau \tag{2.2}$$

where T is a sufficiently large time interval compared to the time scale of the turbulence [20]. It is assumed that this definition for the average applies to any quantity. By taking the average of equation (2.1), we get by definition $\bar{\bar{U}} = \bar{U}$ and $\bar{u} = 0$.

The equations of motion for a viscous fluid are the Navier-Stokes equations. Here we make the assumptions of constant viscosity and incompressible fluid, meaning the density of the fluid is constant along the flow. In this case the Navier-Stokes equations can be written in the form [21]

$$\frac{D\mathbf{U}}{Dt} = -\frac{1}{\rho}\nabla p + \nu\nabla^2\mathbf{U}. \tag{2.3}$$

Here

$$\frac{D}{Dt} = \frac{\partial}{\partial t} + \mathbf{U}\cdot\nabla, \tag{2.4}$$

which is the convective derivative describing the acceleration of a fluid element, ρ is the density of the fluid, p is the pressure and ν is the viscosity. Additionally, we have the continuity equation

$$\frac{\partial\rho}{\partial t} + \nabla\cdot(\rho\mathbf{U}) = 0, \tag{2.5}$$

that governs the conservation of mass in the system. In the case of an incompressible fluid this reduces to

$$\nabla\cdot\mathbf{U} = \frac{\partial U_i}{\partial x_i} = 0. \tag{2.6}$$

The equation (2.3) is nonlinear, which makes it difficult to solve. In fact, the turbulent behaviour transpires because of this nonlinearity. The above equations apply also in nonturbulent cases, so in order to see the turbulent terms explicitly, the equations need to be written in terms of the turbulent quantities and averaged. We write $U_i = \bar{U}_i + u_i$ and $p = \bar{p} + \tilde{p}$, insert them into (2.3) and then average both sides

of the equation. Note that (2.3) can be written in index form as

$$\frac{\partial U_i}{\partial t} + U_j \frac{\partial U_i}{\partial x_j} = -\frac{1}{\rho}\frac{\partial p}{\partial x_i} + \nu \frac{\partial^2 U_i}{\partial x_j \partial x_j}. \tag{2.7}$$

After substitution the left-hand side yields

$$\begin{aligned}
\overline{\frac{DU_i}{Dt}} &= \frac{\partial}{\partial t}\overline{\bar{U}_i + u_i} + \overline{\left(\bar{U}_j + u_j\right)\frac{\partial}{\partial x_j}\left(\bar{U}_i + u_i\right)} \\
&= \frac{\partial}{\partial t}\left(\bar{\bar{U}}_i + \underbrace{\bar{u}_i}_{=0}\right) + \overline{\bar{U}_j \frac{\partial \bar{U}_i}{\partial x_j}} + \overline{\bar{U}_j \frac{\partial u_i}{\partial x_j}} + \overline{u_j \frac{\partial \bar{U}_i}{\partial x_j}} + \overline{u_j \frac{\partial u_i}{\partial x_j}} \\
&= \frac{\partial \bar{U}_i}{\partial t} + \bar{U}_j \frac{\partial \bar{U}_i}{\partial x_j} + \bar{U}_j \frac{\partial \bar{u}_i}{\partial x_j} + \bar{u}_j \frac{\partial \bar{U}_i}{\partial x_j} + \overline{u_j \frac{\partial u_i}{\partial x_j}} \\
&= \frac{\partial \bar{U}_i}{\partial t} + \bar{U}_j \frac{\partial \bar{U}_i}{\partial x_j} + \overline{u_j \frac{\partial u_i}{\partial x_j}}.
\end{aligned} \tag{2.8}$$

Performing the same procedure to the right-hand side is much simpler and in the end we end up with

$$\frac{\partial \bar{U}_i}{\partial t} + \bar{U}_j \frac{\partial \bar{U}_i}{\partial x_j} = -\frac{1}{\rho}\frac{\partial \bar{p}}{\partial x_i} + \nu \frac{\partial^2 \bar{U}_i}{\partial x_j \partial x_j} + \overline{u_j \frac{\partial u_i}{\partial x_j}}. \tag{2.9}$$

When this is compared with (2.3), we see that the mean quantities follow a similar equation, but the nonlinear term has given a contribution which involves the turbulent velocity fluctuations. Averaging the continuity equation (2.6) results in

$$\frac{\partial \bar{U}_i}{\partial x_i} = 0, \qquad \frac{\partial u_i}{\partial x_i} = 0, \tag{2.10}$$

so by adding $\overline{u_i \partial u_j / \partial x_j} = 0$ to the right-hand side of (2.9) and by multiplying both sides by ρ, we find

$$\rho\left(\frac{\partial \bar{U}_i}{\partial t} + \bar{U}_j \frac{\partial \bar{U}_i}{\partial x_j}\right) = -\frac{\partial \bar{p}}{\partial x_i} + \frac{\partial}{\partial x_j}\left(\rho\nu \frac{\partial \bar{U}_i}{\partial x_j} + \rho\overline{u_i u_j}\right). \tag{2.11}$$

The terms on the right-hand side can be interpreted as stresses, hence we can see that in addition to the stresses by pressure and the viscous stresses, we now have the turbulent stresses $\rho\overline{u_i u_j}$, which are known as Reynolds stresses [20]. These quantities are as of yet not known and if one tries to derive more equations relating

these variables, more statistical unknowns appear. Therefore the system of equations is not closed and there always exists more unknowns than equations relating them. This is known as the closure problem of turbulence and is the reason why no rigorous statistical theories of turbulence exist [21].

The Navier-Stokes equations can also be used to examine the change of energy in turbulent flows. In order to get a kinetic energy term, we take a dot product $\mathbf{U}\cdot$ on both sides of (2.3), yielding

$$\begin{aligned}
\mathbf{U}\cdot\frac{D\mathbf{U}}{Dt} &= -\frac{1}{\rho}\mathbf{U}\cdot\nabla p+\nu\mathbf{U}\cdot\left(\nabla^2\mathbf{U}\right)+\left(\mathbf{U}\cdot\nabla\right)\left(\nabla\cdot\mathbf{U}\right)\\
\Rightarrow U_i\frac{DU_i}{Dt} &= -\frac{1}{\rho}U_j\frac{\partial p}{\partial x_j}+\nu U_i\frac{\partial^2 U_i}{\partial x_j\partial x_j}+U_i\frac{\partial^2 U_j}{\partial x_i\partial x_j}\\
\Rightarrow \frac{D}{Dt}\frac{U_iU_i}{2} &= -\frac{1}{\rho}U_j\frac{\partial p}{\partial x_j}+\nu U_i\frac{\partial}{\partial x_j}\left(\frac{\partial U_i}{\partial x_j}+\frac{\partial U_j}{\partial x_i}\right),
\end{aligned}\tag{2.12}$$

where we have added zero to the right-hand side of the equation with the help of equation (2.6). To separate the change of energy due to dissipation from the work done by viscous stresses, we massage the right-hand side a little by once again adding a zero

$$\begin{aligned}
&\nu U_i\frac{\partial}{\partial x_j}\left(\frac{\partial U_i}{\partial x_j}+\frac{\partial U_j}{\partial x_i}\right)+\underbrace{\nu\frac{\partial U_i}{\partial x_j}\left(\frac{\partial U_i}{\partial x_j}+\frac{\partial U_j}{\partial x_i}\right)-\nu\left(\frac{\partial U_i}{\partial x_j}+\frac{\partial U_j}{\partial x_i}\right)\frac{\partial U_i}{\partial x_j}}_{=0}\\
&=\nu\frac{\partial}{\partial x_j}U_i\left(\frac{\partial U_i}{\partial x_j}+\frac{\partial U_j}{\partial x_i}\right)-\nu\left(\frac{\partial U_i}{\partial x_j}+\frac{\partial U_j}{\partial x_i}\right)\frac{\partial U_i}{\partial x_j}.
\end{aligned}$$

Now by using the above equation with (2.4) and (2.6) we get

$$\begin{aligned}
\frac{\partial}{\partial t}\frac{U_iU_i}{2} = -\frac{\partial}{\partial x_j}U_j\left(\frac{p}{\rho}+\frac{U_iU_i}{2}\right)+\nu\frac{\partial}{\partial x_j}U_i\left(\frac{\partial U_i}{\partial x_j}+\frac{\partial U_j}{\partial x_i}\right)\\
-\nu\left(\frac{\partial U_i}{\partial x_j}+\frac{\partial U_j}{\partial x_i}\right)\frac{\partial U_i}{\partial x_j}.
\end{aligned}\tag{2.13}$$

This equation describes the local change of kinetic energy per unit mass and time. On the right-hand side, the first term is the work done by the total dynamic pressure, the term in the middle is the work done by the viscous stresses and lastly we have the dissipation term [20]. In order to get a similar equation in terms of turbulent

quantities, we again need to take time averages. We substitute $U_i = \bar{U}_i + u_i$, $p = \bar{p} + \tilde{p}$ and $U_i U_i = \bar{U}_i \bar{U}_i + 2\bar{U}_i u_i + u_i u_i$ and average both sides of Eq. (2.13). When the dust settles, we get

$$\begin{aligned}\frac{\partial}{\partial t}\frac{\bar{U}_i\bar{U}_i}{2} + \frac{\partial}{\partial t}\frac{\overline{u_i u_i}}{2} = &-\frac{\partial}{\partial x_j}\bar{U}_j\left(\frac{\bar{p}}{\rho} + \frac{\bar{U}_i\bar{U}_i}{2}\right) - \frac{\partial}{\partial x_j}\frac{\overline{u_j\tilde{p}}}{\rho} - \frac{\partial}{\partial x_j}\frac{\overline{u_j u_i u_i}}{2} - \frac{1}{2}\frac{\partial}{\partial x_j}\bar{U}_j\overline{u_i u_i} \\ &- \frac{\partial}{\partial x_j}\bar{U}_i\overline{u_i u_j} + \nu\frac{\partial}{\partial x_j}\bar{U}_i\left(\frac{\partial\bar{U}_i}{\partial x_j} + \frac{\partial\bar{U}_j}{\partial x_i}\right) + \nu\frac{\partial}{\partial x_j}\overline{u_i\left(\frac{\partial u_i}{\partial x_j} + \frac{\partial u_j}{\partial x_i}\right)} \\ &- \nu\left(\frac{\partial\bar{U}_i}{\partial x_j} + \frac{\partial\bar{U}_j}{\partial x_i}\right)\frac{\partial\bar{U}_i}{\partial x_j} - \nu\overline{\left(\frac{\partial u_i}{\partial x_j} + \frac{\partial u_j}{\partial x_i}\right)\frac{\partial u_i}{\partial x_j}}.\end{aligned} \tag{2.14}$$

To get rid of the mean flow terms, similar massaging can be done to (2.9), as was done in order to reach equation (2.12). After contracting it with U_i and modifying the last two terms, it can be written in the form

$$\begin{aligned}\frac{\partial}{\partial t}\frac{\bar{U}_i\bar{U}_i}{2} = &-\frac{\partial}{\partial x_j}\bar{U}_j\left(\frac{\bar{p}}{\rho} + \frac{\bar{U}_i\bar{U}_i}{2}\right) + \overline{u_i u_j}\frac{\partial\bar{U}_i}{\partial x_j} - \frac{\partial}{\partial x_j}\bar{U}_i\overline{u_i u_j} \\ &+ \nu\frac{\partial}{\partial x_j}\bar{U}_i\left(\frac{\partial\bar{U}_i}{\partial x_j} + \frac{\partial\bar{U}_j}{\partial x_i}\right) - \nu\left(\frac{\partial\bar{U}_i}{\partial x_j} + \frac{\partial\bar{U}_j}{\partial x_i}\right).\end{aligned} \tag{2.15}$$

Subtracting this from (2.14) and rearranging some of the terms leads us to the turbulence energy equation

$$\begin{aligned}\underbrace{\frac{D}{Dt}\frac{\overline{u_i u_i}}{2}}_{(1)} = &\underbrace{-\frac{\partial}{\partial x_j}\overline{u_j\left(\frac{\tilde{p}}{\rho} + \frac{u_i u_i}{2}\right)}}_{(2)} \underbrace{-\overline{u_i u_j}\frac{\partial\bar{U}_i}{\partial x_j}}_{(3)} + \underbrace{\nu\frac{\partial}{\partial x_j}\overline{u_i\left(\frac{\partial u_i}{\partial x_j} + \frac{\partial u_j}{\partial x_i}\right)}}_{(4)} \\ &\underbrace{- \nu\overline{\left(\frac{\partial u_i}{\partial x_j} + \frac{\partial u_j}{\partial x_i}\right)\frac{\partial u_i}{\partial x_j}}}_{\equiv\epsilon \quad (5)}.\end{aligned} \tag{2.16}$$

Here the terms can be given the following physical interpretations [20]:

(1) The change of kinetic energy of turbulence including the convective transport term.

(2) The work by the total dynamic pressure of turbulence.

(3) The work of deformation of the mean motion by the turbulence shear stresses.

(4) The work by the viscous shear stresses of turbulence.

(5) The viscous dissipation by turbulence, denoted ϵ

All of these quantities are per unit of mass and time. Term (3) usually has a positive sign and is also known as the turbulence production term as it extracts energy from the mean motion and transfers it to the turbulent motion.

2.2 Isotropic turbulence

From now on we discuss the simplest possible case of turbulence. We assume the turbulence to be homogeneous, stationary and isotropic. Homogeneity means that the statistical properties of turbulence do not change with spatial translations, that is, they don't change with position. In stationary turbulence the statistics are independent of the origin of time and statistical parameters, such as mean and variance, are independent of time. From this it also follows that correlators are functions of time differences. Finally, isotropic turbulence is independent of rotations and reflections. Actual turbulent flows fulfil none of these assumptions, so this case is only hypothetical. Regardless, this type of turbulence is the most treated one both theoretically and experimentally due to its simplicity, and is also used in almost all of the cosmological models regarding gravitational wave generation from turbulence. It still gives valuable knowledge about the theoretical framework of turbulence and acts as a basis for more complicated models.

In order to study the statistical behaviour of turbulence, we need to study correlations between velocity fluctuations of different points in the flow field. To this end, we shall convert the Navier-Stokes equation into an evolution equation for the velocity correlation functions. Let A and B be two points in the flow field. When

we plug $\bar{U}_i = \bar{U}_i + u_i(x,t)$ into the Navier-Stokes equation (2.3), we get at point A

$$\left[\frac{\partial}{\partial t}u_i + \left(\bar{U}_k + u_k\right)\frac{\partial u_i}{\partial x_k} = -\frac{1}{\rho}\frac{\partial p}{\partial x_i} + \nu\frac{\partial^2 u_i}{\partial x_k \partial x_k}\right]_A . \tag{2.17}$$

From here on out we don't write down the time dependence of u explicitly to keep the notation compact. It is however good to keep in mind that all quantities containing u are still dependent on time. After multiplying (2.17) by $(u_j)_B$ and taking into account that derivatives at point A only operate on quantities at that point, the equation gives

$$\begin{aligned}(u_j)_B\frac{\partial}{\partial t}(u_i)_A + \left[\bar{U}_k + (u_k)_A\right]\left(\frac{\partial}{\partial x_k}\right)_A (u_i)_A(u_j)_B = -\frac{1}{\rho}\left(\frac{\partial}{\partial x_i}\right)_A p_A(u_j)_B \\ + \nu\left(\frac{\partial^2}{\partial x_k \partial x_k}\right)_A (u_i)_A(u_j)_B.\end{aligned} \tag{2.18}$$

We can also multiply the equation at point B by $(u_i)_A$ and we get the same equation but with AB and ij interchanged. Next we add these two equations together, use the continuity condition (2.10) and take the time average on both sides to obtain

$$\begin{aligned}&\frac{\partial}{\partial t}\overline{(u_i)_A(u_j)_B} + \left[\left(\frac{\partial}{\partial x_k}\right)_A \overline{(u_i)_A(u_k)_A(u_j)_B} + \left(\frac{\partial}{\partial x_k}\right)_B \overline{(u_i)_A(u_k)_B(u_j)_B}\right] \\ &\quad + \bar{U}_k\left[\left(\frac{\partial}{\partial x_k}\right)_A \overline{(u_i)_A(u_j)_B} + \left(\frac{\partial}{\partial x_k}\right)_B \overline{(u_i)_A(u_j)_B}\right] \\ &\quad = -\frac{1}{\rho}\left[\left(\frac{\partial}{\partial x_i}\right)_A \overline{p_A(u_j)_B} + \left(\frac{\partial}{\partial x_j}\right)_B \overline{p_B(u_i)_A}\right] \\ &\quad + \nu\left[\left(\frac{\partial^2}{\partial x_k \partial x_k}\right)_A + \left(\frac{\partial^2}{\partial x_k \partial x_k}\right)_B\right]\overline{(u_i)_A(u_j)_B}.\end{aligned} \tag{2.19}$$

It can be shown that in the case of isotropic turbulence $\overline{p_A(u_j)_B} = \overline{p_B(u_i)_A} = 0$. Due to isotropy, the quantities cannot depend on any direction, hence the only vector that can appear in the expressions is the radius vector $\mathbf{r}$. Then $\overline{p_A(u_j)_B}$ is of the form $f(r)\hat{\mathbf{r}}$ and the continuity equation (2.10) requires the divergence to be zero. Writing the divergence in spherical coordinates and solving the resulting differential equation gives $f(r) = (\text{constant})/r^2$, which does not stay finite at $r = 0$ and thus the constant must be zero, proving the statement $\overline{p_A(u_j)_B} = 0$. We shall also conduct a

change of variables of the form $r_k = (x_k)_B - (x_k)_A$, which leads to

$$\left(\frac{\partial}{\partial x_k}\right)_A = \frac{\partial r_k}{\partial (x_k)_A}\frac{\partial}{\partial r_k} = -\frac{\partial}{\partial r_k} \qquad \left(\frac{\partial}{\partial x_k}\right)_B = \frac{\partial r_k}{\partial (x_k)_B}\frac{\partial}{\partial r_k} = \frac{\partial}{\partial r_k}$$

$$\left(\frac{\partial^2}{\partial x_k \partial x_k}\right)_A = \left(\frac{\partial^2}{\partial x_k \partial x_k}\right)_B = \frac{\partial^2}{\partial r_k \partial r_k}$$

and (2.19) becomes

$$\frac{\partial}{\partial t}\overline{(u_i)_A (u_j)_B} - \frac{\partial}{\partial r_k}\overline{(u_i)_A (u_k)_A (u_j)_B} + \frac{\partial}{\partial r_k}\overline{(u_i)_A (u_k)_B (u_j)_B} = 2\nu \frac{\partial^2}{\partial r_k \partial r_k}\overline{(u_i)_A (u_j)_B}. \quad (2.20)$$

We now define the second and third order correlation tensors

$$Q_{i,j} = \overline{(u_i)_A (u_j)_B} \qquad S_{ik,j} = \overline{(u_i)_A (u_k)_A (u_j)_B}, \quad (2.21)$$

and reflectional invariance gives $S_{i,kj} = -S_{kj,i}$, which leads to

$$\frac{\partial}{\partial t} Q_{i,j} = \frac{\partial}{\partial r_k}\left(S_{ik,j} + S_{kj,i}\right) + 2\nu \frac{\partial^2}{\partial r_k \partial r_k} Q_{i,j}. \quad (2.22)$$

Now that the notationally intricate part is behind us, we start to denote the average value in a more explicit way that is often used in statistical physics

$$Q_{i,j}(\mathbf{r}) = \overline{(u_i)_A (u_j)_B} \equiv \langle u_i(\mathbf{x}_A) u_j(\underbrace{\mathbf{x}_A + \mathbf{r}}_{=\mathbf{x}_B}) \rangle \equiv \langle u_i(\mathbf{x}) u_j(\mathbf{x} + \mathbf{r}) \rangle , \quad (2.23)$$

where the independence of $\mathbf{x}$ follows from the definition of homogeneous turbulence. From the continuity equation (2.10) it follows that

$$\frac{\partial Q_{i,j}}{\partial r_i} = \frac{\partial Q_{i,j}}{\partial r_j} = 0, \qquad \frac{\partial S_{ik,j}}{\partial r_j} = 0 \quad (2.24)$$

and another important relation is

$$\frac{1}{2} Q_{i,i}(0) = \frac{\overline{u_i u_i}}{2} \equiv \frac{1}{2}\left\langle \mathbf{u}^2 \right\rangle , \quad (2.25)$$

which is the kinetic energy of turbulence per unit of mass. In the isotropic and homogeneous case, $\bar{U}_i$ is constant in time and space, and all spatial derivatives of

local mean turbulent quantities vanish, so the turbulence energy equation (2.16) reduces to

$$\frac{\partial}{\partial t}\frac{\langle \mathbf{u}^2 \rangle}{2} = -\epsilon. \tag{2.26}$$

Hence, the change of turbulent kinetic energy equals the viscous dissipation and the turbulent flow is a decaying one [20].

2.3 Energy spectrum

An important tool in analysing the statistical theory of turbulence is the Fourier transform, for it can be used to determine how the kinetic energy of turbulence will be distributed across the different eddy sizes, each corresponding to a certain frequency in the Fourier space. Such a distribution is called the energy spectrum, and due to its importance, the Fourier representation can be said to be the natural language of isotropic homogeneous turbulence. To begin with, we define the three-dimensional Fourier transforms of the velocity correlation functions as

$$Q_{i,j}(\mathbf{k}) = \int Q_{i,j}(\mathbf{r}) e^{-i\mathbf{k}\cdot\mathbf{r}}\, d^3x, \qquad Q_{i,j}(\mathbf{r}) = \frac{1}{(2\pi)^3}\int Q_{i,j}(\mathbf{k}) e^{i\mathbf{k}\cdot\mathbf{r}}\, d^3k \tag{2.27}$$

$$S_{ik,j}(\mathbf{k}) = \int S_{ik,j}(\mathbf{r}) e^{-i\mathbf{k}\cdot\mathbf{r}}\, d^3x, \qquad S_{ik,j}(\mathbf{r}) = \frac{1}{(2\pi)^3}\int S_{ik,j}(\mathbf{k}) e^{i\mathbf{k}\cdot\mathbf{r}}\, d^3k, \tag{2.28}$$

where $\mathbf{k}$ is the three-dimensional wave vector. In isotropic and homogeneous turbulence $Q_{i,j}(\mathbf{r}) = Q_{i,j}(-\mathbf{r})$ and as a result $Q_{i,j}(\mathbf{k}) = Q_{i,j}(-\mathbf{k}) = Q^*_{i,j}(\mathbf{k})$, which means the functions $Q_{i,j}(\mathbf{k})$ are real. From (2.25) and (2.27) we get the relation

$$\frac{1}{2}Q_{i,i}(0) = \frac{1}{2}\left\langle \mathbf{u}^2 \right\rangle = \frac{1}{16\pi^3}\int Q_{i,i}(\mathbf{k})\, d^3k. \tag{2.29}$$

In spherical coordinates the volume element is $d^3k = k^2 \sin(\theta)\, dk\, d\theta\, d\phi$, and since the velocity correlations are independent of angles, the angular integrals give 4π, which leads to

$$\frac{1}{2}\left\langle \mathbf{u}^2 \right\rangle = \int_0^\infty \frac{1}{4\pi^2} k^2 Q_{i,i}(k)\, dk. \tag{2.30}$$

It is now apparent that $Q_{i,i}(k)$ represents the spectral density of the kinetic energy per unit mass in k-space. We define the three-dimensional energy spectrum as

$$E(k) = \frac{1}{4\pi^2} k^2 Q_{i,i}(k), \tag{2.31}$$

so (2.30) becomes

$$\frac{1}{2}\left\langle \mathbf{u}^2 \right\rangle = \int_0^\infty E(k)\, dk, \tag{2.32}$$

where $E(k)\, dk$ is the energy in the fluctuations whose wavenumber is in the range $[k, k + dk]$.

We may also use the Fourier transforms to transfer the equation (2.22) into Fourier space. Plugging in the inverse transforms of the velocity correlations and calculating the derivatives yields

$$\begin{aligned} \frac{1}{(2\pi)^3}\int \left[\frac{\partial}{\partial t} Q_{i,j}(\mathbf{k}) - ik_k \left[S_{ik,j}(\mathbf{k}) + S_{kj,i}(\mathbf{k})\right] - 2\nu i^2 k_k k_k Q_{i,j}(\mathbf{k})\right] e^{i\mathbf{k}\cdot\mathbf{r}}\, d^3k = 0 \\ \Rightarrow \frac{\partial}{\partial t} Q_{i,j}(\mathbf{k}) = ik_k \left[S_{ik,j}(\mathbf{k}) + S_{kj,i}(\mathbf{k})\right] - 2\nu k^2 Q_{i,j}(\mathbf{k}). \end{aligned} \tag{2.33}$$

The tensor structure can be extracted from the above equation by applying the properties of isotropy. The general structure of an isotropic tensor of rank two can be shown to be [20]

$$Q_{i,j}(\mathbf{k}) = A(k)\delta_{ij} + B(k)k_i k_j, \tag{2.34}$$

where A and B are even functions of k. Inserting the inverse Fourier transforms of the correlations into the continuity equation (2.24) allows us to write it in the Fourier space as

$$k_i Q_{i,j}(\mathbf{k}) = k_j Q_{i,j}(\mathbf{k}) = 0, \qquad k_j S_{ik,j}(\mathbf{k}) = 0. \tag{2.35}$$

This condition requires

$$\left(A + Bk^2\right) k_j = 0 \tag{2.36}$$

and we can replace B in (2.34) to find

$$Q_{i,j}(\mathbf{k}) = A(k)\left(\delta_{ij} - \frac{k_i k_j}{k^2}\right) \equiv P(k) P_{ij}(\hat{\mathbf{k}}), \tag{2.37}$$

where we have just renamed the function A and defined the projector

$$P_{ij}(\hat{\mathbf{k}}) = \delta_{ij} - \frac{k_i k_j}{k^2} = \delta_{ij} - \hat{k}_i \hat{k}_j. \tag{2.38}$$

The same procedure can be performed in the case of the rank three velocity correlations. The general expression for an isotropic tensor of the third order is [20]

$$S_{ik,j}(\mathbf{k}) = A(k) k_i k_k k_j + B(k) k_j \delta_{ik} + C(k) \left(k_k \delta_{ij} + k_i \delta_{kj}\right). \tag{2.39}$$

Substitution into (2.35) gives

$$B\delta_{ik} = -\frac{k_i k_k}{k^2} \left(Ak^2 + 2C\right) \tag{2.40}$$

and when this is used to replace $B(k)$ in (2.39), the terms with $A(k)$ cancel and we are left with

$$S_{ik,j}(\mathbf{k}) = iF(k) \left(k_k \delta_{ij} + k_i \delta_{kj} - 2k_i k_k k_j / k^2\right), \tag{2.41}$$

where we have put $C(k) \equiv iF(k)$. The imaginary unit has been included because $S_{ik,j}(\mathbf{k})$ are imaginary[1] so the inclusion makes the function $F(k)$ real. After a straightforward calculation we have

$$ik_k \left[S_{ik,j}(\mathbf{k}) + S_{kj,i}(\mathbf{k})\right] = -2F(k) \left(k^2 \delta_{ij} - k_i k_j\right) = -2k^2 F(k) P_{ij}(\hat{\mathbf{k}}). \tag{2.42}$$

We are now ready to substitute equations (2.37) and (2.42) into (2.33), and since every term is proportional to the projector $P_{ij}(\hat{\mathbf{k}})$, which cannot be zero for all i and j, we get

$$\frac{\partial}{\partial t} P(k) = -2k^2 F(k) - 2\nu k^2 P(k). \tag{2.43}$$

The function $P(k)$ can be related to the energy spectrum $E(k)$ via equations (2.31)

[1] It follows from isotropy that $S_{ik,j}(-\mathbf{r}) = -S_{ik,j}(\mathbf{r})$, then by using the equation of the inverse Fourier transform (2.28), one gets $S_{ik,j}(-\mathbf{k}) = S^*_{ik,j}(\mathbf{k}) = -S_{ik,j}(\mathbf{k})$, which implies $S_{ik,j}(\mathbf{k})$ is purely imaginary.

and (2.37)

$$E(k) = \frac{1}{4\pi^2} k^2 Q_{i,i}(k) = \frac{k^2}{4\pi^2} P(k) \underbrace{P_{ii}(\hat{\mathbf{k}})}_{=\delta_{ii}-1=2} \tag{2.44}$$

$$\Rightarrow E(k) = \frac{k^2}{2\pi^2} P(k). \tag{2.45}$$

So in terms of the energy spectrum, the equation (2.43) can be written as

$$\frac{\partial}{\partial t} E(k) = -\frac{k^4}{\pi^2} F(k) - 2\nu k^2 E(k). \tag{2.46}$$

This is the energy balance equation of the various spectral components in the turbulent flow. If we integrate the equation on both sides with respect to k, we can give each term a physical interpretation

$$\frac{\partial}{\partial t} \int_0^k E(k)\, dk = -\frac{1}{\pi^2} \int_0^k k^4 F(k)\, dk - 2\nu \int_0^k k^2 E(k)\, dk. \tag{2.47}$$

The left-hand side describes the change of kinetic energy of the eddies with wavenumbers between 0 and k. The second term on the right-hand side is negative and contains viscosity, so it is the loss of energy due to dissipation in this wavenumber range. This leaves the first term on the right-hand side, which can be given the following interpretation [20]: It describes the transfer of energy or the energy redistribution in the spectrum in the region between wavenumbers 0 and k. The wavenumbers are related to the scales by $k = 2\pi/L$, meaning that large scales correspond to small wavenumbers and vice versa, therefore the flow of energy in the turbulent cascade is from small wavenumbers to larger ones.

The rate of the dissipation of energy in terms of the energy spectrum can be determined from the above equation. The term containing $F(k)$ came from the triple velocity correlations in equation (2.22). Looking at eq. (2.42), we conclude that the right-hand side is the Fourier transform of $\partial/\partial r_k \left(S_{ik,j} + S_{kj,i}\right)$, hence by using the inverse transform we get the following relation

$$\frac{\partial}{\partial r_k} \left[S_{ik,j}(\mathbf{r}) + S_{kj,i}(\mathbf{r})\right] = \frac{1}{(2\pi)^3} \int \left[-2k^2 F(k) P_{ij}(\hat{\mathbf{k}})\right] e^{i\mathbf{k}\cdot\mathbf{r}}\, d^3k. \tag{2.48}$$

When $r \to \infty$, the left-hand side becomes zero on account of the homogeneity, and from the right-hand side we get

$$\int k^2 F(k)\, d^3k = 0 \quad \Rightarrow \quad \int_0^\infty k^4 F(k)\, dk = 0. \tag{2.49}$$

This is an expected result, for the function $F(k)$ transfers energy from small scales to large scales, meaning it is negative at small k and becomes positive at some stage. The integral grants zero because energy is only transferred, not destroyed. Therefore, by taking the integration limits to infinity in equation (2.47), the first term on the right-hand side disappears and we are left with

$$\frac{\partial}{\partial t} \int_0^\infty E(k)\, dk = -2\nu \int_0^\infty k^2 E(k)\, dk. \tag{2.50}$$

If we now use the definition of the power spectrum (2.32) and compare the equation with the turbulence energy equation for homogeneous turbulence (2.26), the dissipation becomes

$$\epsilon = 2\nu \int_0^\infty k^2 E(k)\, dk. \tag{2.51}$$

In theory, the energy spectrum can be solved from (2.46) but here we again bump into the closure problem of turbulence, for the energy-transfer-spectrum function $F(k)$ is not known. However, we can still get a good idea of its shape by looking at its properties and by using dimensional analysis. As mentioned earlier, the function $A(k) \equiv P(k)$ in equation (2.34) is an even function and its series expansion around $k = 0$ starts with a term that goes like k^2. Then according to equation (2.45), the first term in the series expansion of $E(k)$ is proportional to k^4. We also know that energy is dissipated into heat by viscous effects at small scales, so $E(k)$ decreases monotonically to zero as $k \to \infty$. Thus as k increases, the energy spectrum function starts to increase rapidly from zero as k^4 until it reaches a maximum value at k_e, which marks the range of energy-containing eddies, and then begins to decrease.

The equation (2.46) can be solved in the simple case, where the term containing $F(k)$ is assumed to be negligible compared to the other terms, that is, the interaction

between the eddies is very small and no transfer of energy takes place between them. Then

$$\frac{\partial}{\partial t}E(k) = -2\nu k^2 E(k), \tag{2.52}$$

which can be solved by integrating. The result is

$$E(k,t) = E(k,t_0)e^{-2\nu k^2(t-t_0)}. \tag{2.53}$$

This shows that at larger values of k, the the decrease of kinetic energy becomes larger or in other words, the smaller eddies decay at a higher rate than the larger ones. The spectrum is very weakly dependent on time for very small values of k, which can be seen from

$$\lim_{k\to 0}\frac{\partial}{\partial t}E(k,t) = 0. \tag{2.54}$$

This shows that most of the dissipation takes place at large values of k. Let us denote the wavenumber k_d with the eddies that are responsible for the largest contribution to the total dissipation. It is usually defined so that the Reynolds number associated with the corresponding length scale equals unity [22]. We shall also assume that the value of the Reynolds number is large so that the ranges of the energy-containing eddies and the eddies with the largest dissipation are far apart, that is $k_e \ll k_d$. According to a hypothesis made by Kolmogorov in 1941, there exists a range of high wavenumbers ($k \gg k_e$) where the turbulence is in statistical equilibrium and can be determined by two parameters: the total dissipation ϵ and the viscosity ν [23]. This range is known as the universal equilibrium range. The viscosity is prominent only on the smallest scales, so there exists a subrange of the equilibrium range in the shorter wavenumbers, which is not affected by viscosity. It is called the inertial subrange, depends only on ϵ and is located at ($k_e \ll k \ll k_d$) when the Reynolds number of turbulence is large.

At smaller wavenumbers outside the equilibrium range, there is the range of energy-containing eddies. This range can be taken to be dependent on ϵ, ν and time

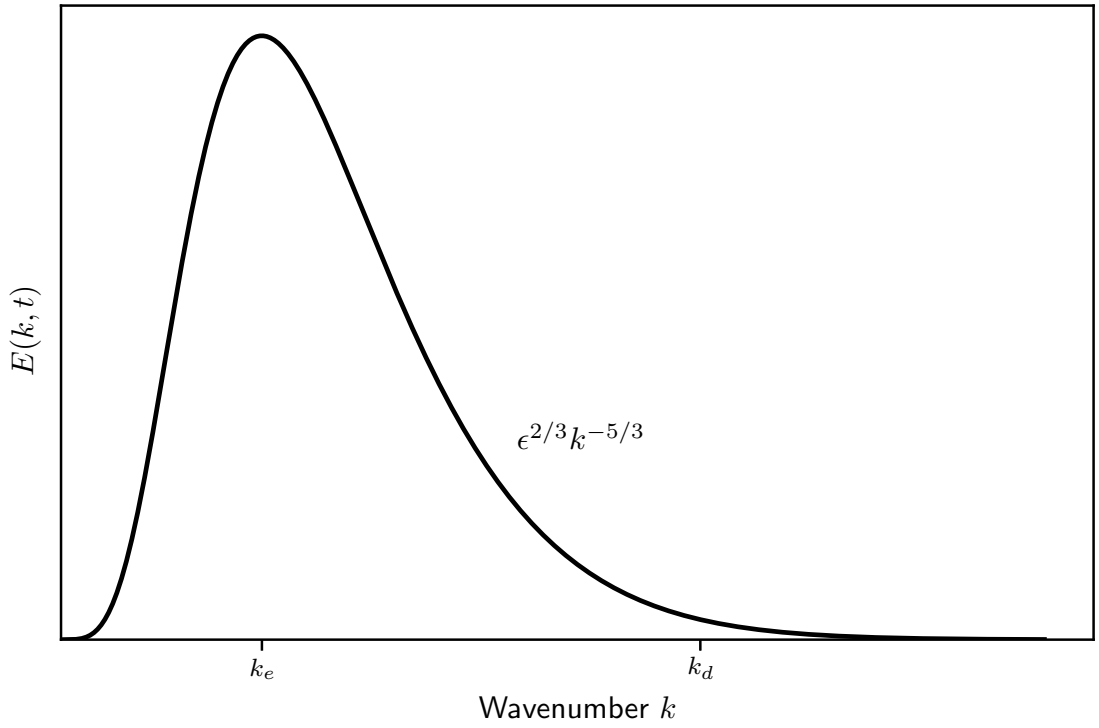

Figure 2.1: Form of the energy spectrum $E(k,t)$.

t. The dependence of time follows from the fact that the relative change of kinetic energy of the turbulence is of the same order as the frequency corresponding to the wavenumber k_e [20]. It is also noteworthy that even though viscosity is negligible on this range, the viscous dissipation taking place at k_d still affects the shape of the spectrum near its maximum, hence the dependence on ν. In the lower wavenumber range of the energy-containing eddies the spectrum can once again be taken to be independent of viscosity, as was the case on the other side of the maximum in the inertial subrange. On even lower wavenumbers the time dependence disappears and the spectrum is dependent only on ϵ, and finally in the lowest wavenumber range it is proportional to k^4 and doesn't depend on any of the aforementioned quantities.

Based on the properties of each of these ranges, it is possible to predict the form of the spectrum on a given range. The prediction is the most precise on the

ranges that depend only on one parameter. A commonly used result is the shape of the energy spectrum on the inertial subrange, which depends only on ϵ. Therefore we can write

$$E(k) \propto \epsilon^a k^b. \tag{2.55}$$

These quantities have the following dimensions

$$\begin{aligned} [k] &= [1/L] \\ [E] &= \left[L^3/T^2\right] \\ [\epsilon] &= \left[L^2/T^3\right], \end{aligned}$$

where L is the unit of length and T is the unit of time. The unit of E follows directly from equation (2.32). Substituting these into (2.55) leads to the system of equations of the form

$$\begin{cases} 3 = 2a - b \\ 2 = 3a \end{cases} \quad \Rightarrow \quad \begin{cases} a = \frac{2}{3} \\ b = -\frac{5}{3} \end{cases},$$

so the form of the energy spectrum is

$$E(k) = A\epsilon^{2/3}k^{-5/3}, \qquad k_e \ll k \ll k_d. \tag{2.56}$$

The result was originally presented by Kolmogorov and is often called the Kolmogorov law. The constant A has been found experimentally to be about 1.5 [24].

3. Gravitational waves from turbulence

3.1 Solving the GW equation

Gravitational waves arise from general relativity by considering small perturbations of space-time. The metric is written as $g_{uv} = \bar{g}_{uv} + h_{uv}$, where $\bar{g}_{uv}$ is the background metric and h_{uv} is the metric perturbation. Linearising the Einstein equations to first order in h_{ij} and assuming a Friedmann-Lemaître-Robinson-Walker (FLRW) background gives the propagation equations for gravitational waves. In the tranverse traceless gauge [25] the equations read [4][1]

$$\frac{d^2}{dt^2}h_{ij}(\mathbf{x},t) + 3H\frac{d}{dt}h_{ij}(\mathbf{x},t) - \frac{1}{a^2}\nabla^2 h_{ij}(\mathbf{x},t) = 16\pi G T_{ij}^{TT}, \tag{3.1}$$

where $a(t)$ is the scale factor, $H = \dot{a}/a$ is the Hubble parameter, G is the universal gravitational constant, ∇^2 is the Laplacian operating on comoving coordinates and T_{ij}^{TT} is the transverse traceless part of the energy momentum tensor, which acts as a source term. In order to solve this equation, we transform it to Fourier space. Writing h_{ij} in the transverse traceless gauge leaves only two degrees of freedom, which correspond to two polarization states. Then $h_{ij}(\mathbf{x},t)$ can be written as

$$h_{ij}(\mathbf{x},t) = \sum_{r=+,\times}\int \frac{d^3k}{(2\pi)^3} h_r(\mathbf{k},t) e^{i\mathbf{k}\cdot\mathbf{x}} e_{ij}^r(\hat{\mathbf{k}}), \tag{3.2}$$

[1]This chapter primarily follows this reference and many of the equations in the following pages are taken from it.

where the amplitudes satisfy $h_r(-\mathbf{k},t) = h_r^*(\mathbf{k},t)$ and $e_{ij}^r(\hat{\mathbf{k}})$ are real symmetric transverse and traceless polarization tensors. Explicitly, they read

$$e_{ij}^+(\hat{\mathbf{k}}) = \hat{m}_i\hat{m}_j - \hat{n}_i\hat{n}_j \tag{3.3}$$

$$e_{ij}^\times(\hat{\mathbf{k}}) = \hat{m}_i\hat{n}_j + \hat{n}_i\hat{m}_j, \tag{3.4}$$

where $\hat{\mathbf{m}}$ and $\hat{\mathbf{n}}$ are unit vectors orthogonal to $\hat{\mathbf{k}}$ and to each other. Hence, they satisfy the property

$$e_{ij}^r(\hat{\mathbf{k}})e_{ij}^{r'}(\hat{\mathbf{k}}) = 2\delta_{rr'}. \tag{3.5}$$

The inverse Fourier transform of T_{ij}^{TT} can also be decomposed into the polarization states $r = +, \times$ and is

$$T_{ij}^{TT}(\mathbf{x},t) = \sum_{r=+,\times}\int \frac{d^3k}{(2\pi)^3}\Pi_r(\mathbf{k},t)e^{i\mathbf{k}\cdot\mathbf{x}}e_{ij}^r(\hat{\mathbf{k}}), \tag{3.6}$$

where

$$\begin{aligned}\Pi_{ij}(\mathbf{k},t) = T_{ij}^{TT}(\mathbf{k},t) &= \sum_{r=+,\times}\Pi_r(\mathbf{k},t)e_{ij}^r(\hat{\mathbf{k}}) \\ &= \left[P_{il}(\hat{\mathbf{k}})P_{jm}(\hat{\mathbf{k}}) - \frac{1}{2}P_{ij}(\hat{\mathbf{k}})P_{lm}(\hat{\mathbf{k}})\right]T_{lm}(\mathbf{k},t)\end{aligned} \tag{3.7}$$

is the transverse traceless part of the energy momentum tensor in Fourier space, also known as the anisotropic stress, which can be presented in this way using the projectors introduced in previous chapter in equation (2.38) [26]. Gravitational waves are only sourced by the transverse and traceless part of $T_{ij}(\mathbf{x},t)$, so using its definition for a perfect fluid (4.2), we can write $T_{ij}(\mathbf{x},t) = wu_i(\mathbf{x},t)u_j(\mathbf{x},t)$, where $w = \rho + p$ is the fluid enthalpy density, which is taken to be a constant throughout space and evaluated at the time of phase transition. Then

$$T_{ij}(\mathbf{k},t) = \mathcal{F}\left[T_{ij}(\mathbf{x},t)\right] = w\mathcal{F}\left[u_i(\mathbf{x},t)u_j(\mathbf{x},t)\right] = w\mathcal{F}\left[u_i(\mathbf{x},t)\right] * \mathcal{F}\left[u_j(\mathbf{x},t)\right], \tag{3.8}$$

where in the last step the Fourier convolution theorem has been utilized. Now the Fourier transform of the energy momentum tensor can be written in the form

$$T_{ij}(\mathbf{k},t) = \frac{w}{(2\pi)^3}\int d^3q\, u_i(\mathbf{q},t)u_j(\mathbf{k}-\mathbf{q},t). \tag{3.9}$$

Transforming the equation (3.1) to Fourier space using (3.2) and (3.6) results in

$$\frac{d^2}{dt^2}h_r(\mathbf{k},t) + 3H\frac{d}{dt}h_r(\mathbf{k},t) + \frac{k^2}{a^2}h_r(\mathbf{k},t) = 16\pi G\Pi_r(\mathbf{k},t), \tag{3.10}$$

where k is the comoving wavenumber. Writing the equation in terms of the conformal time $d\eta = dt/a(t)$ leads to

$$\frac{d^2}{d\eta^2}h_r(\mathbf{k},\eta) + \frac{2}{a}\frac{da}{d\eta}\frac{d}{d\eta}h_r(\mathbf{k},\eta) + k^2h_r(\mathbf{k},\eta) = 16\pi Ga^2\Pi_r(\mathbf{k},\eta). \tag{3.11}$$

Solving the equation becomes more convenient by defining $\mathcal{H}_r(\mathbf{k},\eta) = a(\eta)h_r(\mathbf{k},\eta)$, after which the equation reads as

$$\frac{d^2}{d\eta^2}\mathcal{H}_r(\mathbf{k},\eta) + \left(k^2 - \frac{1}{a}\frac{d^2a}{d\eta^2}\right)\mathcal{H}_r(\mathbf{k},\eta) = 16\pi Ga^3\Pi_r(\mathbf{k},\eta). \tag{3.12}$$

During the radiation dominated era $a \propto t^{1/2}$. By using the definition of the conformal time one gets $a \propto \eta$. This means that the last term on the left-hand side of the equation vanishes. Writing $a = a_*\eta$ and moving to a dimensionless variable $x = k\eta$ gives

$$\frac{d^2}{dx^2}\mathcal{H}_r(\mathbf{k},x) + \mathcal{H}_r(\mathbf{k},x) = \frac{16\pi Ga_*^3}{k^5}x^3\Pi_r(\mathbf{k},x). \tag{3.13}$$

This equation can be solved by using the Green's function method. The solution is

$$\mathcal{H}_r(\mathbf{k},x) = \int dy\, G(x,y)\frac{16\pi Ga_*^3}{k^5}y^3\Pi_r(\mathbf{k},y), \tag{3.14}$$

where $G(x,y)$ is the Green's function, which can be solved from

$$\frac{d^2}{dx^2}G(x,y) + G(x,y) = \delta(x-y). \tag{3.15}$$

The solution is obtained, for example, by using the Laplace transform. If the source is turned on at $x_1 = k\eta_1$ and stops at $x_2 = k\eta_2$, so that at x_1 we have $h_{ij} = \dot{h}_{ij} = 0$, Laplace transforming the equation gives

$$\widetilde{G}(s,y) = \frac{e^{-sy}}{s^2+1}, \tag{3.16}$$

from which the Green's function is obtained by Laplace inverse transform as

$$G(x,y) = \theta(x-y)\sin(x-y). \tag{3.17}$$

Here $\theta(x-y)$ is the Heaviside step function. Substitution into (3.14) and using the step function to shift the upper limit of the integral gives

$$\mathcal{H}_r(\mathbf{k},x) = \frac{16\pi G a_*^3}{k^5}\int_{x_1}^{x} dy\, y^3 \sin(x-y)\Pi_r(\mathbf{k},y). \tag{3.18}$$

This holds while the source is active, that is $x < x_2$. When $x > x_2$, the right-hand side of the equation (3.13) is zero and the solution is

$$\mathcal{H}_r(\mathbf{k},x) = A_r(k)\cos(x) + B_r(k)\sin(x). \tag{3.19}$$

The solution needs to remain continuous at $x = x_2$, so writing $\sin(x-y) = \sin(x)\cos(y) - \sin(y)\cos(x)$ in (3.18) and comparing with the above gives

$$A_r(k) = -\frac{16\pi G a_*^3}{k^5}\int_{x_1}^{x_2} dy\, y^3 \sin(y)\Pi_r(\mathbf{k},y) \tag{3.20}$$

$$B_r(k) = \frac{16\pi G a_*^3}{k^5}\int_{x_1}^{x_2} dy\, y^3 \cos(y)\Pi_r(\mathbf{k},y). \tag{3.21}$$

Now the solution at $x > x_2$ can be written as

$$h_r(\mathbf{k},x) = \frac{16\pi G a_*^3}{a(\eta)k^5}\int_{x_1}^{x_2} dy\, y^3 \sin(x-y)\Pi_r(\mathbf{k},y). \tag{3.22}$$

This result shows the effect of the expansion of the universe on the GW wave amplitude, namely that it decays like a^{-1}.

In the case of cosmological turbulence, it is often assumed that the expansion of the universe can be neglected during the period of time the source is active. This means that the duration of the source is short compared to the Hubble time, which should be a good approximation for early-universe phase-transitions [15, 27]. Then the expansion term in (3.11) can be dropped and the equation becomes

$$\frac{d^2}{d\eta^2}h_{ij}(\mathbf{k},\eta) + k^2 h_{ij}(\mathbf{k},\eta) = 16\pi G a_*^2 \Pi_{ij}(\mathbf{k},\eta). \tag{3.23}$$

or

$$\frac{d^2}{dt^2}h_{ij}(\mathbf{k},t) + k^2_{\mathrm{phys}}h_{ij}(\mathbf{k},t) = 16\pi G\Pi_{ij}(\mathbf{k},t). \tag{3.24}$$

in terms of physical time and physical wavenumber $k_{\mathrm{phys}} = k/a$. The form of the equation is very similar to (3.13) and solving the equation is carried out in a similar manner. The solutions in this case can be found, for example, in [15, 28].

3.2 General stochastic source

Because turbulence is a stochastic process, the generated gravitational wave background is also stochastic. Therefore, the amplitude h_{ij} is a random variable and obtaining relevant results requires statistical analysis. The quantity often calculated is the two-point correlation function $\langle h_{ij}h_{ij}\rangle$, where $\langle\cdots\rangle$ denotes ensemble average. The background is often approximated to be statistically isotropic and homogeneous, unpolarised and Gaussian [29]. Under these assumptions, the ergodic hypothesis is valid and states, that ensemble, temporal and spatial averages all give the same result.

The quantity usually used to characterize cosmological backgrounds is the spectrum of energy density per logarithmic frequency interval divided by the current value of the critical density

$$h^2\Omega_{\mathrm{GW}}(f) = \left(\frac{h^2}{\rho_c}\frac{d\rho_{GW}}{d\log f}\right)_0, \tag{3.25}$$

where h is included because now the equation is not affected by the observational uncertainty of the value of $H_0 = 100\,h\,\mathrm{km/s/Mpc}$, for $\rho_c = 3H^2/8\pi G$. The present day frequency can be related to the wavenumber by $f = k/2\pi a_0$. Under the statistical assumptions made earlier, $\Omega_{\mathrm{GW}}(f)$ contains all information about the stochastic background. Other useful and often used characterizations of the background are the characteristic amplitude $h_c(f)$ and the spectral density $S_h(f)$. The characteristic

amplitude per unit logarithmic interval of frequency is defined as [30]

$$\langle h_{ij}(\mathbf{x},t)h_{ij}(\mathbf{x},t)\rangle = 2\int_0^\infty d(\log f)\, h_c^2(f) = 2\int_0^\infty \frac{dk}{k}\, h_c^2(k,t). \tag{3.26}$$

The factor of two is usually included, because the left-hand side of the equation contains two contributions where the two-point functions contain only amplitudes with the same polarization, either + or ×. In an unpolarized background the two-point functions with mixed polarizations disappear and the ones with matching polarizations are equal. The spectral density is related to $h_c(f)$ by [30]

$$h_c^2(f) = 2fS_h(f). \tag{3.27}$$

The characteristic amplitude can now be related to the power spectrum of the Fourier amplitudes by defining

$$\Big\langle h_r(\mathbf{k},\eta)h_p^*(\mathbf{q},\eta)\Big\rangle = (2\pi)^3\delta(\mathbf{k}-\mathbf{q})\delta_{rp}\mathcal{P}(k,\eta), \tag{3.28}$$

which follows from the statistical assumptions made earlier, and then calculating $\langle h_{ij}(\mathbf{x},\eta)h_{ij}(\mathbf{x},\eta)\rangle$ using the expansion in equation (3.2) and comparing it with equation (3.26). This gives

$$\langle h_{ij}(\mathbf{x},\eta)h_{ij}(\mathbf{x},\eta)\rangle = 4\int \frac{d^3k}{(2\pi)^3}\int \frac{d^3q}{(2\pi)^3}\,\langle h_r(\mathbf{k},\eta)h_r^*(\mathbf{q},\eta)\rangle\, e^{i\mathbf{x}\cdot(\mathbf{k}-\mathbf{q})}, \tag{3.29}$$

where we have used the property

$$\sum_r\sum_{r'} e_{ij}^r(\hat{\mathbf{k}})e_{ij}^{r'}(\hat{\mathbf{k}}) = 4, \tag{3.30}$$

made a change of variables $\mathbf{q}\to-\mathbf{q}$ and also used the property $h_r(-\mathbf{q},t) = h_r^*(\mathbf{q},t)$. We can now substitute equation (3.28) into this expression, after which the q-integral is easily performed with the help of the δ-function, which kills off the exponential function. Writing $d^3k = k^2\,dk\,d\Omega$ and performing the integral over the angles $\int d\Omega = 4\pi$, we have

$$\langle h_{ij}(\mathbf{x},\eta)h_{ij}(\mathbf{x},\eta)\rangle = \frac{16\pi}{(2\pi)^6}\int_0^\infty dk\, k^2\mathcal{P}(k,\eta) \overset{(3.26)}{=} 2\int_0^\infty \frac{dk}{k}\, h_c^2(k,\eta). \tag{3.31}$$

Comparison gives

$$\mathcal{P}(k,\eta) = \frac{(2\pi)^3}{8\pi k^3} h_c^2(k,\eta), \tag{3.32}$$

and (3.28) becomes

$$\left\langle h_r(\mathbf{k},\eta) h_p^*(\mathbf{q},\eta) \right\rangle = \frac{8\pi^5}{k^3} \delta(\mathbf{k}-\mathbf{q}) \delta_{rp} h_c^2(k,\eta). \tag{3.33}$$

The next step is to relate $\Omega_{\rm GW}(f)$ and $h_c(f)$. In order to do that, we need to relate the GW energy density ρ_{GW} to a two-point function containing the amplitudes. Such a relation can be derived from General Relativity by using second order perturbation theory and by averaging the second order Ricci tensor to obtain [26]

$$T_{\mu\nu}^{\rm GW} = \frac{\left\langle \nabla_\mu h_{\alpha\beta} \nabla_\nu h^{\alpha\beta} \right\rangle}{32\pi G}, \tag{3.34}$$

where T is the effective energy momentum tensor of GWs and ∇ is the covariant derivative. The energy density of gravitational waves is given by $T_{00}^{\rm GW}$. For the FLRW metric at first order in perturbation theory, the covariant derivative reduces to a regular time derivative. In the transverse traceless gauge $h_{\mu 0} = 0$, so the equation can be written as

$$\rho_{\rm GW} = \frac{\left\langle \dot{h}_{ij} \dot{h}_{ij} \right\rangle}{32\pi G} = \frac{\left\langle h'_{ij} h'_{ij} \right\rangle}{32\pi G a^2(\eta)} = \int_0^\infty \frac{dk}{k} \frac{d\rho_{\rm GW}}{d(\log k)}. \tag{3.35}$$

Here dots denote time derivatives and primes denote differentiation with respect to conformal time. By looking at the expansion (3.2), it is evident, that the conformal time derivatives only act on h_r, so it is natural to assume that an equation of the form (3.33) exists also in this case. It can be written as

$$\left\langle h'_r(\mathbf{k},\eta) h'^*_p(\mathbf{q},\eta) \right\rangle = \frac{8\pi^5}{k^3} \delta(\mathbf{k}-\mathbf{q}) \delta_{rp} h'^2_c(k,\eta). \tag{3.36}$$

Now the general solution at $x > x_2$, that is equation (3.19), can be used to relate h_c and h'_c. We write it as

$$h_r(\mathbf{k},\eta) = \frac{1}{a(\eta)} \left[A_r(k) \cos(k\eta) + B_r(k) \sin(k\eta) \right] \tag{3.37}$$

and now

$$\left\langle h_r(\mathbf{k},\eta)h_p^*(\mathbf{q},\eta)\right\rangle = \frac{1}{a^2(\eta)}\Big[\left\langle A_r(k)A_p^*(k)\cos^2(k\eta)\right\rangle + \left\langle B_r(k)B_p^*(k)\sin^2(k\eta)\right\rangle + \frac{1}{2}\left\langle \Big(A_r(k)B_p^*(k) + A_p^*(k)B_r(k)\Big)\sin(2k\eta)\right\rangle\Big], \quad (3.38)$$

which has been obtained by taking into account the presence of a delta function that imposes $k = q$. We can make further progress by averaging the above equation over multiple periods in addition to taking the ensemble average. The last term containing $\sin(2k\eta)$ can then be dropped because it oscillates around zero and thus also averages to zero. In the first two terms, the $\sin^2$ and $\cos^2$ can be replaced by their average values of 1/2. Then the result becomes

$$\left\langle h_r(\mathbf{k},\eta)h_p^*(\mathbf{q},\eta)\right\rangle = \frac{1}{2a^2(\eta)}\left[\left\langle A_r(k)A_p^*(q)\right\rangle + \left\langle B_r(k)B_p^*(q)\right\rangle\right]. \quad (3.39)$$

Next, we calculate $\left\langle h_r'(\mathbf{k},\eta)h_p'^*(\mathbf{q},\eta)\right\rangle$. Differentiating with respect to conformal time we get

$$h_r'(\mathbf{k},\eta) = \frac{1}{a(\eta)}\Big[k\left[B_r(k)\cos(k\eta) - A_r(k)\sin(k\eta)\right] - H_{\rm conf}\left[A_r(k)\cos(k\eta) + B_r(k)\sin(k\eta)\right]\Big], \quad (3.40)$$

Where $H_{\rm conf} = a'/a$. After some calculus and averaging over the oscillating functions, the result is

$$\left\langle h_r'(\mathbf{k},\eta)h_p'^*(\mathbf{q},\eta)\right\rangle = \frac{1}{2a^2(\eta)}(k^2 + H_{\rm conf}^2)\left[\left\langle A_r(k)A_p^*(q)\right\rangle + \left\langle B_r(k)B_p^*(q)\right\rangle\right]. \quad (3.41)$$

When it comes to detectors, only the sub-Hubble scales ($k \gg H_{\rm conf}$) are of interest. Therefore, we can drop the $H_{\rm conf}^2$ term and use (3.39) to get

$$\left\langle h_r'(\mathbf{k},\eta)h_p'^*(\mathbf{q},\eta)\right\rangle \simeq \frac{k^2}{2a^2(\eta)}\left[\left\langle A_r(k)A_p^*(q)\right\rangle + \left\langle B_r(k)B_p^*(q)\right\rangle\right] \quad (3.42)$$

$$= k^2\left\langle h_r(\mathbf{k},\eta)h_p^*(\mathbf{q},\eta)\right\rangle. \quad (3.43)$$

This requires that

$$h_c'^2(k,\eta) = k^2 h_c^2(k,\eta). \quad (3.44)$$

Using the expansion for $h_{ij}(\mathbf{x},\eta)$ in (3.35) with (3.36) and (3.44) gives

$$\frac{1}{16\pi G a^2(\eta)}\int_0^\infty dk\, k h_c^2(k,\eta) = \int_0^\infty \frac{dk}{k}\frac{d\rho_{\rm GW}}{d(\log k)} \tag{3.45}$$

$$\Rightarrow \Omega_{\rm GW}(k,\eta) = \frac{1}{\rho_c}\frac{d\rho_{\rm GW}}{d(\log k)} = \frac{k^2}{6H^2(\eta)a^2(\eta)}h_c^2(k,\eta). \tag{3.46}$$

Therefore because $h_c \propto a^{-1}(\eta)$, the GW energy density scales as $\propto a^{-4}(\eta)$ with the expansion of the universe. Solving for the value of h_c today and substituting $k = 2\pi f a$ and the value of H_0 yields the relation

$$h_c(f) = 1.268\cdot 10^{-18}\left(\frac{\rm Hz}{f}\right)\sqrt{h^2\Omega_{\rm GW}(f)}. \tag{3.47}$$

The two-point function $\left\langle h_r(\mathbf{k},\eta)h_p^*(\mathbf{q},\eta)\right\rangle$ can now be calculated explicitly using the solution obtained in the previous section. This is achieved either by substituting (3.20) and (3.21) into (3.39) and using the trigonometric property $\cos(a-b) = \sin a\sin b + \cos a\cos b$ or by using the solution (3.22) directly and writing

$$\sin(x-y)\sin(x-z) = \frac{1}{2}\left[\cos(y-z) - \cos(y+z-2x)\right], \tag{3.48}$$

where the latter term averages to zero. The result is

$$\left\langle h_r(\mathbf{k},\eta)h_p^*(\mathbf{q},\eta)\right\rangle = \frac{2^7\pi^2G^2a_*^6}{a^2k^{10}}\int_{x_1}^{x_2} dy\, y^3\int_{x_1}^{x_2} dz\, z^3\cos(y-z)\left\langle \Pi_r(\mathbf{k},y)\Pi_p^*(\mathbf{q},z)\right\rangle. \tag{3.49}$$

For a statistically isotropic, homogeneous, unpolarized and Gaussian background, the source can also be treated in a similar manner. Therefore, The power spectrum of the Fourier components of the tensor anisotropic stress can be expressed as follows

$$\left\langle \Pi_r(\mathbf{k},\eta)\Pi_p^*(\mathbf{q},\zeta)\right\rangle = (2\pi)^3\delta(\mathbf{k}-\mathbf{q})\delta_{rp}\Pi(k,\eta,\zeta). \tag{3.50}$$

Here $\Pi(k,\eta,\zeta)$ is called the unequal-time correlator of the tensor-type anisotropic stress, which characterizes the source. Substituting this into (3.49) and comparing the resulting equation with (3.33) gives the characteristic amplitude as

$$h_c(k,\eta) = \frac{2^7G^2a_*^6}{a^2k^7}\int_{x_1}^{x_2} dy\, y^3\int_{x_1}^{x_2} dz\, z^3\cos(y-z)\Pi(k,y,z) \tag{3.51}$$

and with equation (3.46) the energy density spectrum today becomes[2]

$$h^2\Omega_{\rm GW} = \frac{h^2}{H_0^2}\frac{64G^2a_*^6}{3a_0^4k^5}\int_{x_1}^{x_2} dy\, y^3 \int_{x_1}^{x_2} dz\, z^3 \cos(y-z)\Pi(k,y,z) \tag{3.52}$$

$$= \frac{h^2}{H_0^2}\frac{64G^2}{3a_0^4}k^3\int_{\eta_1}^{\eta_2} d\eta\, a^3(\eta)\int_{\eta_1}^{\eta_2} d\zeta\, a^3(\zeta)\cos\left[k(\eta-\zeta)\right]\Pi(k,\eta,\zeta), \tag{3.53}$$

where the dimensionless variables have been expressed in terms of conformal time. Now the computation of the spectrum is reduced to the determination of the the unequal-time correlator of the source.

Gravitational waves interact extremely weakly with matter, therefore after production they can be assumed to propagate freely trough spacetime. If one considers modes well inside the Hubble horizon ($k \gg H_{\rm conf}$) or short lasting sources, the expansion of the universe can be neglected. Then the expansion term in (3.11) is dropped. In this case, in order to get the value of the desired quantity today, one needs to take into account that the solutions are redshifted (stretched) with the expansion of the universe. For example, the energy density goes like $\rho_{\rm GW} \propto a^{-4}$, so the spectrum today in terms of the energy density at the time of production (denoted by p) reads

$$h^2\Omega_{\rm GW} = h^2\left(\frac{a_p}{a_0}\right)^4\frac{1}{\rho_c}\left(\frac{d\rho_{\rm GW}}{d(\log k)}\right)_p. \tag{3.54}$$

The scale factor at the time of production is related to the present value by the standard assumption of adiabatic expansion of the universe. Then the conservation of the total entropy requires

$$g_{*S}(T)T^3a^3 = \text{const.} \tag{3.55}$$

The function $g_{*S}(T)$ is is the number of degrees of freedom associated with entropy

[2]The numerical prefactor differs from that of [4] because of using a slightly different normalization for the unequal-time correlator. There is also a mistake of a factor 2 in [4], which results from using a wrong formula when calculating $\langle h_r(\mathbf{k},\eta)h_p^*(\mathbf{q},\eta)\rangle$.

at the temperature T [31]. Then it follows that

$$\frac{a_p}{a_0} = \left(\frac{g_{*S}(T_0)}{g_{*S}(T_p)}\right)^{\frac{1}{3}} \left(\frac{T_0}{T_p}\right). \tag{3.56}$$

Now $g_{*S}(T_0)$ and T_0 can be replaced by their well-known values of 3.909 and $2.348 \cdot 10^{-4}\,\mathrm{eV}$ respectively. Also during the radiation dominated era $g_{*S}(T) \approx g_*(T)$, which is the number of relativistic degrees of freedom. With these, the ratio becomes

$$\frac{a_p}{a_0} \approx 7.97 \cdot 10^{-16} \left(\frac{100}{g_*(T_p)}\right)^{\frac{1}{3}} \left(\frac{100\,\mathrm{GeV}}{T_p}\right), \tag{3.57}$$

which can now be used, for example, in equation (3.54) or to determine the shift in frequency, which goes like a^{-1}. During the radiation dominated era, the total energy density is related to temperature by

$$\rho_{\mathrm{rad}} = \frac{\pi^2}{30} g_*(T) T^4, \tag{3.58}$$

which can be used to express the Hubble parameter as

$$H_p^2 = \frac{8\pi G}{3}\rho_p = \frac{8\pi^3 g_*(T_p) T_p^4}{90 m_{\mathrm{Pl}}^2}, \tag{3.59}$$

where $m_{\mathrm{Pl}} = 1/\sqrt{G}$ is the Planck mass. This relation is often used to include the Hubble parameter in the results.

3.3 Cosmological turbulence

Cosmological turbulence is generated as a result of bubble collisions from first-order phase transitions that cause stirring of the fluid. Classical turbulence analysis, the one discussed in Chapter 2, only holds and is tested for fluids that are non-relativistic and incompressible. Neither of these features is true for the radiation-dominated plasma in the early universe and no general model exists for turbulence with relativistic velocities. Additionally, there are things, like shock formation, that further

complicate the situation. This problem is typically solved by extending the non-relativistic classical results under the approximation that the speed of the fluid on a scale L, denoted v_L, is bounded by the sound speed of the fluid $c_s = 1/\sqrt{3}$ for radiation-dominated plasma. The approximation is justified by arguing that velocities well over c_s lead to shock formation and thus to significant thermal dissipation and loss of energy [15]. The fluid is expected to be only moderately relativistic with a γ-factor close to unity. Then the error resulting from using the non-relativistic model is expected to within the uncertainty of the calculation. Also according to the numerical simulations in [32, 33], the Kolmogorov spectrum is recovered even in the relativistic case.

As the bubbles collide, the fluid is stirred on a characteristic length scale L_S. After the phase transition has ended, the number of small bubbles is much larger than the number of large ones, but the energy density in the large bubbles dominates the total energy density [34]. Thus, L_S can be approximated as the size of the largest bubbles at the time of collision $L_S \sim R_*$. On this scale, a large amount of energy is being injected into the system and under suitable conditions a turbulent cascade develops, where energy is transferred from large scales to small scales trough deformation of eddies. They can be given a characteristic velocity v_L called eddy velocity and a turnover time $\tau_L = L/v_L$ on a given scale L. On scales larger than L_S there is no correlated fluid motion. The eddies are dissipated on a scale L_d, so eddies only exist in the interval $L_d < L < L_S$, meaning that L_S marks the size of the largest eddies[3].

In the case that the stirring of the fluid is continuous, turbulence becomes fully developed in a time interval of the order of the eddy turnover time on the scale L_*. The length of the strirring depends on the duration of the phase transition, which

[3]Here L_S and L_d correspond to the wavenumbers k_e and k_d of figure 2.1. Therefore the power spectrum gains its maximum at a wavenumber corresponding to the size of the largest eddies.

is typically assumed to be considerably shorter than one Hubble time H^{-1}. In fact, turbulence described with a Kolmogorov model can only be generated if $\tau_S < H^{-1}$, where τ_S is the eddy turnover time on the stirring scale. The Reynolds' number of the fluid is expected to be very large, of the order 10^{13} at the electroweak epoch at $T \sim 100\,\mathrm{GeV}$ [35], meaning that the stirring and dissipation scales are far apart and a wide range of scales exists between them. In this region the energy spectrum follows the Kolmogorov law. The contributions to the energy spectrum from scales smaller than L_d are neglected in the case of cosmological turbulence, because the dissipation range contains so little energy that it is not relevant in the context of a cosmological treatment.

Turbulence remains stationary as long as energy is being injected. After the phase transition ends, the stirring stops and the turbulence begins to decay. If this occurs before the turbulence has time to become fully developed (short lasting source), the cascade develops but the turbulence is not stationary. The lifetime of an eddy on a given scale is also of the order of the eddy turnover time τ_L, so the eddies decay in a way that there are time displacements between their existence. These displacements lead to phase shift between the gravitational waves generated at two different frequencies, which has no effect on gravitational wave generation. Therefore in this case, the turbulence can be modelled as stationary and fully developed lasting for a time τ_S [15]. If the stirring lasts a lot longer than τ_S (long lasting source), the duration of turbulence is virtually the same as the duration of the phase transition.

We focus on the non-helical case, so that the generated gravitational waves are not polarized. Polarized GWs could be generated by anisotropic stresses of the helical primordial magnetic fields [36] or by macroscopic parity violations [37]. Helical turbulence produces circularly polarized gravitational waves [38] and their amplitude is believed to be below the detection range of any near future GW detectors [39]. The results from the previous chapter can be easily generalized to the

case where polarizations are ignored, so that all quantities are presented in terms of Π_{ij} and h_{ij} instead of the ones with polarization subscript $r = (+, \times)$. Then all equations maintain their form but in some cases the preceding numerical factors are slightly different due to the lack of polarization tensors when calculating the two-point functions.

Turbulence generates anisotropic stress in the fluid, which in turn acts as a source for gravitational waves. In the last section it was shown that in order to determine the GW energy density spectrum, one needs to calculate the anisotropic stress power spectrum

$$\left\langle \Pi_{ij}(\mathbf{k}, t_1)\Pi^*_{ij}(\mathbf{k}', t_2)\right\rangle = (2\pi)^3\delta(\mathbf{k}-\mathbf{k}')\Pi(k, t_1, t_2). \tag{3.60}$$

at different times, substitute it into (3.53) and evaluate the integrals. Using equation (3.7), this can be written as

$$\left\langle \Pi_{ij}(\mathbf{k}, t_1)\Pi^*_{ij}(\mathbf{k}', t_2)\right\rangle = \mathcal{P}_{abcd}\left\langle T_{ab}(\mathbf{k}, t_1)T^*_{cd}(\mathbf{k}', t_2)\right\rangle, \tag{3.61}$$

where

$$\mathcal{P}_{abcd} = \left[P_{ia}(\hat{\mathbf{k}})P_{jb}(\hat{\mathbf{k}}) - \frac{1}{2}P_{ij}(\hat{\mathbf{k}})P_{ab}(\hat{\mathbf{k}})\right]\left[P_{ic}(\hat{\mathbf{k}}')P_{jd}(\hat{\mathbf{k}}') - \frac{1}{2}P_{ij}(\hat{\mathbf{k}}')P_{cd}(\hat{\mathbf{k}}')\right]. \tag{3.62}$$

Now using the Fourier transform of the energy-momentum tensor, equation (3.9), gives

$$\langle T_{ab}(\mathbf{k}, t_1)T^*_{cd}(\mathbf{k}', t_2)\rangle = w^2\int\frac{d^3k}{(2\pi)^3}\int\frac{d^3s}{(2\pi)^3}\left\langle u_a(\mathbf{q}, t_1)u_b(\mathbf{k}-\mathbf{q}, t_1)u^*_c(\mathbf{s}, t_2)u^*_d(\mathbf{k}'-\mathbf{s}, t_2)\right\rangle. \tag{3.63}$$

The quantity contains a product of four velocity components evaluated at two different times. To make progress, the typical approximation is to use Wick's theorem, even though the turbulent velocity field is not Gaussian. This way one does not need to use equations that involve higher order correlators and the calculation reduces to a product of velocity power spectra. This (hopefully) gives the right order of

magnitude for the four-point function. The same trick is also used in more complex studies of turbulence [21]. Using Wick's theorem and the relation $u(-\mathbf{k}) = u^*(\mathbf{k})$, the equation (3.63) becomes

$$\begin{aligned}\langle T_{ab}(\mathbf{k},t_1)T^*_{cd}(\mathbf{k}',t_2)\rangle =& w^2 \int \frac{d^3k}{(2\pi)^3}\int \frac{d^3s}{(2\pi)^3}\times \\ &\Big[\langle u_a(\mathbf{q},t_1)u^*_b(\mathbf{q}-\mathbf{k},t_1)\rangle \langle u_c(-\mathbf{s},t_2)u^*_d(\mathbf{k}'-\mathbf{s},t_2)\rangle + \\ &\langle u_a(\mathbf{q},t_1)u^*_c(\mathbf{s},t_2)\rangle \langle u_b(\mathbf{k}-\mathbf{q},t_1)u^*_d(\mathbf{k}'-\mathbf{s},t_2)\rangle + \\ &\langle u_a(\mathbf{q},t_1)u^*_d(\mathbf{k}'-\mathbf{s},t_2)\rangle \langle u_b(\mathbf{k}-\mathbf{q},t_1)u^*_c(\mathbf{s},t_2)\rangle \Big].\end{aligned} \tag{3.64}$$

The two-point functions can be calculated by using the Fourier transforms of the velocity components and the properties of statistical isotropy. After substitution, we have

$$\left\langle u_i(\mathbf{k},t_1)u^*_j(\mathbf{q},t_2)\right\rangle = \int d^3x \int d^3x'\, e^{i(\mathbf{q}\cdot\mathbf{x}'-\mathbf{k}\cdot\mathbf{x})}\langle u_i(\mathbf{x},t_1)u_j(\mathbf{x}',t_2)\rangle\,. \tag{3.65}$$

Writing $\mathbf{x}' = \mathbf{x}+\mathbf{r}$ and using equation (2.23) gives

$$\begin{aligned}\left\langle u_i(\mathbf{k},t_1)u^*_j(\mathbf{q},t_2)\right\rangle &= \int d^3r\, Q_{ij}(r,t_1,t_2)e^{i\mathbf{q}\cdot\mathbf{r}}\int d^3x\, e^{i\mathbf{x}\cdot(\mathbf{q}-\mathbf{k})} \\ &= (2\pi)^3\delta(\mathbf{k}-\mathbf{q})\int d^3r\, Q_{ij}(r,t_1,t_2)e^{i\mathbf{k}\cdot\mathbf{r}},\end{aligned} \tag{3.66}$$

where the definition of the δ-function has been used to replace the x-integral and $\mathbf{q}$ has been replaced by $\mathbf{k}$, as imposed by the δ-function. Making the change of variables $\mathbf{r} \to -\mathbf{r}$ with $Q_{ij}(\mathbf{r}) = Q_{ij}(-\mathbf{r})$ shows, that the r-integral is just the Fourier transform of $Q_{ij}(\mathbf{r},t_1,t_2)$. Then using eq. (2.37), we get

$$\left\langle u_i(\mathbf{k},t_1)u^*_j(\mathbf{q},t_2)\right\rangle = (2\pi)^3\delta(\mathbf{k}-\mathbf{q})P_{ij}(\hat{\mathbf{k}})P(k,t_1,t_2), \tag{3.67}$$

which shows that at equal time, the function $P(k,t)$ is the turbulent velocity power spectrum and is related to the energy spectrum by the equation (2.45). After substituting this into (3.64), the first term becomes non-zero, due to the product of δ-functions, only when $\mathbf{k} = \mathbf{k}' = 0$ so it does not give a contribution. In the remaining terms, the delta functions simplify to $\delta(\mathbf{k}-\mathbf{k}')$ after integration over s and we

have

$$\langle T_{ab}(\mathbf{k},t_1)T^*_{cd}(\mathbf{k}',t_2)\rangle = w^2\delta(\mathbf{k}-\mathbf{k}')\int d^3q\,\mathcal{O}_{abcd}P(q,t_1,t_2)P(|\mathbf{k}-\mathbf{q}|,t_1,t_2), \quad (3.68)$$

where

$$\mathcal{O}_{abcd} = P_{ac}(\hat{\mathbf{q}})P_{bd}(\widehat{\mathbf{k}-\mathbf{q}}) + P_{ad}(\hat{\mathbf{q}})P_{bc}(\widehat{\mathbf{k}-\mathbf{q}}) \quad (3.69)$$

The projectors $P_{ij}(\hat{\mathbf{k}})$ fulfil

$$P_{ij}(\hat{\mathbf{k}})P_{jk}(\hat{\mathbf{k}}) = P_{ik}(\hat{\mathbf{k}}), \qquad P_{ij}(\hat{\mathbf{k}})\hat{\mathbf{k}}_j = 0, \quad (3.70)$$

so after putting $\mathbf{k}=\mathbf{k}'$ as required by the δ-function, the operator $\mathcal{P}_{abcd}$ becomes

$$\mathcal{P}_{abcd}(\hat{\mathbf{k}}) = P_{ab}(\hat{\mathbf{k}})P_{bd}(\hat{\mathbf{k}}) - \frac{1}{2}P_{ab}(\hat{\mathbf{k}})P_{cd}(\hat{\mathbf{k}}). \quad (3.71)$$

Now the anisotropic stress power spectrum (3.61) is going to contain the contraction $\mathcal{P}_{abcd}\mathcal{O}_{abcd}$. Writing it out explicitly gives

$$\begin{aligned}\mathcal{P}_{abcd}\mathcal{O}_{abcd} =& P_{ac}(\hat{\mathbf{k}})P_{ac}(\hat{\mathbf{q}})P_{bd}(\hat{\mathbf{k}})P_{bd}(\widehat{\mathbf{k}-\mathbf{q}}) + P_{ac}(\hat{\mathbf{k}})P_{ad}(\hat{\mathbf{q}})P_{bd}(\hat{\mathbf{k}})P_{bc}(\widehat{\mathbf{k}-\mathbf{q}})\\ &- \frac{1}{2}P_{ab}(\hat{\mathbf{k}})P_{ac}(\hat{\mathbf{q}})P_{cd}(\hat{\mathbf{k}})P_{bd}(\widehat{\mathbf{k}-\mathbf{q}}) - \frac{1}{2}P_{ab}(\hat{\mathbf{k}})P_{ad}(\hat{\mathbf{q}})P_{cd}(\hat{\mathbf{k}})P_{bc}(\widehat{\mathbf{k}-\mathbf{q}}).\end{aligned} \quad (3.72)$$

This can be calculated using the definition of P_{ij} in eq. (2.38). The calculation is somewhat tedious but straightforward. It gives, term by term

$$P_{ac}(\hat{\mathbf{k}})P_{ac}(\hat{\mathbf{q}})P_{bd}(\hat{\mathbf{k}})P_{bd}(\widehat{\mathbf{k}-\mathbf{q}}) = (1+\gamma^2)(1+\beta^2), \quad (3.73)$$

where $\gamma = \hat{\mathbf{k}}\cdot\hat{\mathbf{q}}$, $\beta = \hat{\mathbf{k}}\cdot(\widehat{\mathbf{k}-\mathbf{q}})$, and

$$\begin{aligned}P_{ac}(\hat{\mathbf{k}})P_{ad}(\hat{\mathbf{q}})P_{bd}(\hat{\mathbf{k}})P_{bc}(\widehat{\mathbf{k}-\mathbf{q}}) &= P_{ab}(\hat{\mathbf{k}})P_{ac}(\hat{\mathbf{q}})P_{cd}(\hat{\mathbf{k}})P_{bd}(\widehat{\mathbf{k}-\mathbf{q}})\\ &= P_{ab}(\hat{\mathbf{k}})P_{ad}(\hat{\mathbf{q}})P_{cd}(\hat{\mathbf{k}})P_{bc}(\widehat{\mathbf{k}-\mathbf{q}})\\ &= \alpha^2+\beta^2-2\gamma\beta\alpha+\gamma^2\beta^2+\gamma^2,\end{aligned} \quad (3.74)$$

where $\alpha = \hat{\mathbf{q}}\cdot(\widehat{\mathbf{k}-\mathbf{q}})$. It can now be seen that the last two terms in (3.72) cancel with the second term. Then the anisotropic stress power spectrum becomes

$$\left\langle \Pi_{ij}(\mathbf{k},t_1)\Pi^*_{ij}(\mathbf{k}',t_2)\right\rangle = w^2\delta(\mathbf{k}-\mathbf{k}')\int d^3q\,P(q,t_1,t_2)P(|\mathbf{k}-\mathbf{q}|,t_1,t_2)(1+\gamma^2)(1+\beta^2). \quad (3.75)$$

Comparison with eq. (3.50) gives the unequal time correlator as

$$\Pi(k,t_1,t_2) = w^2 \int \frac{d^3q}{(2\pi)^3} P(q,t_1,t_2)P(|\mathbf{k}-\mathbf{q}|,t_1,t_2)(1+\gamma^2)(1+\beta^2). \tag{3.76}$$

In order to calculate the integral, one needs to know how the source behaves in time. In practise this means writing out the time dependence in terms of the equal time velocity power spectra for both t_1 and t_2 by using a so-called de-correlation function. After that a specific model for turbulence consists of specifying the function $P(k,t)$.

When the time dependence of the source and the correlation between t_1 and t_2 has been specified, and the integrals in (3.76) and (3.53) have been evaluated, the energy density spectrum is going to depend on quantities characterising turbulence, such as L_S, L_d, τ_S and v_S. The final step is relating these quantities to parameters characterising the phase transition. These are: (1) β^{-1}, which is the duration of the phase transition determined by the bubble nucleation rate $\Gamma = \Gamma_0 e^{\beta t}$, (2) $\alpha = \rho_{\rm vac}/\rho^*_{\rm rad}$, the ratio of the vacuum energy density released in the transition to the radiation energy density in the universe at the time of the phase transition, which characterises the strength of the PT, (3) v_w, the bubble wall speed in the rest frame of the fluid far away from the bubble, and (4) T_p, the temperature of the thermal bath at the time of GW production. Now the size of the largest bubbles (also the stirring scale, as $R_* \sim L_S$) can be written as $R_* \simeq v_w\beta^{-1}$, and β can also be connected with the strength of the PT, α, because strong PTs last longer. The parameters T_p, β and α are determined directly by the underlying physics, for instance, from the general properties of the effective potential. However, the same does not apply to v_w. Instead, it is determined by the microscopic interactions related to the bubble propagation. When considering GW production, it can be determined by defining a friction parameter that describes the interaction between the plasma and the bubble wall [40]. Generally, the higher the strength of the PT α, the higher bubble wall velocities will be obtained.

3.4 Models presented thus far

Turbulence is an incoherent source and that is why the analysis of the resulting gravitational waves is not straightforward. Different models solve the GW equation in slightly different ways, model the time dependence of the source using different de-correlators, include different parts of the turbulence velocity power spectrum and some include features like the decay of turbulence while others do not. Often the models also include the magnetohydrodynamic (MHD) turbulence, which has not been discussed here. This section is going to contain information about the history of the study of GW production from turbulence and highlight the main differences between each model.

The first analysis is by Kamionkowski et al from 1994 [16]. Instead of integrating the GW equation, they resorted to using simple dimensional arguments with the quadrupole approximation, which holds for small values of v_w. They have also only considered the Kolmogorov inertial range law (2.56) and extended it to the stirring scale L_S, completely ignoring the energy contents of scales larger than L_S. The extension of the Kolmogorov spectrum leads to the overestimation of the turbulent kinetic energy density and thus also the GW amplitude. The dependence between the GW spectrum and frequency is found to be $h^2\Omega_{\mathrm{GW}}(f) \propto f^{-9/2}$.

The subsequent analysis is from Kosowsky et al from 2002 [15], which instead of dimensional analysis solves the GW equation and calculates the GW spectrum in a fully analytical way. They also consider only the extended inertial range part of the spectrum and leave out the low wavenumber range of the velocity power spectrum. The source is assumed to be stationary and turned on instantly at a certain time, so that the development of turbulence is not taken into account. The decay has also been neglected, which is not the best of approximations because the turbulence is going to remain stationary only as long as the fluid is stirred and the duration of the phase transition is of course finite. Also the assumption of a

stationary source is not fully justified in cosmological context [41] and leads to the anisotropic stress power spectrum only depending on a time difference. There is also an error in the calculation, where a wrong dispersion relation has been used [28, 41]. They have set the gravitational wave oscillation frequency to the frequency of the source $\omega \propto k^{3/2}$ at the time when the turbulent source turns off, so that at later times when the GWs propagate freely, the dispersion relation differs from the usual dispersion relation $\omega = k$. They end up with $h^2\Omega_{\mathrm{GW}}(f) \propto f^{-7/2}$.

The paper by Dolgov et al 2002 [42] extends the results found in [15] by considering a more general energy spectrum instead of the standard Kolmogorov spectrum. This is achieved by introducing small deviations from the Kolmogorov case. The analysis leans heavily upon the results found in [15], so it also contains the same flaws described earlier.

The analysis by Caprini and Durrer 2006 [28] has tried to improve the previous results by also taking into account the largest scales. They also use the Kolmogorov law $P(k) \propto k^{-11/3}$ on the high-k region and intersect it with the very large scale $P(k) \propto k^2$ behaviour. The GW spectrum now covers the entire wavenumber range, but the peak amplitude of the source is still overestimated. They have also corrected the error with the dispersion relation mentioned earlier along with proposing a new way of calculating the ensemble average in a way that the time dependence of the turbulent flow is not lost. This is achieved by heuristically introducing oscillatory behaviour to the turbulent velocity field, which in turn makes the source non-stationary. They find a spectrum $h^2\Omega_{\mathrm{GW}}(f) \propto f^{-8/3}$ in the high-k range.

The paper by Gogoberidze et al from 2007 [27] revisits the case of [15] with stationary Kolmogorov turbulence, this time utilizing some methods used in aeroacoustics. Unlike the papers mentioned earlier, the analysis is carried out in real space instead of using the usual Fourier space methods. The time dependence of turbulence is modelled using the Gaussian Kraichnan time de-correlation function.

For high frequencies, they find that the spectrum behaves as $h^2\Omega_{\mathrm{GW}}(f) \propto f^{-9/2}$.

Lastly, the 2009 analysis by Caprini et al. [35] takes into account the entire wavenumber range by using the Von Kármán interpolation formula [43], which describes the power spectrum in a more realistic way and corrects the overestimation of the peak amplitude present in the previous models. They also model the source continuously so that it is not turned on and off instantly, but takes some time to build up to full power and to turn off completely. Another significant difference compared to earlier models is the inclusion of the decay of turbulence. They argue that in the case of high Reynolds number turbulence, the fluid can still remain turbulent for many Hubble times after the stirring has stopped. This means that the expansion of the universe can no longer be neglected when solving the GW equation and the source has to be treated as a long lasting one. Also, instead of using the Kraichnan de-correlator, they have opted to use the so-called top hat correlator. This is because in their case the Kraichnan function failed to produce a positive energy density spectrum, and according to them, the top hat model gives a similar behaviour to that of the Kraichnan model while still giving a positive result. They get a high frequency behaviour that goes like $h^2\Omega_{\mathrm{GW}}(f) \propto f^{-5/3}$.

4. Shock waves in the early universe

4.1 Relativistic fluid equations in linear theory

In this chapter we follow mainly [44], where it is found that under the usually assumed initial conditions for cosmological perturbations, small amplitude acoustic waves steepen and form shocks in the radiation fluid of the very early universe. We begin by writing the relativistic fluid equations in flat Minkowski spacetime. They follow from the energy-momentum conservation condition of general relativity, which states

$$\nabla_\mu T^{\mu\nu} = \partial_\mu T^{\mu\nu} = 0, \tag{4.1}$$

where ∇_μ is the covariant derivative, which reduces to partial derivative in flat space. We assume a perfect fluid, for which the energy-momentum tensor reads as

$$T^{\mu\nu} = (\rho + p)u^\mu u^\nu + p\eta^{\mu\nu}. \tag{4.2}$$

Here $u = \gamma(1, \mathbf{v})$ is the fluid 4-velocity, ρ is the energy density of the fluid and p is the hydrostatic pressure. In the rest frame the energy-momentum tensor simplifies to $T = \mathrm{diag}(\rho, p, p, p)$. Now the fluid equations can be written as

$$\partial_\mu \left((\rho + p)u^\mu u^\nu\right) + \partial_\mu \eta^{\mu\nu} p = 0. \tag{4.3}$$

The equation with $\nu = 0$ can be written in the form

$$\frac{\partial}{\partial t}\left(\gamma^2(\rho+p)\right) + \frac{\partial}{\partial x^i}\left(\gamma^2(\rho+p)v^i\right) - \frac{\partial p}{\partial t} = 0$$

$$\Rightarrow \frac{\partial p}{\partial t} - \frac{\partial}{\partial t}\left(\frac{\rho+p}{1-\mathbf{v}^2}\right) - \nabla\cdot\left(\frac{(\rho+p)\mathbf{v}}{1-\mathbf{v}^2}\right) = 0, \tag{4.4}$$

which is the relativistic counterpart of the continuity equation. In the same way we get for $\nu = i$ the three equations

$$\frac{\partial}{\partial t}\left((\rho+p)\gamma^2 v^i\right) + \frac{\partial}{\partial x^j}\left((\rho+p)\gamma^2 v^i v^j\right) + \frac{\partial p}{\partial x^i} = 0$$

$$\Rightarrow \frac{\partial p}{\partial x^i} + v^i \underbrace{\left[\frac{\partial}{\partial t}\left(\frac{\rho+p}{1-\mathbf{v}^2}\right) + \nabla\cdot\left(\frac{(\rho+p)\mathbf{v}}{1-\mathbf{v}^2}\right)\right]}_{=\partial_t p \quad (4.4)} + \frac{\rho+p}{1-\mathbf{v}^2}\left(\frac{\partial v^i}{\partial t} + \mathbf{v}\cdot\nabla v^i\right). \tag{4.5}$$

Here we have used the continuity equation to replace the contents of the square brackets in the second term. The three equations can now be combined, and rearranging gives us the relativistic form of the Euler equation

$$\frac{\partial \mathbf{v}}{\partial t} + \mathbf{v}\cdot\nabla\mathbf{v} = -\frac{1-\mathbf{v}^2}{\rho+p}\left(\nabla p + \mathbf{v}\frac{\partial p}{\partial t}\right). \tag{4.6}$$

Here, once again, the equations of motion are non-linear, making it difficult to find exact solutions. One way to simplify the equations is to study the evolution of small-amplitude perturbations. This is allowed, since according to observations, the very early radiation dominated universe is found to be nearly homogeneous and isotropic with the FLRW background. The deviations from the background grew over time but remained small during this period.

We assume Gaussian, scalar, linear, adiabatic, growing mode perturbations

$$\rho = \rho_0 + \delta\rho(t,\mathbf{x})$$

$$p = p_0 + \delta p(t,\mathbf{x}) \tag{4.7}$$

$$\mathbf{v} = \mathbf{v}_0 + \delta\mathbf{v}(t,\mathbf{x}) = \delta\mathbf{v}(t,\mathbf{x}), \tag{4.8}$$

where ρ_0, p_0 and $\mathbf{v}_0$ denote the constant background values. Here we have set $\mathbf{v_0} = 0$, because small perturbations lead to small velocities. The idea is to plug these in

to equations (4.4) and (4.6), then expand to first-order, keeping only terms, which contain exactly one perturbation or only background quantities, the so called zeroth order terms. The second order terms are deemed very small, that is $\delta\rho^2 \simeq \delta p^2 \simeq \mathbf{v}^2 \simeq \delta\rho\,\delta p \simeq \mathbf{v}\,\delta\rho \simeq \cdots \simeq 0$, which allows us to immediately drop the non-linear term in (4.6). We have also the barotropic equation of state for the radiation fluid $p = c_s^2\rho$, where $c_s = 1/\sqrt{3}$ is the speed of sound. In this case the perturbations are necessarily adiabatic, fulfilling the property $\delta p = c_s^2\delta\rho$. Lastly, we define the fractional density perturbation

$$\delta = \frac{\delta\rho}{\rho_0}. \tag{4.9}$$

We are now ready to substitute the perturbations into the continuity and Euler equations. The former yields

$$\begin{aligned} &\cancel{\frac{\partial\delta\rho}{\partial t}} - \frac{\partial\delta\rho}{\partial t} - \cancel{\frac{\partial\delta\rho}{\partial t}} - \nabla\cdot(\rho_0 + p_0)\mathbf{v} = 0 \\ &\Rightarrow \dot{\delta} = -(1+c_s^2)\nabla\cdot\mathbf{v}, \end{aligned} \tag{4.10}$$

where the dot denotes time derivative. By using the velocity potential $\mathbf{v} = \nabla\phi$, this can also be written as

$$\dot{\delta} = -(1+c_s^2)\nabla^2\phi. \tag{4.11}$$

Similar treatment of the Euler equations gives

$$\frac{\partial\mathbf{v}}{\partial t} = -\frac{1}{\rho_0 + \delta\rho + p_0 + \delta p_0}\nabla\delta p, \tag{4.12}$$

where we can do the following expansion

$$\begin{aligned} \frac{1}{\rho_0 + \delta\rho + p_0 + \delta p_0} &= \frac{1}{\rho_0 + p_0}\Big(1 + \underbrace{\frac{\delta\rho + \delta p}{\rho_0 + p_0}}_{\ll 1}\Big)^{-1} \\ &\simeq \frac{1}{\rho_0 + p_0}\Big(1 - \frac{\delta\rho + \delta p}{\rho_0 + p_0}\Big) \end{aligned} \tag{4.13}$$

and (4.12) becomes

$$\begin{aligned} \frac{\partial\mathbf{v}}{\partial t} &= -\frac{1}{\rho_0 + p_0}\nabla\delta p \\ \Rightarrow \frac{\partial\mathbf{v}}{\partial t} &= -\frac{c_s^2}{1+c_s^2}\nabla\delta. \end{aligned} \tag{4.14}$$

Substituting the velocity potential and integrating allows us to write this also as

$$\dot{\phi} = -\frac{c_s^2}{1+c_s^2}\delta. \tag{4.15}$$

To take into account the expansion of the universe, the equations can be written in comoving coordinates χ that follow the expansion of space instead of the physical proper coordinates where distances between objects grow as the universe expands. The relation between the two is

$$\mathbf{r} = \frac{a(t)}{a_0}\chi, \tag{4.16}$$

where $a(t)$ is the scale factor and $a_0 \equiv 1$ is the value of the scale factor today. To write equations (4.10) and (4.14) in comoving coordinates, one needs to transform the velocities and derivatives

$$\begin{aligned} \mathbf{v} = \dot{\mathbf{r}} &= \dot{a}\chi + a\dot{\chi} \\ &= H\mathbf{r} + a\tilde{\mathbf{u}} \end{aligned} \tag{4.17}$$

and

$$\begin{aligned} \dot{\mathbf{v}} = \ddot{\mathbf{r}} &= \ddot{a}\chi + 2\dot{a}\dot{\chi} + a\ddot{\chi} \\ &= \frac{\ddot{a}}{a}\mathbf{r} + 2\dot{a}\tilde{\mathbf{u}} + a\dot{\tilde{\mathbf{u}}}, \end{aligned} \tag{4.18}$$

where H is the Hubble parameter and $\tilde{\mathbf{u}} = \partial_t\chi$. Here we drop the large terms containing $\mathbf{r}$ because they correspond to v_0, which was taken to be zero in our expansion. The gradient transforms as

$$\nabla = \frac{1}{a}\nabla_\chi. \tag{4.19}$$

Inserting these into the perturbed continuity and acceleration equations leads to

$$\begin{cases} \dot{\delta} + (1+c_s^2)\nabla_\chi \cdot \tilde{\mathbf{u}} = 0 \\ 2\dot{a}\tilde{\mathbf{u}} + a\dot{\tilde{\mathbf{u}}} = -\dfrac{c_s^2}{1+c_s^2}\dfrac{1}{a}\nabla_\chi\delta \end{cases}. \tag{4.20}$$

The terms containing $\tilde{\mathbf{u}}$ can be eliminated by differentiating the first equation with respect to time and by taking the divergence of the second equation and then by writing $\nabla_\chi \cdot \tilde{\mathbf{u}}$ and $\nabla_\chi \cdot \dot{\tilde{\mathbf{u}}}$ in terms of δ. This leads to a second order partial differential equation for the fractional density perturbations

$$\ddot{\delta} + 2H\dot{\delta} = \frac{c_s^2}{a^2}\nabla_\chi^2 \delta. \tag{4.21}$$

The density perturbations can be expanded as a Fourier series in terms of the co-moving wavenumber k

$$\delta(t, \mathbf{x}) = \sum_{\mathbf{k}} \delta_{\mathbf{k}}(t) e^{i\mathbf{k}\cdot\chi} \tag{4.22}$$

and (4.21) becomes

$$\ddot{\delta}_{\mathbf{k}} + 2H\dot{\delta}_{\mathbf{k}} + \frac{c_s^2 k^2}{a^2}\delta_{\mathbf{k}} = 0, \tag{4.23}$$

whose exact solutions are Bessel functions and thus oscillating. Such small amplitude oscillatory motions in a compressible fluid are called sound waves, also known as acoustic waves. Indeed, if we consider very small scales (large k), the term in the middle containing H can be neglected and (4.21) reduces to

$$\frac{\partial^2 \delta}{\partial t^2} = c_s^2 \nabla^2 \delta, \tag{4.24}$$

which is the well-known wave equation. It has a simple general solution in the one dimensional case, where all quantities depend on only one coordinate x, so that we have

$$\frac{\partial^2 \delta}{\partial t^2} = c_s^2 \frac{\partial^2 \delta}{\partial x^2}. \tag{4.25}$$

To obtain the solution we move to new coordinates $u = x - c_s t$ and $v = x + c_s t$. The derivatives transform as

$$\frac{\partial}{\partial x} = \frac{\partial u}{\partial x}\frac{\partial}{\partial u} + \frac{\partial v}{\partial x}\frac{\partial}{\partial v} = \frac{\partial}{\partial u} + \frac{\partial}{\partial v} \tag{4.26}$$

$$\frac{\partial}{\partial t} = \frac{\partial u}{\partial t}\frac{\partial}{\partial u} + \frac{\partial v}{\partial t}\frac{\partial}{\partial v} = c_s\left(\frac{\partial}{\partial v} - \frac{\partial}{\partial u}\right) \tag{4.27}$$

and it follows that

$$\frac{\partial^2}{\partial x^2} = \frac{\partial^2}{\partial u^2} + 2\frac{\partial}{\partial u}\frac{\partial}{\partial v} + \frac{\partial^2}{\partial v^2} \tag{4.28}$$

$$\frac{\partial^2}{\partial t^2} = c_s^2\left(\frac{\partial^2}{\partial u^2} - 2\frac{\partial}{\partial u}\frac{\partial}{\partial v} + \frac{\partial^2}{\partial v^2}\right). \tag{4.29}$$

After inserting these into the wave equation we get

$$\frac{\partial^2 \delta}{\partial u \partial v} = 0, \tag{4.30}$$

which can be solved by integrating twice, first with respect to u and then v. The solution is

$$\begin{aligned} \delta &= F_1(u) + F_2(v) \\ &= F_1(x - c_s t) + F_2(x + c_s t), \end{aligned} \tag{4.31}$$

where F_1 and F_2 are arbitrary functions. The function F_1 represents a travelling plane wave propagated in the positive direction of the x-axis, the so-called right-moving wave. Intuitively, the function F_2 then represents left-moving plane waves and the fractional density perturbation is the sum of these two waves propagating in the opposite directions. It follows from quantum mechanics that cosmological perturbations are generated as standing waves [45] so that in the one dimensional case the initial conditions set the amplitudes and frequencies of F_1 and F_2 to be the same. When considering the full equation (4.21), the $2H\dot{\delta}$ term dampens the solutions decreasing the amplitude of the oscillations with time. The fluid equations hold only for subhorizon scales. The density perturbations on superhorizon scales change very little and remain frozen. All in all, the evolution of the perturbations is the following: After inflation the Hubble radius increases and when a mode crosses it, the mode starts to oscillate as a standing wave. The associated metric perturbations decay and after some time they die off, after which the fluid evolves as if in an unperturbed FLRW background.

4.2 Fluid equations in quadratic theory

As is done in [44], we expand the fluid equations to second order by writing the spatial stresses T^{ij} in terms of the four $T^{0\mu}$, which contain the energy and momentum densities. We also consider very small scales, so that we may neglect the expansion of the universe. From the definition of the energy-momentum tensor (4.2) with the equation of state $p = c_s^2\rho$ we have

$$T^{ij} = (1 + c_s^2)\rho u^i u^j + c_s^2 \rho \delta^{ij}. \tag{4.32}$$

In the same way

$$T^{0i} = (1 + c_s^2)\rho u^0 u^i \tag{4.33}$$

$$\Rightarrow u^i = \frac{T^{0i}}{(1 + c_s^2)\rho\gamma}. \tag{4.34}$$

We can now replace the velocities in (4.32) to express them in terms of T^{0i}. The result is

$$T^{ij} = c_s^2\rho\delta^{ij} + \frac{T^{0i}T^{0j}}{(1 + c_s^2)\rho\gamma^2}. \tag{4.35}$$

We are expanding T^{ij} to second order so we drop all terms that are more than second-order small. From (4.33) we have

$$\begin{aligned} T^{0i} = (1 + c_s^2)\rho\gamma^2 v^i &= (1 + c_s^2)\rho_0(1 + \delta + \cdots)(1 + \mathbf{v}^2 + \cdots)v^i \\ &= (1 + c_s^2)\rho_0 v^i + \text{higher order terms}, \end{aligned} \tag{4.36}$$

meaning that the first term in the expansion of T^{0i} is first-order small. Therefore, the numerator of the last term in (4.35) is already second-order small. This means we only need to take the zeroth-order term of the denominator [1]. The equation

[1] Explicitly, we can write

$$\frac{T^{0i}T^{0j}}{\rho\gamma^2} = \frac{T^{0i}T^{0j}}{\rho_0(1+\delta)}(1 - \mathbf{v}^2) \simeq \frac{T^{0i}T^{0j}}{\rho_0}(1 - \delta)(1 - \mathbf{v}^2) = \frac{T^{0i}T^{0j}}{\rho_0} + \text{3rd order terms}$$

becomes

$$T^{ij} = c_s^2 \rho \delta^{ij} + \frac{T^{0i} T^{0j}}{(1 + c_s^2)\rho_0}. \tag{4.37}$$

We still need to give the energy density ρ in terms of $T^{0\mu}$. To this end, the energy-momentum tensor can be used to write

$$T^{00} = (1 + c_s^2)\rho u^0 u^0 - c_s^2 \rho \tag{4.38}$$

and here we can use the following property of the four velocity

$$u_\mu u^\mu = \eta_{\mu\nu} u^\mu u^\nu = -1 \tag{4.39}$$

to write

$$u^0 u^0 = 1 + u^k u^k. \tag{4.40}$$

Substituting this gives

$$\begin{aligned} T^{00} &= (1 + c_s^2)(1 + u^k u^k)\rho - c_s^2 \rho \\ &= \rho + (1 + c_s^2) u^k u^k \rho, \end{aligned} \tag{4.41}$$

which can be solved for ρ as

$$\rho = \frac{T^{00}}{1 + (1 + c_s^2) u^k u^k}. \tag{4.42}$$

Here u^k is first-order small, so by expanding the denominator with $(1+x)^\alpha \simeq 1+\alpha x$ and by replacing the velocities with T^{0k} by using (4.34) we get

$$\begin{aligned} \rho &\simeq T^{00} - T^{00}(1 + c_s^2) u^k u^k \\ &= T^{00} - \frac{T^{00} T^{0k} T^{0k}}{(1 + c_s^2)\gamma^2 \rho^2}. \end{aligned} \tag{4.43}$$

We again expand the last term to second order in perturbation theory. We write T^{00} in terms of its perturbation δT^{00} as $T^{00} = \widetilde{T}^{00}(1 + \delta T^{00})$. Because $T^{0k} T^{0k}$ is already second order small, the numerator simply becomes $\widetilde{T}^{00} T^{0k} T^{0k}$ and like in expanding (4.35), we only need the zeroth-order term of the denominator. The result is

$$\rho \simeq= T^{00} - \frac{\widetilde{T}^{00} T^{0k} T^{0k}}{(1 + c_s^2)\rho_0^2}. \tag{4.44}$$

At the initial moment $\mathbf{v}$ is zero, so according to (4.36) we have $T^{0k}T^{0k} = 0$. Also by definition $\delta = 0$. Then from (4.44) it follows that $\rho_0 = \widetilde{T}^{00}$, which is the rest frame result. Inserting both to (4.37) gives us the expansion

$$T^{ij} \approx c_s^2 T^{00}\delta^{ij} + \frac{T^{0i}T^{0j} - c_s^2\delta^{ij}T^{0k}T^{0k}}{(1+c_s^2)\widetilde{T}^{00}}. \tag{4.45}$$

Now we can write the fluid equations using this result. We consider them in the one-dimensional case, which leads to

$$\partial_0 T^{0\nu} + \partial_1 T^{1\nu} = 0 \tag{4.46}$$

by using equation (4.1). This contains two equations, one for $\nu = 0$ and one for $\nu = 1$

$$\begin{cases} \partial_t T^{00} + \partial_x T^{10} = 0 \\ \partial_t T^{01} + \partial_x T^{11} = 0 \end{cases}. \tag{4.47}$$

Next, we divide both equations with $\widetilde{T}^{00}$ and use (4.45) to replace T^{11}. We also define $\Pi \equiv T^{01}/\widetilde{T}^{00}$ This yields

$$\begin{cases} \dfrac{\partial}{\partial t}\dfrac{T^{00}}{\widetilde{T}^{00}} + \dfrac{\partial \Pi}{\partial x} = 0 \\ \dfrac{\partial \Pi}{\partial t} + \dfrac{\partial}{\partial x}\left(c_s^2\dfrac{T^{00}}{\widetilde{T}^{00}} + \dfrac{T^{01}T^{01} - c_s^2 T^{01}T^{01}}{(1+c_s^2)\widetilde{T}^{00}\widetilde{T}^{00}}\right) = 0 \end{cases} \tag{4.48}$$

$$\Rightarrow \begin{cases} \dfrac{\partial}{\partial t}\dfrac{T^{00}}{\widetilde{T}^{00}} + \dfrac{\partial \Pi}{\partial x} = 0 \\ \dfrac{\partial \Pi}{\partial t} + c_s^2\dfrac{\partial}{\partial x}\dfrac{T^{00}}{\widetilde{T}^{00}} + \dfrac{1-c_s^2}{1+c_s^2}\dfrac{\partial \Pi^2}{\partial x} = 0 \end{cases}. \tag{4.49}$$

To make progress, the upper equation can be differentiated with respect to x and the lower with respect to t. Then if we multiply the upper one with c_s^2, we notice that it can be used to eliminate the term containing T^{00} in the lower equation, which results in the following second order differential equation

$$\frac{\partial^2 \Pi}{\partial t^2} - c_s^2\frac{\partial^2 \Pi}{\partial x^2} + \frac{1-c_s^2}{1+c_s^2}\frac{\partial^2 \Pi^2}{\partial t \partial x} = 0. \tag{4.50}$$

Here we recognize the first two terms as the wave equation but this time we also have an additional second order term. Thus, we expect the solutions to be plane waves with some additional behaviour caused by this term. To solve the equation for Π, it might be useful to write it again in terms of the coordinates $u = x - c_s t$ and $v = x + c_s t$. We have already transformed the second derivatives of x and t in the previous section, giving us the results (4.28) and (4.29). The cross term follows from (4.26) and (4.27) as

$$\frac{\partial^2}{\partial t \partial x} = c_s \left(\frac{\partial^2}{\partial v^2} - \frac{\partial^2}{\partial u^2} \right) \tag{4.51}$$

and the equation in u and v coordinates becomes

$$-4c_s^2 \frac{\partial^2 \Pi}{\partial u \partial v} + \frac{1 - c_s^2}{1 - c_s^2} c_s \left(\frac{\partial^2}{\partial v^2} - \frac{\partial^2}{\partial u^2} \right) \Pi^2 = 0. \tag{4.52}$$

We define the constant

$$\kappa = \frac{2c_s(1 + c_s^2)}{1 - c_s^2}, \tag{4.53}$$

which leads to

$$2\kappa \frac{\partial^2 \Pi}{\partial u \partial v} + \left(\frac{\partial^2}{\partial u^2} - \frac{\partial^2}{\partial v^2} \right) \Pi^2. \tag{4.54}$$

This is the equation describing the evolution of Π in the aforementioned coordinate system. With a small simplification, it can be used to obtain Burgers' equation.

4.3 Burgers' equation

We consider right-moving linearized waves $\Pi^{(1)}(u)$[2]. In this case, the term containing the double derivative with respect to v can be neglected, as it is a lot smaller than

[2]We can write $\Pi = \Pi^{(1)} + \Pi^{(2)} + \Pi^{(3)} + \cdots$, where $\Pi^{(1)}$ is the first-order term etc. We drop all the other terms and only consider the first-order term, that is $\Pi = \Pi^{(1)}$, unless otherwise stated. This way the equations remain second-order small in perturbation theory.

the corresponding term with u. The equation can now be integrated to obtain

$$\int \frac{\partial}{\partial u}\left(2\kappa\frac{\partial \Pi}{\partial v}+\frac{\partial \Pi^2}{\partial u}\right) du = 0$$

$$\Rightarrow \kappa\frac{\partial \Pi}{\partial v}+\Pi\frac{\partial \Pi}{\partial u}=0. \tag{4.55}$$

This first-order quasilinear partial differential equation is known as Burgers' equation. Like other equations of its kind, it can be solved by using the method of characteristics.

The solution $\Pi(u,v)$ represents the solution surface $(u,v,\Pi(u,v))$ embedded in $\mathbb{R}^3$. The solution surface can also be represented by a level surface $f(u,v,\Pi)=0$ with a suitable function $f(u,v,z)$. In this case we have $f(u,v,\Pi)=\Pi(u,v)-\Pi$. The surface in question fulfils

$$df=\frac{\partial f}{\partial u}du+\frac{\partial f}{\partial v}dv+\frac{\partial f}{\partial z}d\Pi=0. \tag{4.56}$$

Here Π is a function of u and v, so we can write

$$d\Pi=\frac{\partial \Pi}{\partial u}du+\frac{\partial \Pi}{\partial v}dv, \tag{4.57}$$

which gives

$$\left(\frac{\partial f}{\partial u}+\frac{\partial f}{\partial z}\frac{\partial \Pi}{\partial u}\right)du+\left(\frac{\partial f}{\partial v}+\frac{\partial f}{\partial z}\frac{\partial \Pi}{\partial v}\right)dv=0. \tag{4.58}$$

As a result

$$\frac{\partial \Pi}{\partial u}=\frac{\partial f}{\partial u}\Big/\frac{\partial f}{\partial z} \tag{4.59}$$

and

$$\frac{\partial \Pi}{\partial v}=\frac{\partial f}{\partial v}\Big/\frac{\partial f}{\partial z}. \tag{4.60}$$

Inserting these into Burgers' equation (4.55) gives

$$\kappa\frac{\partial f}{\partial v}+\Pi\frac{\partial f}{\partial u}=0. \tag{4.61}$$

We define a vector $\mathbf{a}=(\Pi,\kappa,0)$ and note that in these coordinates $\nabla=(\partial_u,\partial_v,\partial_z)$, so the equation can be written in the form

$$\mathbf{a}\cdot\nabla f=0. \tag{4.62}$$

From the properties of gradient it follows that ∇f is normal to the solution surface at every point on the surface. What this means is that the vector **a** must be a tangent vector of the solution surface. This, by definition, makes $f(u, v, \Pi) = 0$ an integral surface, which is determined by a family of so-called integral curves that sit in the solution surface. These integral curves are also known as characteristics. The vector **a** is the tangent vector of a characteristic curve

$$\frac{d\mathbf{r}(\tau)}{d\tau} = \mathbf{v}\left(\mathbf{r}(\tau)\right), \tag{4.63}$$

where τ is used to parametrize the curve. From these one gets the characteristic equations

$$\begin{aligned} \frac{du}{d\tau} &= \Pi \\ \frac{dv}{d\tau} &= \kappa \\ \frac{d\Pi}{d\tau} &= 0, \end{aligned} \tag{4.64}$$

where the last one immediately gives $\Pi = const \equiv C_1$, meaning that Π remains constant along the characteristic curve. The two remaining equations can be combined to get

$$d\tau = \frac{dv}{\kappa} = \frac{du}{\Pi}, \tag{4.65}$$

which can be solved easily by integrating both sides now that we can treat Π as constant. The solution is

$$u = \frac{\Pi v}{\kappa} + C_2. \tag{4.66}$$

We now have two surfaces $C_1 = \Pi \equiv \phi_1$ and $C_2 = u - \Pi v/\kappa \equiv \phi_2$, whose intersection is the characteristic curve. Therefore in this case the characteristics are straight lines in the u, v-plane. Any smooth surface composed of characteristic curves is a solution of Burgers' equation and the equation for the surface is found by expressing C_1 in terms of C_2. The general solution of (4.55) can be written as

$$G(C_1, C_2) = G(\phi_1, \phi_2) = 0, \tag{4.67}$$

where G is an arbitrary function. This equation can be written in another way by expressing ϕ_1 in terms of an arbitrary function of ϕ_2 as

$$\phi_1 = F(\phi_2), \tag{4.68}$$

or

$$\Pi(u, v) = F\left(u - \frac{\Pi v}{\kappa}\right). \tag{4.69}$$

Let us now impose the initial condition $\Pi(u, 0) = F(u)$, which specifies the shape of the plain wave at $v = 0$. Then the solution of Burgers' equation (4.55) can be solved after specifying the function $\Pi(u, 0)$ from the equation

$$\Pi(u, v) = F\left(u - \frac{\Pi(u, v)v}{\kappa}\right), \tag{4.70}$$

which is only possible analytically in some simple cases.

The steepening of waves is a distinctive feature of Burgers' equation. The wave speed increases with increasing amplitude so that peaks with positive Π move to right and vice versa. Because the peaks move the fastest, eventually they overtake the rest of the pulse leading to the breaking of the waveform. After this moment, called the breaking time, the solutions would become multivalued with three different values of Π corresponding to some u, which represents an unphysical situation. It is said that a discontinuity, or a shock wave, is formed and the wave ceases to be a simple wave. Therefore, after the breaking time the evolution of the wave is no longer governed by Burgers' equation. To determine the evolution of the fluid after breaking, one would have to make use of the local conservation laws.

Shock waves dissipate energy, leading to a damping of the wave. This is apparent, for if one were to continue the bending of the wave after breaking, the height of the profile would decrease leading to a smaller amplitude. The dissipation of energy signifies an increase in the entropy, making the motion irreversible. This is in contrast with the perfect fluid description where entropy is conserved and the dynamics is reversible, which leads to a manifestation of effects forbidden by the

fluid equations. One such effect is the generation of vorticity in the fluid. The increase in entropy also makes it possible to reach the maximum entropy state, corresponding to thermal equilibrium. These effects could be of some importance in solving certain early universe puzzles, such as baryogenesis and the generation of primordial magnetic fields. Lastly, shock collisions also generate gravitational waves, whose contribution to the stochastic gravitational wave background is estimated in [44].

4.4 Steepening of acoustic waves

The breaking time can be determined by looking at the derivative of Π with respect to u. The waves steepen under Burgers' equation and become multivalued right after the moment of breaking. Therefore, the breaking time corresponds to the moment where the derivative $\partial_u \Pi$ becomes infinite. Differentiating the general solution (4.70) with respect to u gives

$$\frac{\partial \Pi}{\partial u} = \frac{\partial F(\phi_2)}{\partial \phi_2} \left(1 - \frac{v}{\kappa} \frac{\partial \Pi}{\partial u} \right). \tag{4.71}$$

We can now solve this for $\partial_u \Pi$. After introducing the notation $\partial_{\phi_2} F(\phi_2) \equiv F'(\phi_2)$ we get

$$\frac{\partial \Pi}{\partial u} = \frac{F'(\phi_2)}{1 + \frac{v}{\kappa} F'(\phi_2)}. \tag{4.72}$$

Thus, the derivative diverges when

$$v \to -\frac{\kappa}{F'(\phi_2)}. \tag{4.73}$$

The same result can be obtained by looking at the characteristics. As mentioned earlier, the characteristics are straight lines in the case of Burgers' equation and from (4.66) we observe that the slope Π/κ can differ between characteristics, making it possible for the characteristics to intersect. This corresponds to the moment where the solution becomes discontinuous. To find the breaking time we need to determine

the time at which the characteristic lines first intersect. From (4.66) it follows that $u(v=0) = C_2 \equiv u_0$ and because Π stays constant along the characteristic line, we can write it by using the designated initial condition as $\Pi(u_0, 0) = F(u_0)$. Now the characteristic line can be written in the form $u = F(u_0)v/\kappa + u_0$. Next, consider two characteristic lines $u = F(u_1)v/\kappa + u_1$ and $u = F(u_2)v/\kappa + u_2$ with $u_2 > u_1$. Their intersection can be found from

$$\frac{F(u_1)v}{\kappa} + u_1 = \frac{F(u_2)v}{\kappa} + u_2 \tag{4.74}$$

and solving for v gives

$$\begin{aligned} v &= \frac{\kappa(u_2 - u_1)}{F(u_1) - F(u_2)} \\ &= -\frac{\kappa}{\frac{1}{u_2-u_1}(F(u_2) - F(u_1))} \\ &= -\frac{\kappa}{\frac{1}{u_2-u_1}\int_{u_1}^{u_2} F'(u)\,du} \\ &= -\frac{\kappa}{F'(\xi)}, \end{aligned} \tag{4.75}$$

which is the same result as (4.73) apart from the naming convention of the variable $\xi \in]u_1, u_2[$. In the last step we have used the first mean value theorem for definite integrals. Because the initial condition is set at $v = x + c_s t = 0$, v increases with time and is always positive. Thus, divergences of the derivative only form on intervals where $F'(\xi) < 0$, that is, on the intervals where the wave is decreasing. To get the moment of shock formation, we have to solve (4.75) for the smallest possible value of v.

We assume the fractional density perturbation to be a standing wave

$$\begin{aligned} \delta &= -\sqrt{2}\epsilon \sin(kx)\cos(kc_s t) \\ &= -\frac{\sqrt{2}\epsilon}{2}\left[\sin(kx + kc_s t) + \sin(kx - kc_s t)\right] \\ &= -\frac{\epsilon}{\sqrt{2}}\left[\sin(kv) + \sin(ku)\right], \end{aligned} \tag{4.76}$$

where we have decomposed it into left- and right-moving waves. We only consider right-moving waves so to first order in perturbation theory δ reads

$$\delta^{(1)} = -\frac{\epsilon}{\sqrt{2}}\sin(ku). \tag{4.77}$$

The linearised Euler and continuity equations (4.15) and (4.11) can now be used to determine $\Pi^{(1)}$. Using equation (4.36), we can relate $\Pi^{(1)}$ to the velocity potential as follows:

$$\begin{aligned}\Pi^{(1)} &= \frac{T^{01(1)}}{\tilde{T}^{00}} = \frac{(1+c_s^2)\cancel{\rho_0}v}{\cancel{\tilde{T}^{00}}} \\ &= (1+c_s^2)\frac{\partial\phi}{\partial x}.\end{aligned} \tag{4.78}$$

On the last line we have used $\mathbf{v} = \nabla\phi$ in one dimensional case. Using this relation to replace the velocity potential in (4.11) gives

$$\frac{\partial\delta^{(1)}}{\partial t} = -\frac{\partial\Pi^{(1)}}{\partial x} \tag{4.79}$$

and furthermore, transforming the derivatives

$$\frac{\partial}{\partial x} = \frac{\partial u}{\partial x}\frac{\partial}{\partial u} = \frac{\partial}{\partial u}, \qquad \frac{\partial}{\partial t} = \frac{\partial u}{\partial t}\frac{\partial}{\partial u} = -c_s\frac{\partial}{\partial u} \tag{4.80}$$

leads to

$$\frac{\partial}{\partial u}\left(\Pi^{(1)} - c_s\delta^{(1)}\right) = 0. \tag{4.81}$$

Now, integrating once in u gives us the result

$$\Pi^{(1)} = c_s\delta^{(1)} = -\frac{c_s\epsilon}{\sqrt{2}}\sin(ku). \tag{4.82}$$

We treat this as the initial waveform, which means

$$\Pi(u,0) = F(u) = -\frac{c_s\epsilon}{\sqrt{2}}\sin(ku) \tag{4.83}$$

and the general solution (4.70) takes the form

$$\Pi(u,v) = F\left(u - \frac{\Pi(u,v)v}{\kappa}\right) = \frac{c_s\epsilon}{\sqrt{2}}\sin\left[k\left(u - \frac{\Pi(u,v)v}{\kappa}\right)\right]. \tag{4.84}$$

It is evident that $\Pi(u, v)$ cannot be solved from this equation analytically. To illustrate the steepening, one would have to develop the function numerically as is done in figure 4.1. However, we can determine the moment of shock formation from (4.73). With $\phi_2 = u - \Pi v/\kappa$

$$F'(\phi_2) = \frac{-c_s\epsilon}{\sqrt{2}} k \cos(k\phi_2) \tag{4.85}$$

and substituting this into the equation for the breaking time yields

$$v = \frac{\sqrt{2}\kappa}{\epsilon c_s k \cos(k\phi_2)}. \tag{4.86}$$

The smallest value of v is obtained when the denominator receives its largest value, that is

$$\cos(k\phi_2) = 1 \quad \Rightarrow \quad k\phi_2 = 2\pi n, \quad n \in \mathbb{Z}. \tag{4.87}$$

Then $\Pi = -2^{(-1/2)} c_s \epsilon k \sin(2\pi n) = 0$ and we get $ku = 2\pi n$. This tells us the breaking points on the u-axis. At these points in this particular case, the steepness of the curves is the same at every moment of time, so derivatives diverge at the same time on 2π intervals. Thus, we can choose $n = 0$, which leads to $u = 0 \Rightarrow x = c_s t$. Then $v = 2c_s t$ and (4.86) becomes

$$t = \frac{\kappa}{\sqrt{2}\epsilon c_s^2 k}. \tag{4.88}$$

Plugging in κ and $c_s = 1/\sqrt{3}$ gives the time scale for shock formation

$$k c_s t \epsilon = \sqrt{8}, \tag{4.89}$$

or in terms of the number of oscillation periods

$$\frac{t}{T} = \frac{\sqrt{2}}{\pi\epsilon}, \tag{4.90}$$

where $T = 2\pi/kc_s$.

The wave steepening can also be seen in perturbation theory. Looking at Π around $u = 0$ allows us to expand the sine in (4.84) with $\sin(a - x) = \sin(a) -$

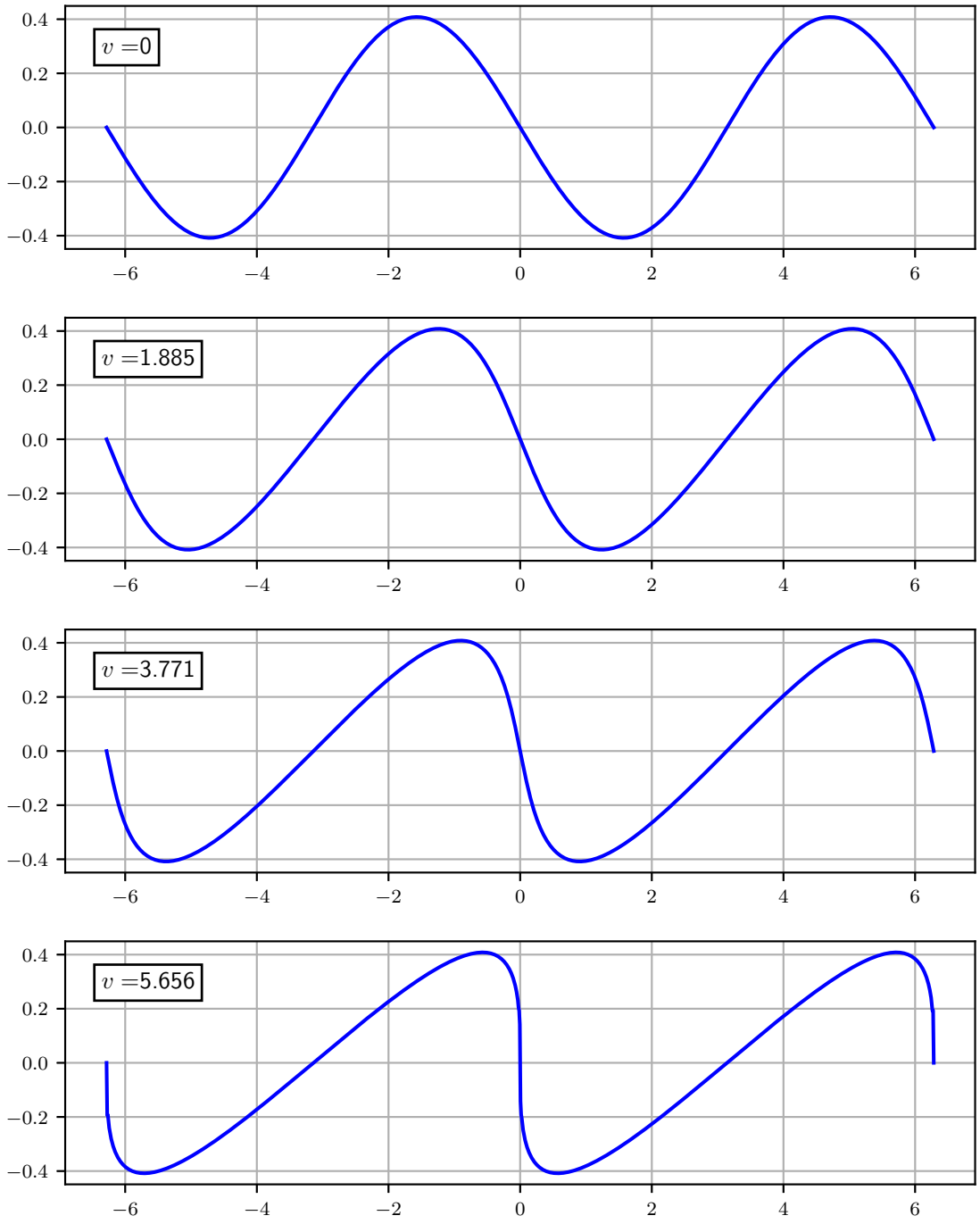

Figure 4.1: Steepening of a sine wave $\Pi(u)$ in Burgers' equation. The initial wave is taken to be that of equation (4.83) with $k = \epsilon = 1$ and $c_s = 1/\sqrt{3}$. Shocks form when $v = 4\sqrt{2} \approx 5.66$, corresponding to $t = 2\sqrt{6} \approx 4.90$, or after $\sqrt{2}/\pi \approx 0.45$ oscillation periods.

$x\cos(a) + \mathcal{O}(x^2)$. The result is

$$\Pi(u,v) \simeq -\frac{c_s\epsilon}{\sqrt{2}}\left[\sin(ku) - \frac{\Pi^{(1)}vk}{\kappa}\cos(ku)\right], \tag{4.91}$$

where on the right-hand side of the equation we use the first-order result recursively. The equation can now be written in the form $\Pi(u,v) = \Pi^{(1)} + \Pi^{(2)}$ with

$$\begin{aligned}\Pi^{(2)} &= -\frac{c_s^2\epsilon^2 vk}{2\kappa}\sin(ku)\cos(ku)\\ &= -\frac{c_s^2\epsilon^2 vk}{4\kappa}\sin(2ku).\end{aligned} \tag{4.92}$$

Now the gradient becomes

$$\frac{\partial\Pi}{\partial u} = -\frac{c_s\epsilon k}{\sqrt{2}}\left[\cos(ku) + \frac{c_s\epsilon kv}{\sqrt{2}\kappa}\cos(2u)\right]. \tag{4.93}$$

In order to see what happens to the gradient at the moment of breaking, we put in the corresponding values $u = 0$ and $v = \sqrt{2}\kappa/(c_s\epsilon k)$. This gives

$$\frac{\partial\Pi}{\partial u} = -\frac{c_s\epsilon k}{\sqrt{2}}(1+1), \tag{4.94}$$

so the second-order term equals the first-order term at the time of breaking.

5. Burgers' turbulence

5.1 Numerical method

In the last chapter it was established that small amplitude waves in the very early universe steepen and form shocks. Next the following question can be presented: How do power spectra evolve in Burgers' equation and what kind of power laws, if any, do they form at the time of breaking? In order to answer this question, we can consider various power spectra numerically and impose random initial conditions. Such a study of Burgers' equation with random solutions is known as Burgers' turbulence or "burgulence" [46].

We consider the one-dimensional case with the linear $\Pi(u, v)$ of Chapter 4. Then, the power spectrum can be defined as

$$P(k) = |\Pi(k)^2|. \tag{5.1}$$

A similar equation follows from the calculation in equations (3.65) - (3.67) in one-dimensional case with $k = k'$ for $u(k)$, which is the velocity in Fourier space. From the definition of Fourier transform and equation (4.36), it follows that $\Pi(k) \propto u(k)$ and $P(k) \propto |u(k)^2|$, so these two definitions of the power spectra differ only by a prefactor. It is however important to note that the turbulence considered in chapters 2 & 3 is governed by the Navier-Stokes equation, where small changes in the initial conditions can lead to vastly different outcomes at later times, which is one of the most important properties of turbulence. Burgers' equation does not have this

property because the equation can be integrated explicitly, as shown by Hopf and Cole in the 1950s[1] [47, 48]. Therefore, it is not a good model for fluid turbulence but can be used as a model for one-dimensional compressible fluids, at least until the moment of shock formation. For these reasons, the power laws are going to be different compared to those of regular fluid turbulence.

The starting point is defining the initial power spectrum $P(k)$. The corresponding $\Pi(k)$ fulfilling (5.1) can be written as

$$\Pi(k) = \sqrt{P(k)}e^{i\phi_k}, \tag{5.2}$$

where ϕ_k is a phase in the complex plane corresponding to a certain value of k. Different phases correspond to different waveforms in real space and thus to random initial conditions to Burgers' equation. The phases are given randomly in such a way that the inverse Fourier transform is real. This is true when $\phi_k = -\phi_{-k}$. The inverse transform yields $\Pi(u)$ and it can then be plugged into Burgers' equation. The numerical method used here is the simple forward Euler method, where the partial derivative with respect to v is written as

$$\frac{\partial \Pi}{\partial v} \approx \frac{\Pi(u, v + \Delta v) - \Pi(u, v)}{\Delta v} \tag{5.3}$$

and the u-derivative is approximated by using a second order accurate central difference

$$\frac{\partial \Pi}{\partial u} \approx \frac{\Pi(u + \Delta u, v) - \Pi(u - \Delta u, v)}{2\Delta u}. \tag{5.4}$$

With these, solving Burgers' equation for $\Pi(u, v + \Delta v)$ gives the scheme

$$\Pi(u, v + \Delta v) = \Pi(u, v) - \frac{\Delta v}{2\kappa \Delta u}\Pi(u, v)\Big[\Pi(u + \Delta u, v) - \Pi(u - \Delta u, v)\Big]. \tag{5.5}$$

On the boundaries, we impose periodic boundary conditions.

[1] This is true both in viscid and inviscid cases. More information about the viscid Burgers' equation in section 5.3.

The method remains stable as long as the latter term remains small, that is $\Delta v \ll \Delta u \ll 1$, where Δu is the stepsize of u. For the sake of simplicity, the factor κ is set to unity from here on. The process is repeated until the moment of breaking v_s, determined by equation (4.73), is reached. Now the wave $\Pi(u, v_s)$ can be transformed back into Fourier space and the power spectrum at the moment of breaking is found by taking the absolute value and raising it to the power of two. The power spectra are plotted on a log-log scale, where power laws appear as straight lines. All in all, the method is as follows:

1. Specify the power spectrum $P(k) = |\Pi(k)|^2$.
2. Solve $\Pi(k) = \sqrt{P(k)}$ and give it random phases corresponding to random initial conditions.
3. Perform an inverse Fourier transform to real space.
4. Evolve $\Pi(u)$ in Burgers' equation using the Eq. (5.5) iteratively with periodic boundary conditions and stop when a shock is formed at v_s.
5. Perform a Fourier transform to obtain $\Pi(k, v_s)$.
6. Calculate and plot the power spectrum $P(k, v_s)$ on a log-log scale and calculate the slope to obtain the power law.

The Python code used to obtain the data used in the following section can be found in the appendix. We use dimensionless variables because we are only interested in the emerging power laws.

5.2 Results

First, let us consider a couple of simple cases starting in real space by defining $\Pi(u)$. What would the corresponding power spectrum look like at the time of breaking, if

$\Pi(u)$ were taken to be a sine wave like in figure 4.1? The result is found in figure (5.1), plotted on a log-log scale. Initially at $v = 0$, the spectrum has a delta spike at $k = 1$, as is expected because the Fourier transform of sine is a sum of two delta spikes, one of which is located on the positive k-axis. As the wave steepens, more spikes appear and at the moment of breaking $v_s \approx 1.414$, the tips of the spikes seem to align in the high-k-range, indicating a power law.

Next, the initial wave is taken to be a simple Gaussian function of the form

$$\Pi(u) = e^{-\frac{u^2}{2}} \tag{5.6}$$

and its evolution and power spectra are found in figures 5.2 and 5.3 respectively. As the Gaussian steepens, its Fourier transform, which is also a Gaussian, widens near the base, leading to an increase in the area under the curve. At the time of breaking, a clear power law emerges in the inertial range at roughly $2 < k < 900$. Fitting a straight line in the said range gives a slope of -2.6623, corresponding to a power law $P(k) \propto k^{-2.6623}$.

Now that we know more or less what to expect, let us move to the method presented in the previous section, where we begin with a power spectrum in the spectral space and make use of random initial conditions. The power spectrum chosen is

$$P(k) = A\frac{\left(\frac{|k|}{k_0}\right)^{\beta}}{\left[1 + \left(\frac{|k|}{k_0}\right)^{\alpha}\right]^{\gamma}}. \tag{5.7}$$

with β, α, γ and k_0 positive.The asymptotic behaviour of the power spectrum goes like $P(k) \simeq k^{\beta-\alpha\gamma}$ when $k \to \infty$, so in order to make sure it decreases to zero at infinity, we must have $\beta < \alpha\gamma$. Then the spectrum has the desired form, where $P(0) = 0$ and as k increases, the spectrum increases until a maximum is reached, after which it decreases asymptotically to zero. The constant k_0 can be used to adjust the width of the spectrum.

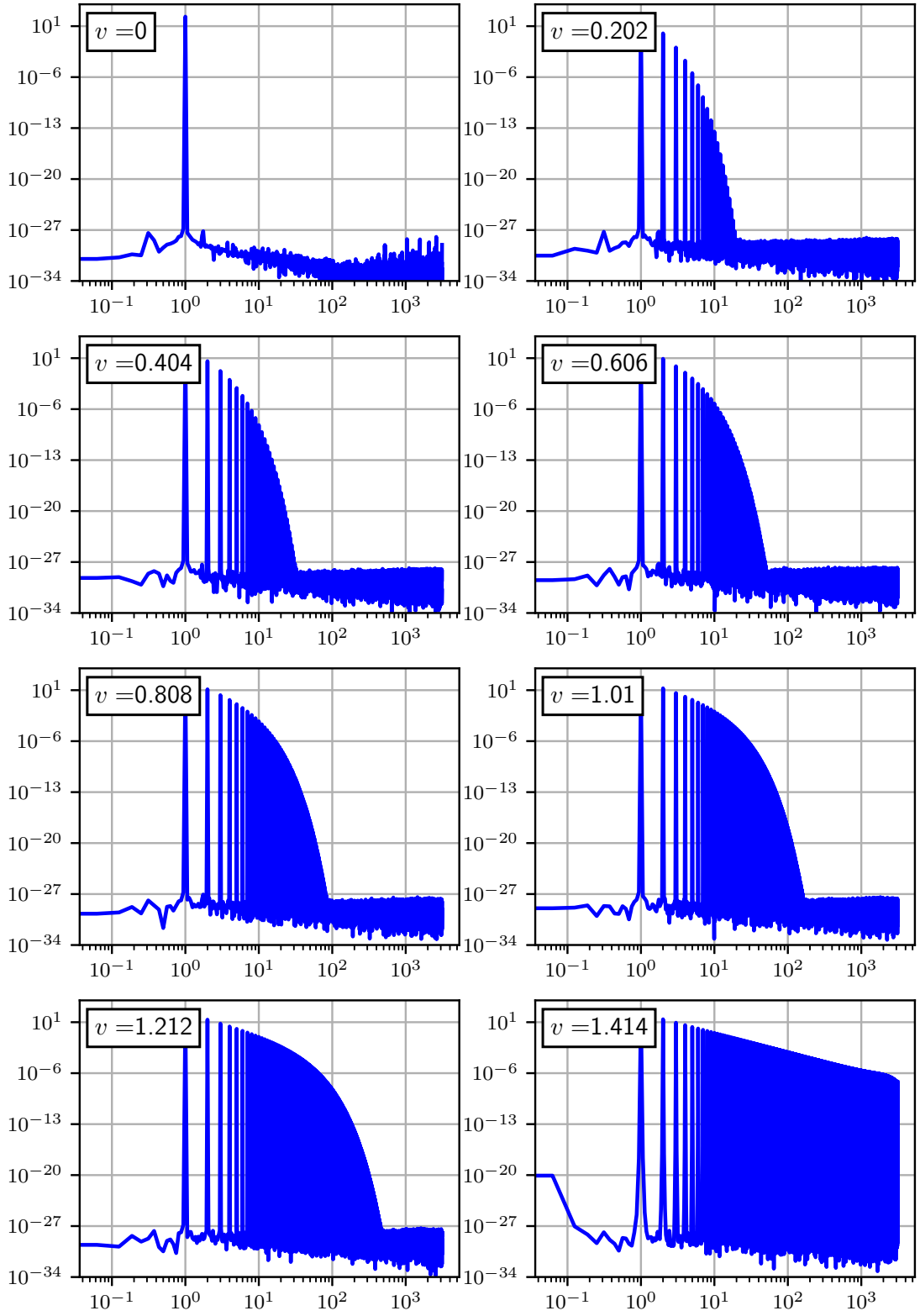

Figure 5.1: The power spectrum $P(k)$ for $\Pi(u) = \sin(u)/\sqrt{2}$. The size of the box is $-32\pi < u < 32\pi$ with stepsizes $\Delta v = 10^{-6}$ and $\Delta u \approx 2 \cdot 10^{-3}$. The graph on the bottom right is plotted at the breaking time and by taking two delta spike tips, a quick back-of-the-envelope calculation gives a slope of about -2.62.

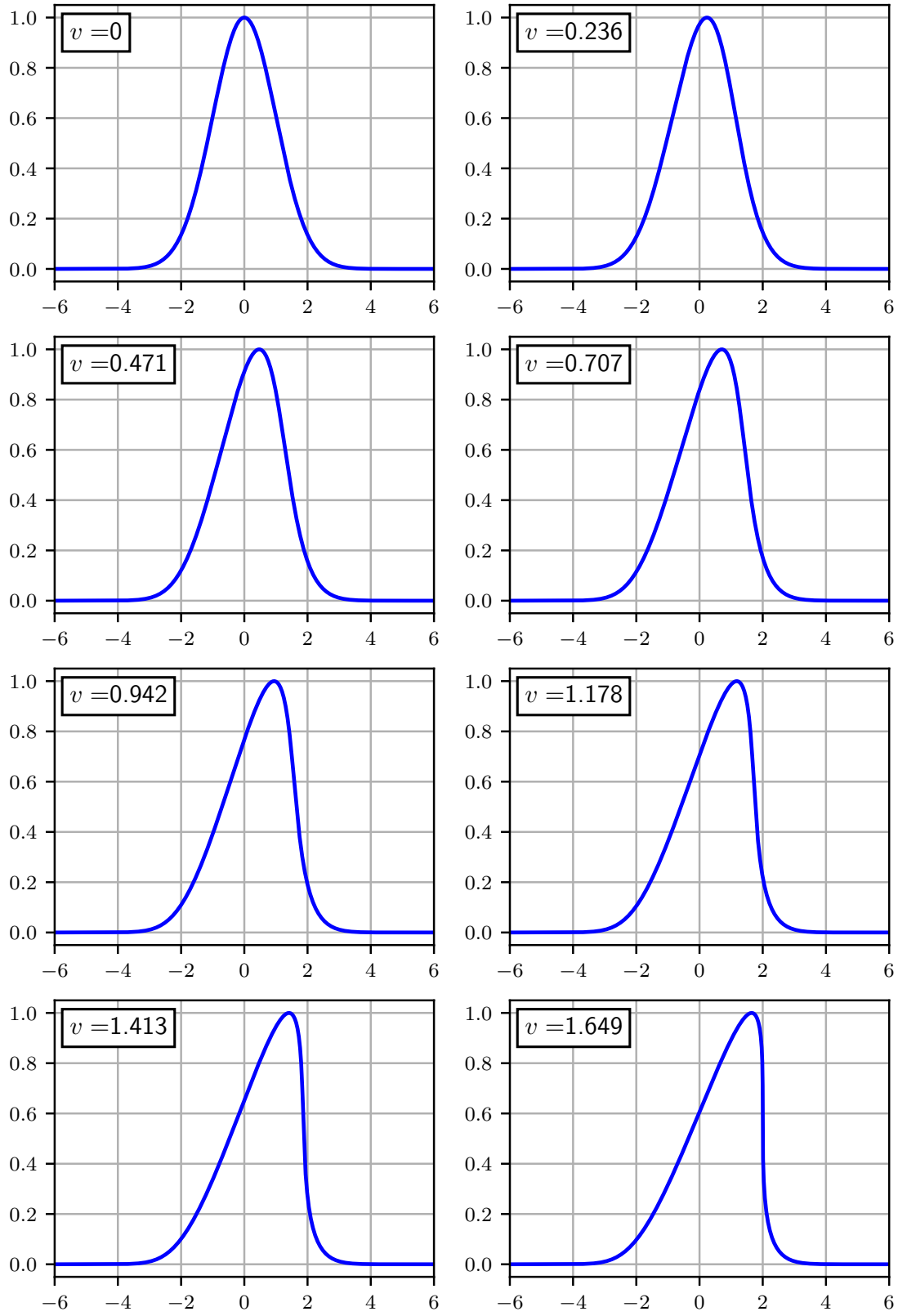

Figure 5.2: The steepening of $\Pi(u)$ of equation (5.6) under Burgers' equation with a box size of $-100 < u < 100$ and $\Delta u = 10^{-3}$, $\Delta v = 10^{-6}$. The graphs are zoomed in to better show the steepening. Corresponding power spectra are found in figure 5.3.

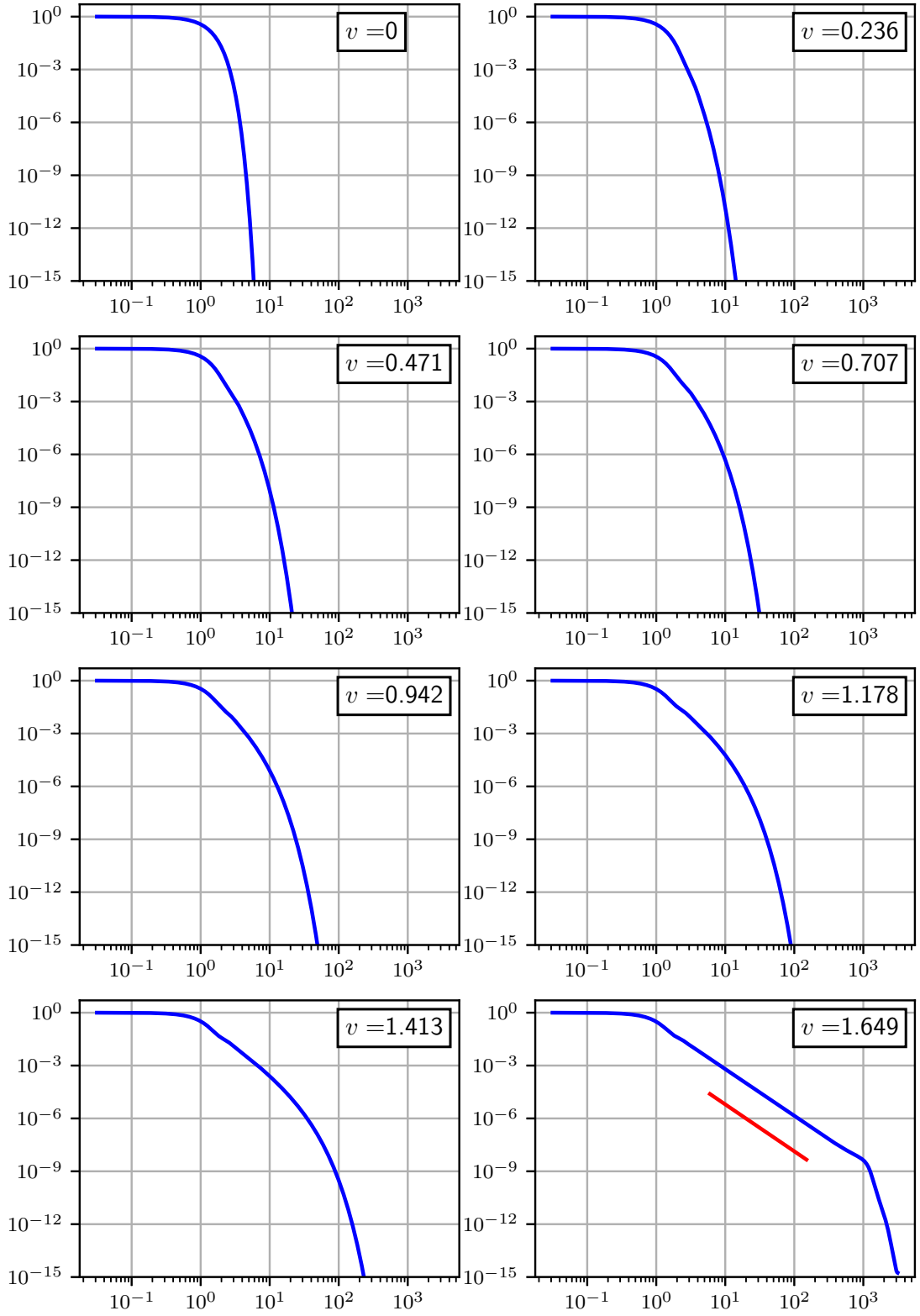

Figure 5.3: The power spectra $P(k)$ for figure 5.2. Linear fit in the inertial range at the time of breaking (red line) gives a slope of -2.6623.

The simulation is very sensitive to certain parameters, especially the size of the simulation box, the stepsizes in u and v, the constant A in (5.7) and the width of the spectrum determined by k_0, so finding a good balance is important to keep the solutions stable under the somewhat fickle Euler method. Increasing the box size makes the computation take considerably longer but increases the resolution in Fourier space, making the spectrum smoother. Other factors affecting the computation time are the stepsizes. There are some distortion effects at breaking time around the point at which the derivative diverges because the Euler method doesn't handle large values very well. To minimize the distortions, Δu should be relatively small. The one used in this chapter is either $\Delta u \approx 10^{-3}$ or $\Delta u \approx 10^{-4}$, and to maintain stability, Δv is chosen to be at least about two order of magnitudes smaller. The computation times can now be made reasonable by fine tuning the coefficient A because it reduces the value of v_s, making the program reach the moment of shock formation sooner. However, increasing A also increases the magnitude of the non-linear term in (5.5), as it goes like A^2 instead of A, like the linear last term. In other words, increasing A too much can make the program unstable.

To begin with, we first consider cases with $k_0 = 1$. In case of figures 5.4, 5.5 and 5.6 we have chosen $A = 500$, $\beta = 2$. $\alpha = 5$, $\gamma = 9/2$, $\Delta u \approx 10^{-3}$ and $\Delta v = 10^{-6}$ with a box size of $-100 < u < 100$. The computation ended up taking a couple of hours on a regular computer. The random initial wave can be seen in figure 5.4. While it is not easy to see the steepening on this scale, it still gives us a good idea of what kind of waves appear as a result of the random phases given to $\Pi(k)$. The evolution of the power spectrum is seen in figure 5.5 and figure 5.6 contains the power spectrum at the time of breaking. Again, there's a clear power law and a linear fit gives a value -2.6542.

Changing the values a bit gives the figures 5.7 and 5.8. The parameters used are $A = 1000$, $\beta = 4$. $\alpha = 8$, $\gamma = 6$ with the same stepsizes and box size as

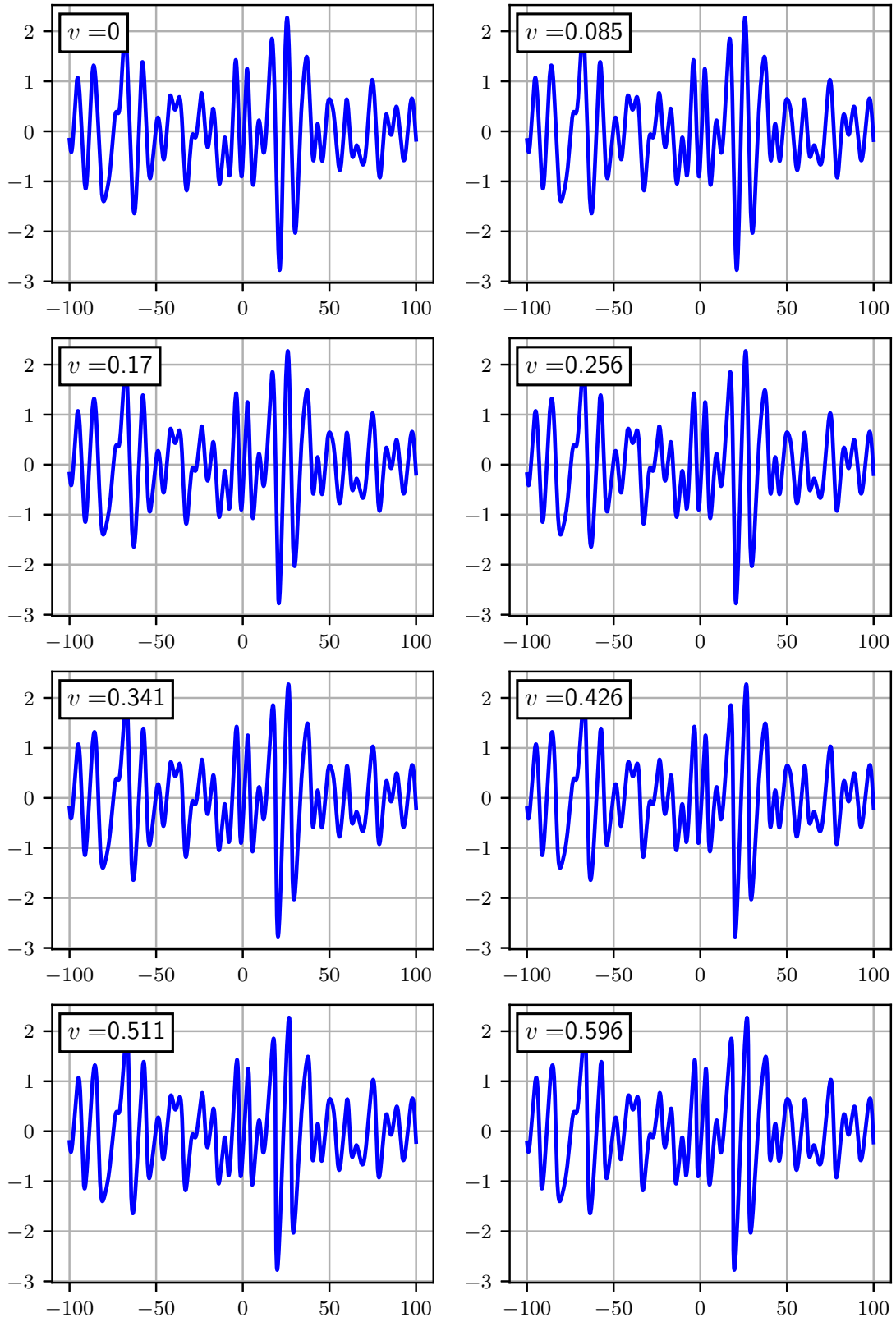

Figure 5.4: Evolution of the wave $\Pi(u)$ corresponding to an initial power spectrum of equation (5.7) with $A = 500$, $\beta = 2$. $\alpha = 5$, $\gamma = 9/2$, $\Delta u \approx 10^{-3}$,$\Delta v = 10^{-6}$ and $k_0 = 1$.

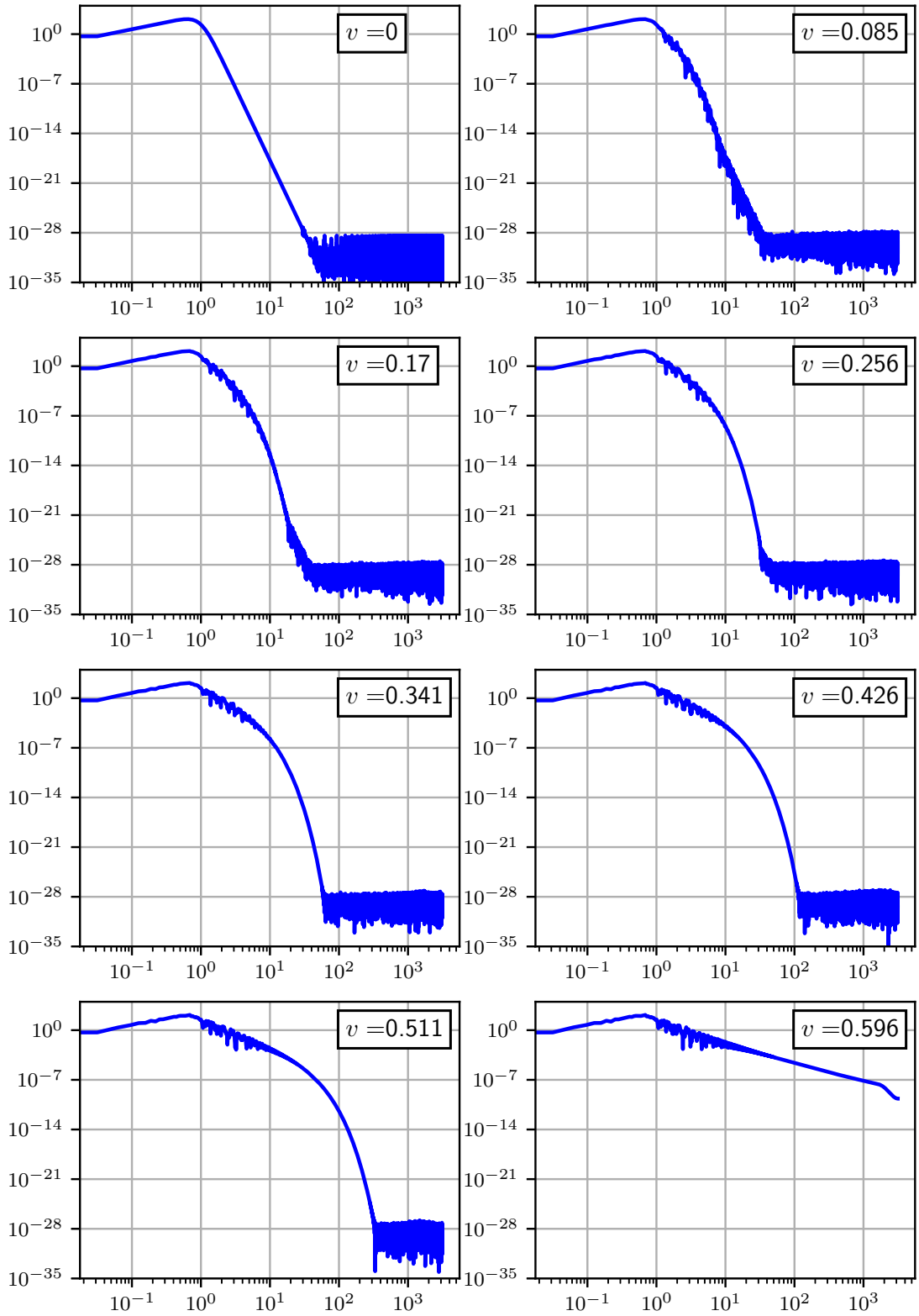

Figure 5.5: Evolution of the power spectrum $P(k)$ in the case of figure 5.4.

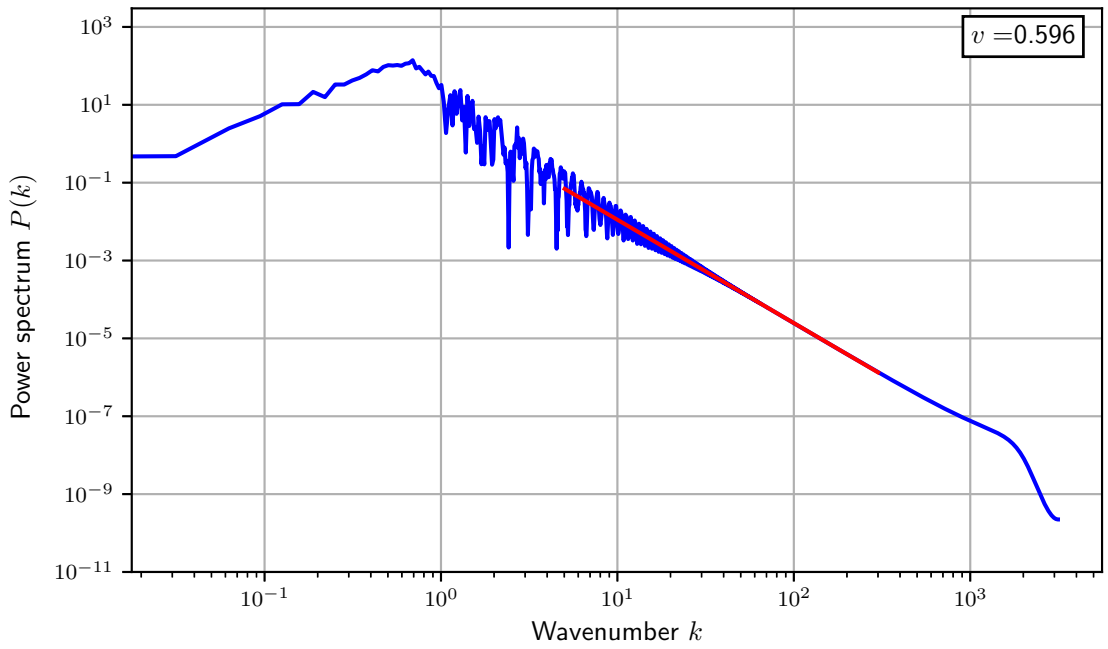

Figure 5.6: The power spectrum of figure 5.5 at the time of shock formation. The slope in the inertial range is found to be about -2.6542.

previously. This time linear fit in the inertial range results in a power law of around -2.6654.

Increasing the width of the power spectrum by increasing the value of k_0 leads to the reduction of the breaking time v_s but also makes the wave in real space denser. The problem is that even with a value as small as $k_0 = 10$, the wave becomes very cramped, meaning that it is necessary to reduce the stepsize of u even further in order to get accurate and stable results, which could also lead to reduction in the stepsize of v. This could make the computation take a very long time. One way to overcome this problem is to reduce the size of the box, meaning that in a sense we are looking at a smaller part of the wave. The price to pay is the reduced accuracy in the Fourier space but this is somewhat compensated by making the spectrum wider in the first place.

Let us put $k_0 = 10$ while keeping α, β and γ the same. The reduction in com-

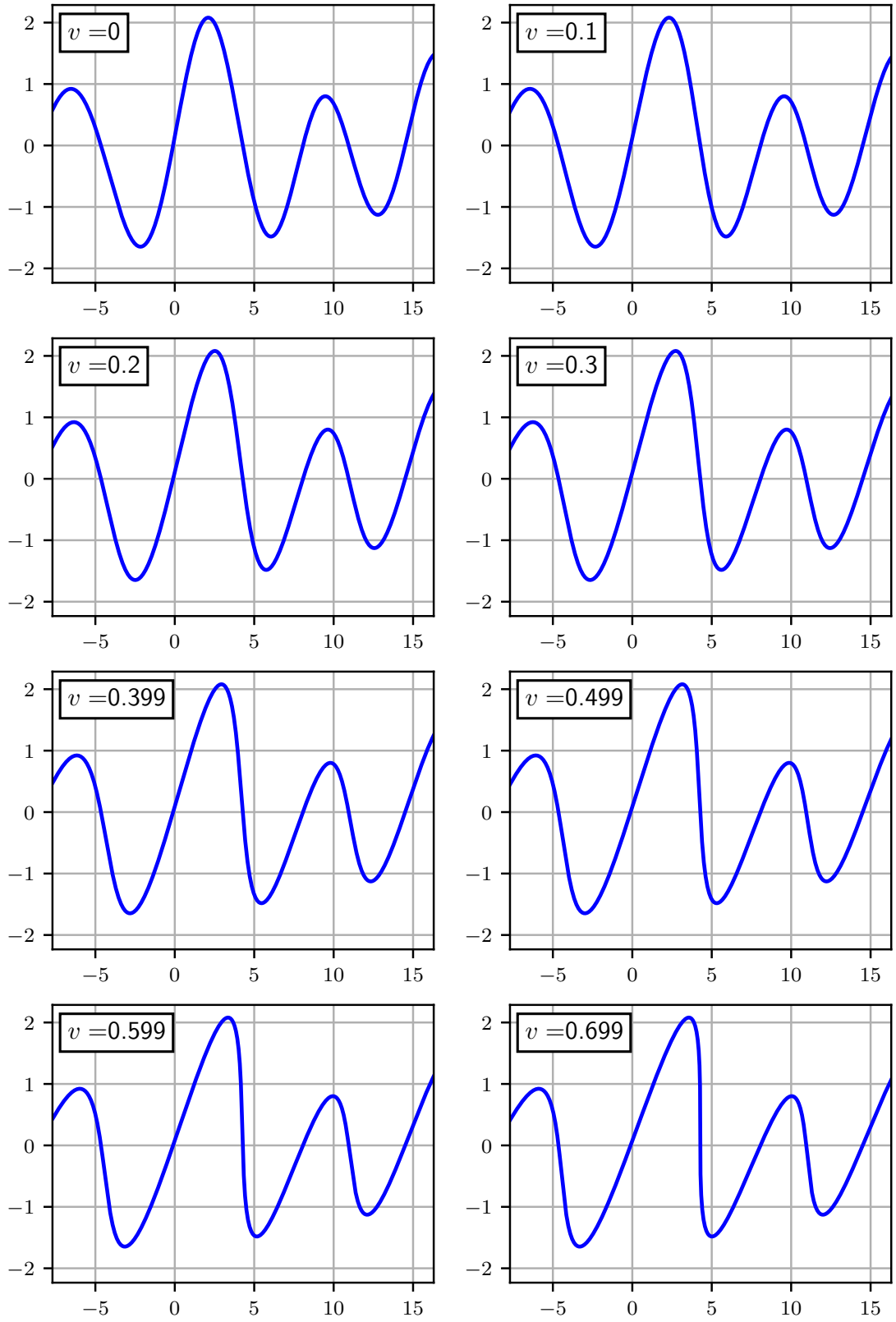

Figure 5.7: Evolution of the wave $\Pi(u)$ corresponding to an initial power spectrum with $A = 1000$, $\beta = 4$. $\alpha = 8$, $\gamma = 6$, $\Delta u = 10^{-3}$,$\Delta v = 10^{-6}$ and $k_0 = 1$. Note that the size of the box is $-100 < u < 100$ and the graphs only contain a part of it to better demonstrate the steepening of the wave.

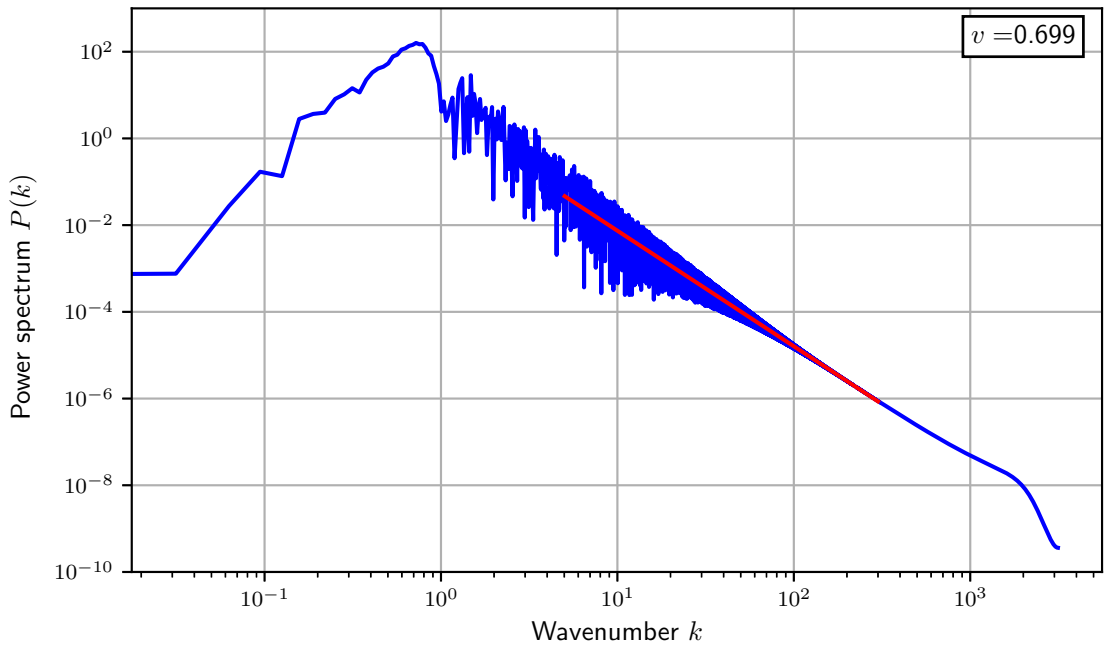

Figure 5.8: The power spectrum of figure 5.7 at the time of shock formation. The linear fit yields a value of -2.6654.

putation time allows us to reduce the value of A to 10, and the program still finishes in a reasonable time. As proposed above, the box size is reduced to $-10 < u < 10$ while still keeping to amount of data points intact, leading to $\Delta u \approx 10^{-4}$. The stepsize of v is kept the same at 10^{-6}. The power spectrum at different values of v is found in figure 5.9. The increase in the value of k_0 has pushed the inertial range to the right by one order of magnitude, as expected. The slope at the time of breaking (fig. 5.10) gives a power law of -2.6675.

The results seem to point towards a formation of an universal power law in the high-k-range at the moment of breaking with a value of about $8/3 \approx -2.66$. This is in agreement with the results found in [49] and their earlier numerical results in [50] [2].

[2] In these the power spectrum is referred to as the energy spectrum.

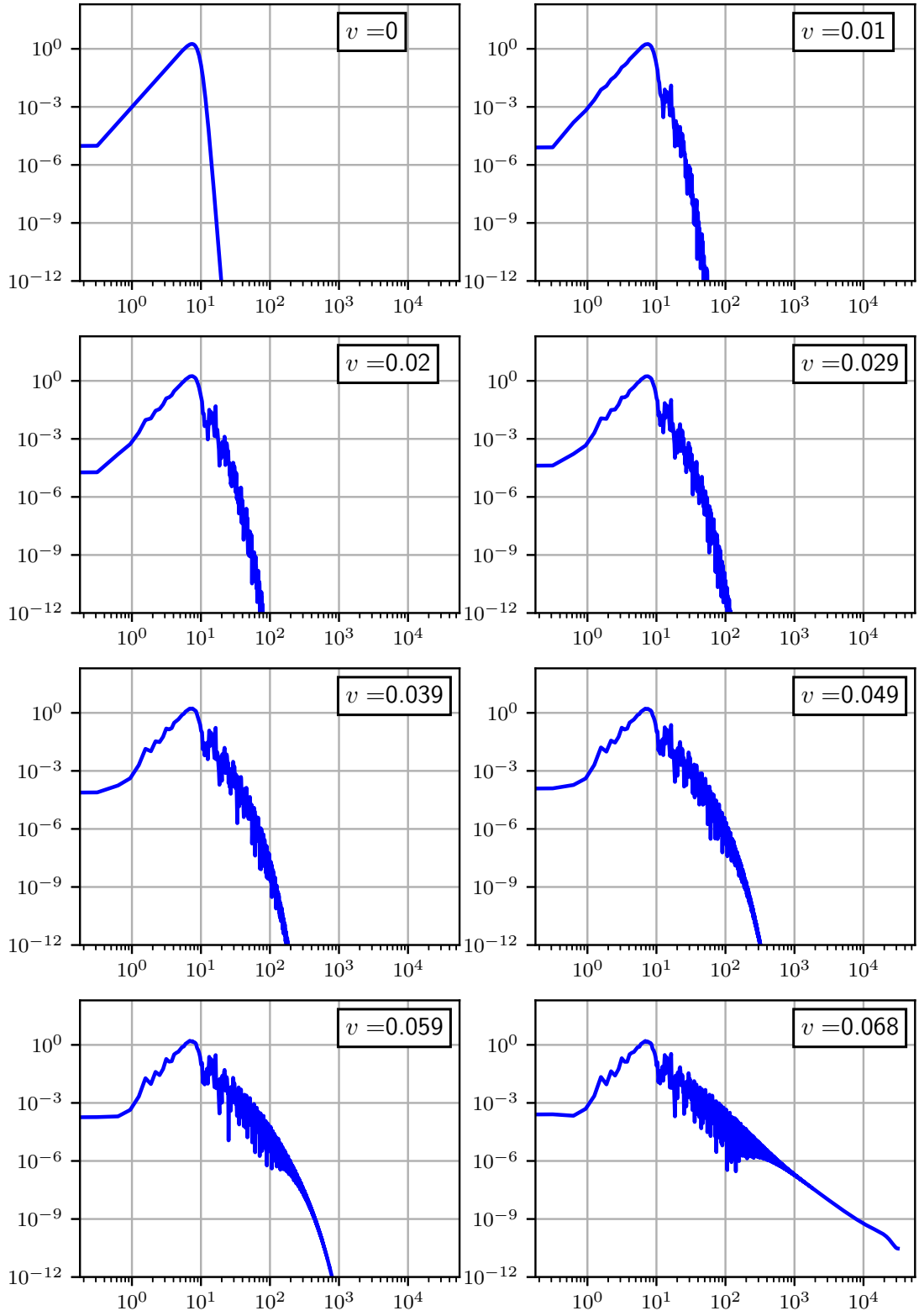

Figure 5.9: Evolution of the power spectrum $P(k)$ with $A = 10$, $\beta = 4$. $\alpha = 8$, $\gamma = 6$, $\Delta u \approx 10^{-4}$,$\Delta v = 10^{-6}$, $k_0 = 10$ and a box size of $-10 < u < 10$.

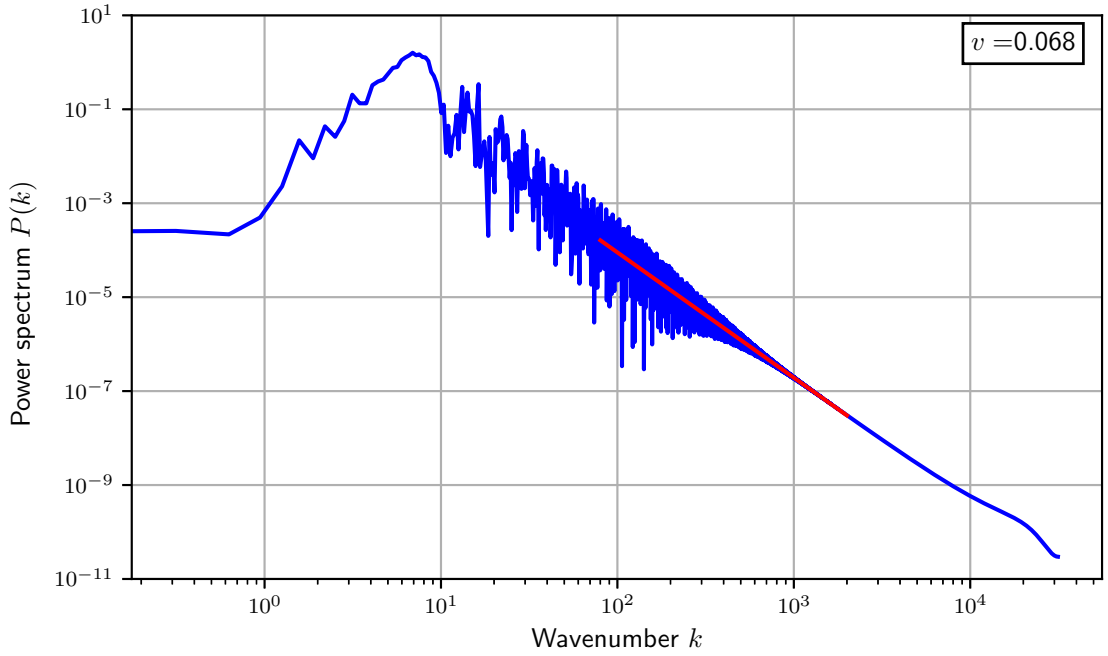

Figure 5.10: The power spectrum of figure 5.7 at $v = v_s$. The power law in the inertial range is found to be -2.6675.

5.3 Viscid case

How would the behaviour of the power spectrum change, if we were to include a dissipative term into Burgers' equation? The viscous Burgers' equation is

$$\frac{\partial \Pi}{\partial v} + \Pi \frac{\partial \Pi}{\partial u} = \nu \frac{\partial^2 \Pi}{\partial u^2} \tag{5.8}$$

and it was studied by J. M. Burgers in the 1930s with a goal to contribute to the study of fluid turbulence. The term on the right-hand side of the equation causes dissipation, leading to a decrease in the wave-amplitude over time. The constant ν is the viscosity.

The first order derivatives are approximated in the same way as in the inviscid case. The second derivative is written using the central difference (5.4) twice with

step $\Delta u/2$, which gives

$$\frac{\partial^2 \Pi}{\partial u^2} \approx \frac{\partial_u \Pi(u + \Delta u/2, v) - \partial_u \Pi(u - \Delta u/2, v)}{\Delta u} \tag{5.9}$$

$$\approx \frac{\Pi(u + \Delta u, v) - 2\Pi(u, v) + \Pi(u - \Delta u, v)}{(\Delta u)^2}. \tag{5.10}$$

Substituting the derivatives to the viscid Burgers' equation yields

$$\Pi(u, v + \Delta v) = \Pi(u, v) + \frac{\Delta v}{\Delta u}\Big[\frac{\nu}{\Delta u}\left(\Pi(u + \Delta u, v) - 2\Pi(u, v) + \Pi(u - \Delta u, v)\right) - \frac{1}{2}\Pi(u, v)\Big(\Pi(u + \Delta u, v) - \Pi(u - \Delta u, v)\Big)\Big]. \tag{5.11}$$

when $\kappa = 1$. The method is sensitive to the value of the viscosity ν and in order to keep the method stable, that is keeping the quantities small on the right-hand side of the equation, one should have $\nu \Delta v < (\Delta u)^2$. For a $\nu < 1$, the condition becomes $\Delta v < (\Delta u)^2$.

We repeat the procedure introduced in the previous section. This time we have chosen $du = 10^{-3}$ and $dv = 10^{-7}$ with a power spectrum (5.7) where $A = 10$, $\alpha = 7$, $\beta = 3$, $\gamma = 9/2$ and $k_0 = 1$ with a box size of $-20 < u < 20$. The value of the viscosity ν is chosen to be 0.01. These parameters with the imposed random initial conditions yield the figure 5.11. It can be seen that with the viscous term, Burgers' equation does not break down when the waves steepen to form shocks. Instead, the steepened waves form a sawtooth-like pattern, whose amplitude reduces with increasing v. The first wave stops steepening around $v = 3.6$, which can be regarded as the shock formation time. Picking a value around that, chosen here to be 3.64, gives the figure 5.12, whose power spectrum in figure 5.13 has a slope of -2.6740 indicated by the red line. Similar results are obtained by changing the parameters of the initial power spectrum, predicting the appearance of the $-8/3$ power law also in the viscid case at the moment of shock formation. This is also in agreement with the findings in [49, 50]. After the breaking time, the power law obtains values smaller than $-8/3$.

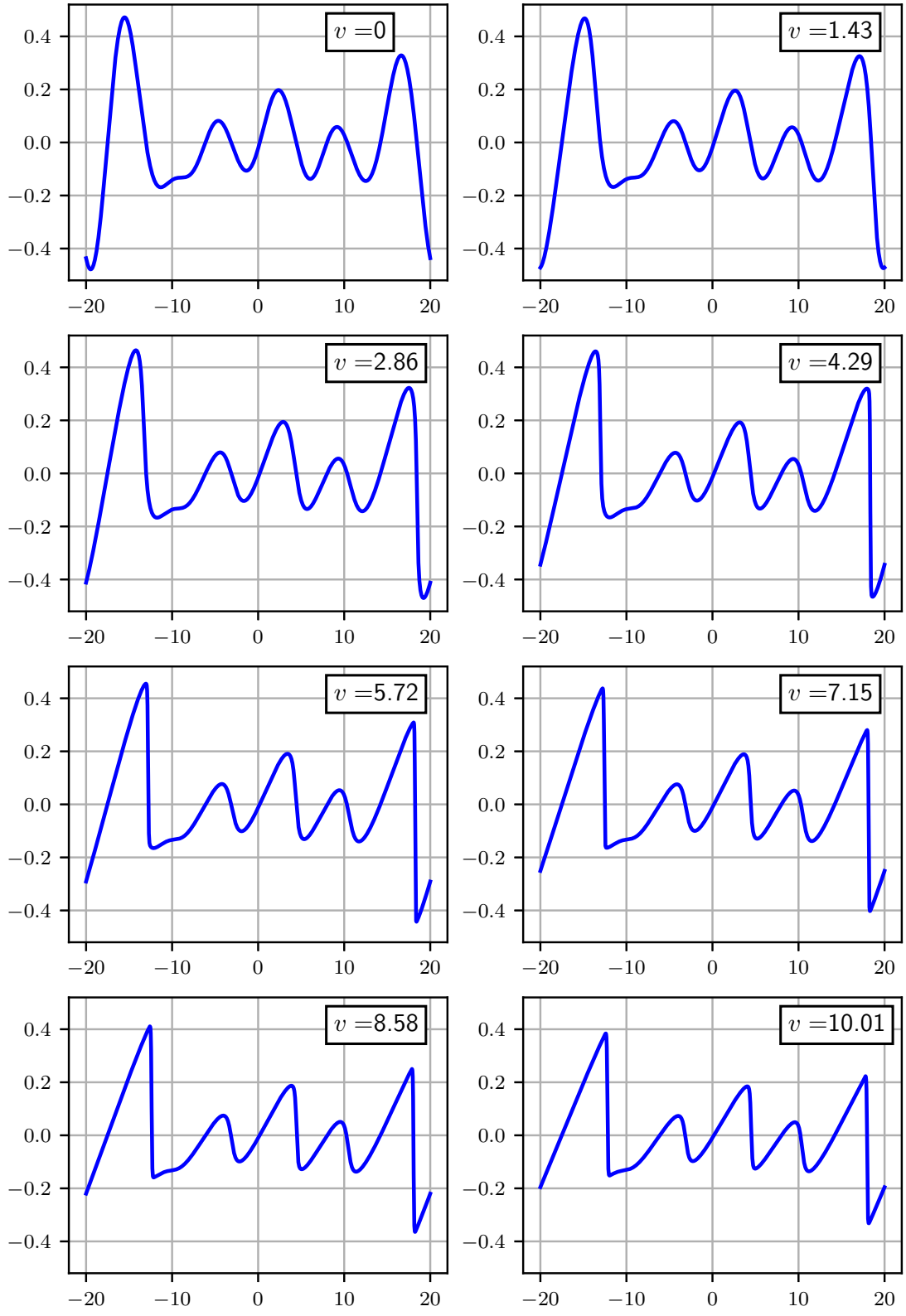

Figure 5.11: Dissipation of the wave $\Pi(u)$ under the viscid Burgers' equation with $\nu = 0.01$ and parameters mentioned at the start of this section.

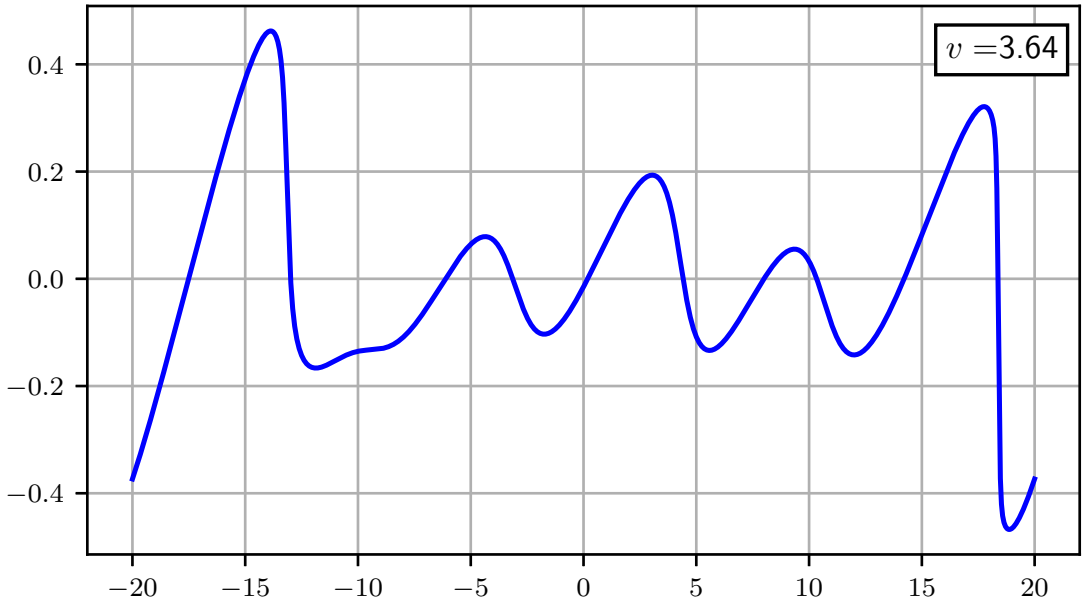

Figure 5.12: The waveform corresponding to figure 5.11 in the vicinity of the shock formation time.

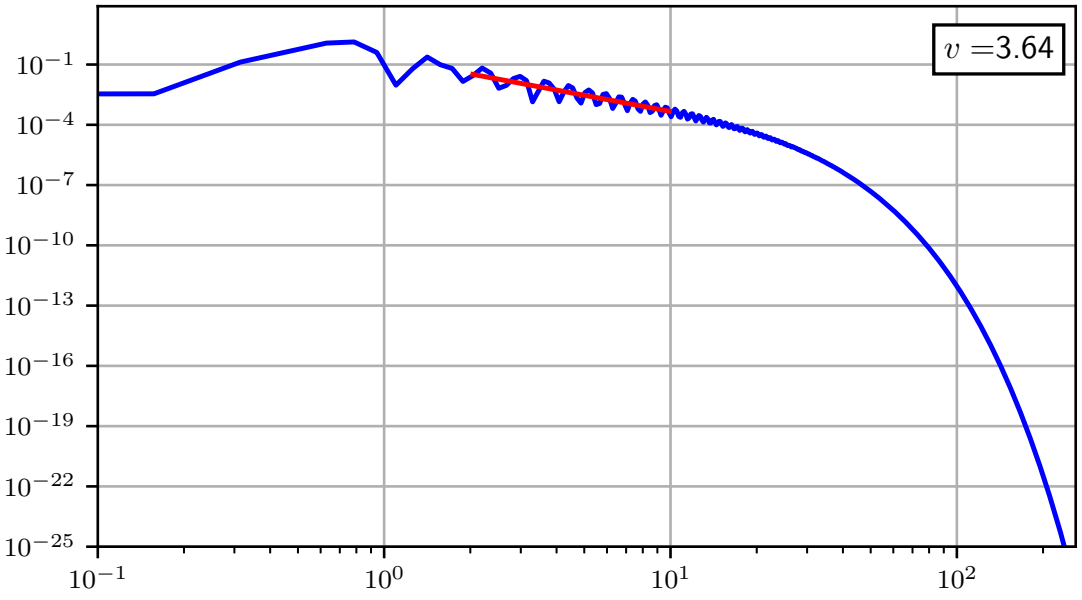

Figure 5.13: The power spectrum of figure 5.12. Linear fit gives a value of -2.6740 for the slope in the low-k-region.

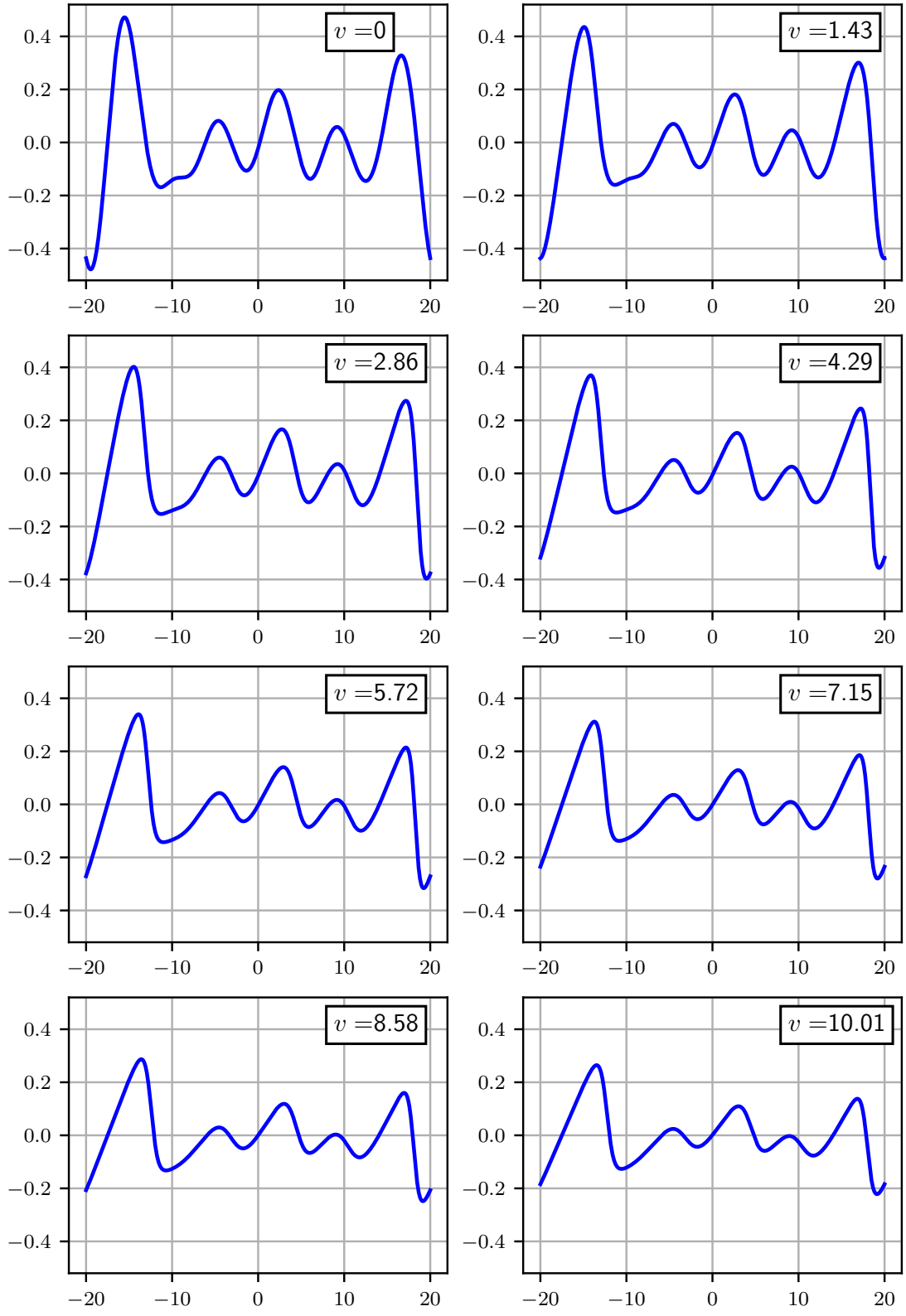

Figure 5.14: The wave of figure (5.11) with $\nu = 0.1$. This illustrates the effects of viscosity to wave steepening. In this case the effects of steepening are less prominent and the breaking time is shifted to a larger value of v.

6. Conclusions

In this thesis, we have discussed cosmological turbulence that originates from first-order phase transitions in the early universe. The transitions proceed by nucleation and expansion of bubbles containing the new phase. The turbulence itself is generated as a result of bubble collisions and the subsequent shocks, both of which cause stirring of the radiation fluid. The models used to analyse cosmological turbulence are based on the classical model of turbulence that was introduced in Chapter 2. In Chapter 3 it was explained how the classical model is utilized in a cosmological context, what are the approximations made and how they are justified.

We also had a look at the relativistic fluid equations for a perfect radiation fluid and expanded them to second order in perturbation theory following and filling in the details in Ref. [44]. In the one-dimensional case, the resulting equations simplified to Burgers' equation for right-moving waves, one of whose defining features is the development of shock waves over time. The equation was solved using the method of characteristics and from the general solution it was possible to obtain the time scale for shock formation.

In Chapter 5 Burgers' equation was analysed numerically using random initial conditions. Even though such a procedure is called Burgers' turbulence, the solutions to Burgers' equation do not manifest the irregular behaviour of regular fluid turbulence. Because of this, it is not a good model for turbulence but the results obtained could still be of some relevance in the study of the onset of cosmologi-

cal turbulence, as it is also generated by shocks. The simulations were carried out by using the simple Euler method with sufficiently small step sizes. In the inviscid case, the results seem to point towards an universal power law of $-8/3$ for the power spectrum at the time of shock formation. The same result is also obtained when a viscous dissipation term is introduced into Burgers' equation. The results are supported by [49, 50] that were unknown to us at the time we obtained our initial results.

We also touched on the gravitational wave generation from cosmological turbulence. Currently the most promising models are those of Refs. [27] and [35], made by different groups, both proclaiming that full numerical simulations of relativistic turbulence are needed in order to find the shortcomings of their models. Gravitational waves from turbulence contribute to the primordial gravitational wave background that may be detectable by future gravitational wave detectors, such as the LISA space observatory, and could provide exquisite information about the very early universe.

A. Code

The following program produces a figure with 8 plots akin to those in Chapter 5 both for the steepening wave and the corresponding power spectrum. The data of each plot is also saved into an .npz file for possible further use.

The program used to produce the data in Chapter 5.

```
import numpy as np
import matplotlib.pyplot as plt
from numpy import sqrt, pi, exp, abs
from numpy.fft import fft, ifft, fftfreq, fftshift, ifftshift

# Parameters
n = 20001                       # Number of datapoints (odd)
u = np.linspace(-10, 10, n,     # Size of the simulation box
                endpoint=False)
du = u[1]-u[0]
dv = 1e-5                       # Stepsize in v (time)
c = 1                           # Speed of sound
kappa = 1                       # Value of kappa in Burgers' equation
v = 0                           # Initial value of v

freq = fftfreq(n, du)           # Fourier space frequencies
freq = fftshift(freq)           # Shift the zero frequency component to the
                                # center of the spectrum
k = 2*pi*freq                   # Values of the wavenumber k

# Options
StartInFourier = True           # Start with a power spectrum or a wave Pi

randInit = True                 # Random initial conditions
# np.random.seed(347667834)     # Remove comment to set a seed

```

```
27  loglog = True                    # Plot the power spectrum on a log-log scale
28  customlimits = False             # Enable a custom plotting range on the log-log
29                                   # plot (vertical axis)
30  miny, maxy = 1e-40, 200          # Plotting range of y if customlimits = True
31
32  dissipation = False              # Include the dissipation term
33  vis = 0.01                       # Value of the viscosity
34
35  usecustomcutoff = False          # Stop the program when v = cutoff
36  cutoff = 10
37
38  slope = True                     # Calculate the slope of the power spectrum in
39  mink, maxk = 10, 110             # the interval [mink, maxk]
40
41  # Define the initial function
42  if StartInFourier:  # Power spectrum
43      A = 10; alfa = 8; beta = 4; gamma = 6; k0 = 1
44      Pk = (A*(abs(k)/k0)**beta)/(1+(abs(k)/k0)**alfa)**(gamma)
45      Fy = sqrt(Pk)
46  else:  # y = Pi
47      e = 1; a = 1
48      y = e*exp(-u**2/(2*a))
49
50  # Fourier inverse transform with random initial conditions
51  if (randInit and StartInFourier):
52      Fy = Fy.astype(complex)
53      im = np.random.uniform(-pi, pi, len(k))
54      half = len(k)//2
55      last = im[-(half+1):]
56      inv = last[::-1]
57      im[:half+1] = -inv
58      Fy = Fy*exp(1j*im)
59      Fy = ifftshift(Fy)
60      dk = k[1].real-k[0].real
61      y = ifft(Fy)*(dk*n)/(sqrt(2*pi))
62      y = fftshift(y)
63      y = y.real
64
65  # Fourier inverse transform without random initial conditions
66  if (StartInFourier and not randInit):
67      Fy = ifftshift(Fy)
68      dk = k[1].real-k[0].real
69      y = ifft(Fy)*(dk*n)/(sqrt(2*pi))
70      y = fftshift(y)
71      y = y.real
72
73  # Calculate the value of v, at which the wave forms a shock
```

```
if not usecustomcutoff:
    der = np.zeros(len(u))
    der[0] = ((y[1]-y[-1])/(2*du))
    der[-1] = (y[0]-y[-2])/(2*du)
    der[1:-1] = (y[2:]-y[:-2])/(2*du)
    cutoff = -kappa/min(der)
    cutoff = cutoff.real
    print("Cutoff: v=" + str(round(cutoff, 2)), flush=True)

# Calculate PI(u) at a later "time" v
def piAtV(y, u, dv, kappa, v0, v):
    y_n = np.zeros(len(u))
    while v0 < v:
        if dissipation:
            y_n[0] = y[0]+(dv/du)*((vis/du)*(y[1]-2*y[0]+y[-1])
                                   - (1/2)*y[0]*(y[1]-y[-1]))
            y_n[-1] = y[-1]+(dv/du)*((vis/du)*(y[0]-2*y[-1]+y[-2])
                                     - (1/2)*y[-1]*(y[0]-y[-2]))
            y_n[1:-1] = y[1:-1]+(dv/du)*((vis/du)*(y[2:]-2*y[1:-1]+y[:-2])
                                         - (1/2)*y[1:-1]*(y[2:]-y[:-2]))
            v0 += dv
            y, y_n = y_n, y
        else:
            y_n[0] = y[0]*(1-(dv/(2*kappa*du))*(y[1]-y[-1]))
            y_n[-1] = y[-1]*(1-(dv/(2*kappa*du))*(y[0]-y[-2]))
            y_n[1:-1] = y[1:-1]*(1-(dv/(2*kappa*du))*(y[2:]-y[:-2]))
            v0 += dv
            y, y_n = y_n, y
    return y, v

# Format plots
def graphFormat(value):
    plt.grid()
    plt.text(0.1, 0.85, r'$v=$' + str(np.round(value, 3)), fontsize=15,
             horizontalalignment='center', verticalalignment='center',
             transform=plt.gca().transAxes)

# Plot and save the power spectrum of y (Pi)
def plotPowerSpectrum(u, y, i):
    y = ifftshift(y)
    Fy = fft(y)*(du/sqrt(2*pi))
    Fy = fftshift(Fy)
    np.savez('four' + str(i), k=k, Fy=Fy)
    print(str(i) + "/8", flush=True)
    if loglog:
        plt.loglog(k, abs(Fy)**2, 'b')
        if slope and (i == 8):
```

```
            cond = (k >= mink) & (k <= maxk)
            Fyfit = np.log10(abs(Fy[cond])**2)
            kran = k[cond]
            kfit = np.log10(kran)
            coeff = np.polyfit(kfit, Fyfit, 1)
            print('slope: ' + str(coeff[0]), flush=True)
            plt.plot(kran, 10**coeff[1]*kran**coeff[0], 'r')
            np.savez('slope', kran=kran, coeff=coeff)
        if customlimits:
            plt.ylim(miny, maxy)
    else:
        plt.plot(k, abs(Fy)**2, 'b')

# Create 2x8 subplots (both in Fourier and real space) at different values of v
d = cutoff/7
for i in range(1, 9):
    if i == 1:
        plt.figure(1)
        plt.subplot(4, 2, i)
        plt.plot(u, y, 'b')
        np.savez('real1', u=u, y=y)
        graphFormat(0)
        plt.title('Real space' + ', ' + r'$n=$' + str(n) + ', ' r'$du=$'
                  + str(du) + ', ' + '$dv=$ ' + str(dv), fontsize=25)

        plt.figure(2)
        plt.subplot(4, 2, i)
        plotPowerSpectrum(u, y, i)
        graphFormat(0)
        plt.title('Fourier space' + ', ' + r'$n=$' + str(n) + ', ' r'$du=$'
                  + str(du) + ', ' + '$dv=$ ' + str(dv), fontsize=25)
    else:
        y, v = piAtV(y, u, dv, kappa, v, d*(i-1))
        plt.figure(1)
        plt.subplot(4, 2, i)
        plt.plot(u, y, 'b')
        np.savez('real' + str(i), u=u, y=y, v=v)
        graphFormat(d*(i-1))

        plt.figure(2)
        plt.subplot(4, 2, i)
        plotPowerSpectrum(u, y, i)
        graphFormat(d*(i-1))

plt.show()
```

References

[1] P. A. R. Ade et al. Planck 2015 results. XIII. Cosmological parameters. *Astron. Astrophys.*, 594:A13, 2016, arXiv:1502.01589 [astro-ph.CO].

[2] B. P. Abbott et al. Observation of Gravitational Waves from a Binary Black Hole Merger. *Phys. Rev. Lett.*, 116(6):061102, 2016, arXiv:1602.03837 [gr-qc].

[3] D. G. Blair. *Detection of gravitational waves.* Cambridge University Press; 1st edition, 1991.

[4] Chiara Caprini and Daniel G. Figueroa. Cosmological Backgrounds of Gravitational Waves. 2018, arXiv:1801.04268 [astro-ph.CO].

[5] J. Allday. *Quarks, Leptons and The Big Bang.* CRC Press; 3rd edition, 2016.

[6] Chiara Caprini et al. Science with the space-based interferometer eLISA. II: Gravitational waves from cosmological phase transitions. *JCAP*, 1604(04):001, 2016, arXiv:1512.06239 [astro-ph.CO].

[7] Norbert Straumann. Cosmological phase transitions. In *3rd PSI Summer School on Condensed Matter Research Zuoz, Switzerland, August 7-14, 2004*, 2004, arXiv:astro-ph/0409042.

[8] Steven Weinberg. Gauge and Global Symmetries at High Temperature. *Phys. Rev.*, D9:3357–3378, 1974.

[9] M. Kachelriess. *Quantum Fields: From the Hubble to the Planck Scale.* Oxford University Press; 1st edition, 2018.

[10] Ariel Mégevand and Santiago Ramírez. Bubble nucleation and growth in slow cosmological phase transitions. *Nucl. Phys.*, B928:38–71, 2018, arXiv:1710.06279 [astro-ph.CO].

[11] Dietrich Bodeker and Guy D. Moore. Can electroweak bubble walls run away? *JCAP*, 0905:009, 2009, arXiv:0903.4099 [hep-ph].

[12] Dietrich Bodeker and Guy D. Moore. Electroweak Bubble Wall Speed Limit. *JCAP*, 1705(05):025, 2017, arXiv:1703.08215 [hep-ph].

[13] Ariel Megevand and Alejandro D. Sanchez. Detonations and deflagrations in cosmological phase transitions. *Nucl. Phys.*, B820:47–74, 2009, arXiv:0904.1753 [hep-ph].

[14] Ariel Megevand and Federico Agustin Membiela. Stability of cosmological deflagration fronts. *Phys. Rev.*, D89(10):103507, 2014, arXiv:1311.2453 [astro-ph.CO].

[15] Arthur Kosowsky, Andrew Mack, and Tinatin Kahniashvili. Gravitational radiation from cosmological turbulence. *Phys. Rev.*, D66:024030, 2002, arXiv:astro-ph/0111483.

[16] Marc Kamionkowski, Arthur Kosowsky, and Michael S. Turner. Gravitational radiation from first order phase transitions. *Phys. Rev.*, D49:2837–2851, 1994, arXiv:astro-ph/9310044.

[17] Dietrich Bodeker and Guy D. Moore. Electroweak Bubble Wall Speed Limit. *JCAP*, 1705(05):025, 2017, arXiv:1703.08215 [hep-ph].

[18] Heather Audley et al. Laser Interferometer Space Antenna. 2017, arXiv:1702.00786 [astro-ph.IM].

[19] Arthur M. Jaffe. The Millennium Grand Challenge in Mathematics. *Notices of the AMS*, 53, 6, 2006.

[20] J. O. Hinze. *Turbulence*. McGraw-Hill College; 2nd edition, 1975.

[21] P. A. Davidson. *Turbulence : an introduction for scientists and engineers*. Oxford University Press, 2004.

[22] L. D. Landau and E. M. Lifshitz. *Fluid Mechanics*. Pergamon press; 2nd edition, 1987.

[23] A. N. Kolmogorov. The local structure of turbulence in incompressible viscous fluid for very large reynolds numbers. *C. R. Acad. Sci. URSS*, 30, 1941.

[24] S. B. Pope. *Turbulent flows*. Cambridge University Press, 2000.

[25] Eanna E. Flanagan and Scott A. Hughes. The Basics of gravitational wave theory. *New J. Phys.*, 7:204, 2005, arXiv:gr-qc/0501041.

[26] K. S. Thorne C. W. Wisner and J. A. Wheeler. *Gravitation*. W. H. Freeman, San Francisco, 1973.

[27] Grigol Gogoberidze, Tina Kahniashvili, and Arthur Kosowsky. The Spectrum of Gravitational Radiation from Primordial Turbulence. *Phys. Rev.*, D76:083002, 2007, arXiv:0705.1733 [astro-ph].

[28] Chiara Caprini and Ruth Durrer. Gravitational waves from stochastic relativistic sources: Primordial turbulence and magnetic fields. *Phys. Rev.*, D74:063521, 2006, arXiv:astro-ph/0603476.

[29] Bruce Allen. The Stochastic gravity wave background: Sources and detection. In *Relativistic gravitation and gravitational radiation. Pro-*

ceedings, School of Physics, Les Houches, France, September 26-October 6, 1995, pages 373–417, 1996, arXiv:gr-qc/9604033.

[30] Michele Maggiore. Gravitational wave experiments and early universe cosmology. *Phys. Rept.*, 331:283–367, 2000, arXiv:gr-qc/9909001.

[31] Lars Husdal. On Effective Degrees of Freedom in the Early Universe. *Galaxies*, 4(4):78, 2016, arXiv:1609.04979 [astro-ph.CO].

[32] Raphael Micha and Igor I. Tkachev. Relativistic turbulence: A Long way from preheating to equilibrium. *Phys. Rev. Lett.*, 90:121301, 2003, arXiv:hep-ph/0210202.

[33] Jungyeon Cho. Simulation of relativistic force-free magnetohydrodynamic turbulence. *Astrophys. J.*, 621:324, 2005, arXiv:astro-ph/0408318.

[34] Michael S. Turner, Erick J. Weinberg, and Lawrence M. Widrow. Bubble nucleation in first order inflation and other cosmological phase transitions. *Phys. Rev.*, D46:2384–2403, 1992.

[35] Chiara Caprini, Ruth Durrer, and Geraldine Servant. The stochastic gravitational wave background from turbulence and magnetic fields generated by a first-order phase transition. *JCAP*, 0912:024, 2009, arXiv:0909.0622 [astro-ph.CO].

[36] Chiara Caprini, Ruth Durrer, and Tina Kahniashvili. The Cosmic microwave background and helical magnetic fields: The Tensor mode. *Phys. Rev.*, D69:063006, 2004, arXiv:astro-ph/0304556.

[37] Stephon Alexander and Nicolas Yunes. Parametrized post-Newtonian expansion of Chern-Simons gravity. *Phys. Rev.*, D75:124022, 2007, arXiv:0704.0299 [hep-th].

[38] Tina Kahniashvili, Grigol Gogoberidze, and Bharat Ratra. Polarized cosmological gravitational waves from primordial helical turbulence. *Phys. Rev. Lett.*, 95:151301, 2005, arXiv:astro-ph/0505628.

[39] Chiara Caprini, Ruth Durrer, and Elisa Fenu. Can the observed large scale magnetic fields be seeded by helical primordial fields? *JCAP*, 0911:001, 2009, arXiv:0906.4976 [astro-ph.CO].

[40] Jose R. Espinosa, Thomas Konstandin, Jose M. No, and Geraldine Servant. Energy Budget of Cosmological First-order Phase Transitions. *JCAP*, 1006:028, 2010, arXiv:1004.4187 [hep-ph].

[41] Pierre Binetruy, Alejandro Bohe, Chiara Caprini, and Jean-Francois Dufaux. Cosmological Backgrounds of Gravitational Waves and eLISA/NGO: Phase Transitions, Cosmic Strings and Other Sources. *JCAP*, 1206:027, 2012, arXiv:1201.0983 [gr-qc].

[42] Alexander D. Dolgov, Dario Grasso, and Alberto Nicolis. Relic backgrounds of gravitational waves from cosmic turbulence. *Phys. Rev.*, D66:103505, 2002, arXiv:astro-ph/0206461.

[43] T. Von Kármán. Progress in the Statistical Theory of Turbulence. *Proceedings of the National Academy of Sciences of the United States of America*, 34:530, 1948.

[44] Ue-Li Pen and Neil Turok. Shocks in the Early Universe. *Phys. Rev. Lett.*, 117(13):131301, 2016, arXiv:1510.02985 [astro-ph.CO].

[45] N. G. Sànchez and A. Zichichi. *Current Topics in Astrofundamental Physics: The Early Universe*. Springer Science & Business Media, 2012.

[46] U. Frisch and J. Bec. 'Burgulence'. In *Les Houches 2000 Summer*

School: Session 74: New Trends in Turbulence Les Houches, France, July 31-September 2, 2000, 2000, arXiv:nlin/0012033.

[47] J.D. Cole. On a quasi-linear parabolic equation occurring in aerodynamics. *Quart. Appl. Math.*, 9:225–236, 1951.

[48] E. Hopf. The partial differential equation $u_t + uu_x = u_{xx}$. *Comm. Pure Appl. Math.*, 3:201–230, 1950.

[49] D. Pelinovsky et al. Universal power law for the energy spectrum of breaking Riemann waves. *JETP Letters*, 98(4):237–241, 2013, arXiv:1307.0248v1 [math-ph].

[50] E. Kartashova and E. Pelinovsky. Universal breaking point asymptotic for energy spectrum of Riemann waves in weakly nonlinear nondispersive media. 2013, arXiv:1303.2885v2 [physics.flu-dyn].